DYNAMIC REMODELING OF THE PULMONARY MICROENVIRONMENT CONTROLS TRANSFORMING GROWTH FACTOR-BETA ACTIVATION AND ALVEOLAR TYPE II EPITHELIAL TO MESENCHYMAL TRANSITION

A Dissertation
Presented to
The Academic Faculty

by

Marilyn Markowski Dysart

In Partial Fulfillment
of the Requirements for the Degree
Doctor of Philosophy in Biomedical Engineering in the
Wallace H. Coulter Department of Biomedical Engineering at Georgia Tech and Emory University

Georgia Institute of Technology
May 2014

DYNAMIC REMODELING OF THE PULMONARY MICROENVIRONMENT CONTROLS TRANFORMING GROWTH FACTOR-BETA ACTIVATION AND ALVEOLAR TYPE II EPITHELIAL TO MESENCHYMAL TRANSITION

Approved by:

Dr. Thomas Barker, Advisor
Wallace H. Coulter Department of Biomedical Engineering
Georgia Institute of Technology

Dr. Lou Ann Brown
Department of Pediatrics
Emory University School of Medicine

Dr. Todd McDevitt
Wallace H. Coulter Department of Biomedical Engineering
Georgia Institute of Technology

Dr. Tatiana Segura
Department of Chemical and Biomolecular Engineering
University of California Los Angeles

Dr. Edward Botchwey
Wallace H. Coulter Department of Biomedical Engineering
Georgia Institute of Technology

Date Approved: February 28, 2014

I would like to dedicate this dissertation to several people. First, to my deceased mother, Carol, who was my inspiration to pursue a PhD, and taught me invaluable lessons throughout my life. Second, to my father, Edward, who provided me unconditional moral support and encouraged me to continue during moments of doubt. Finally, I dedicate this to my husband, Fred, who has been a constant source of support and encouragement throughout the challenges of graduate school. I am truly thankful to have had each of you in my life.

ACKNOWLEDGEMENTS

This work could not have been accomplished without the guidance, support, encouragement and input from a number of people. I would first like to thank my advisor, Dr. Thomas H. Barker for helping to shape the overall direction of my work in the Matrix Biology and Engineering Lab. I especially want to thank Tom for his guidance and mentoring after joining his lab already two years into my graduate career. He was a pivotal part in giving me the opportunity to pursue research that was of great interest to me in a timely manner while still focusing on my professional development for my specific career goals. I would secondly like to thank my committee members, Dr. Todd McDevitt, Dr. Edward Botchwey, Dr. Lou Ann Brown, and Dr. Tatiana Segura for their valuable insight about alveolar cell and pulmonary biology, fibronectin integrin interactions and subsequent cell signaling, and for their comments and suggestions that improved the quality of this work. Finally, I would like to thank Dr. Ted Russell and the graduate students in his lab for their collaboration on the collection of particulate matter without much of this work could not be accomplished.

I would like to thank the members of the Matrix Biology and Engineering Lab, who all work extremely hard to produce high quality research. I would specifically like to thank Dr. Ashley Brown, with whom this work would not have been possible without. I am extremely grateful for her expertise in EMT and alveolar cell biology, her continual mentoring, and her assistance in training me on many assays and experimental techniques that made this work possible. I also want to thank Ashley for her friendship and willingness to listen when experiments were failing. I would like to thank Dr. Lizhi Cao

for his many insightful conversations on fibronectin structure and mechanics and Vince Fiore for assistance in AFM and insight on the role of substrate rigidity in EMT. I thank Alison Douglas for her assistance in learning protein purification techniques and troubleshooting the FPLC. I would also like to thank the newer members of our lab, Dwight Chambers, Victoria Stefanelli, Haylee Bachman, and John Nicosia for their fresh insight and helpful comments as well as their continuing support as I was pushing to finish this work. Finally, I would like to thank my undergraduate assistant Mercedes de la Sierra for her help in polyacrylamide gel production, cell culture maintenance, and protein purification.

I would also like to thank my friends and family for their invaluable support and friendships through this process. The individuals I have met in graduate school that I consider friends are too numerous to name. There are a few, however, that cannot go unmentioned. Specifically I thank Eric Alonas, who was the first person I met after moving to Atlanta, for his unwavering friendship, coffee breaks, occasional necessary happy hours, and for keeping me sane while trying to plan a wedding while in graduate school. I would also like to recognize Akhil Srinivasan, Jeenah Jung, Kristin Loomis, Patricia Pacheco, Alex Calhoun, and Eli Fine. These friends have been there for me when the challenges of graduate school seemed too great to overcome. I will never forget the many amazing experiences we have shared together.

I would like to express the deepest gratitude to my family. I would first like to thank my deceased mom, Dr. Carol Markowski, for inspiring me to pursue a PhD. She was the single most important person in my life: my best friend and mentor. Thank you for always standing behind me and believing I would succeed. I will miss you always and

love you forever. To Dr. Edward Markowski, my dad, for his love and support over the years. Thank you for always being there for me, even when I was calling for statistical advice at midnight! To my sister Pamela Markowski, thank you for believing in me and being so proud of my work. I hope my work will inspire your students to love science the way we both do. I would also like to thank my new family members, Samuel Dysart, Susan Rooney, and Mahlon Dysart for welcoming me into your family and for all your encouragement. Finally to all my friends who are truly family: Amanda Ramkvist, Liz Martin, Bridget Holroyd, Jennifer Kamens, Matt Henley, Jim Anderson, Anthony Clark, and Mac Nance, thank you for the unwavering support not only through this journey, but for the past 10+ years. I could not have gotten to where I am without each and every one of you.

Finally to my husband Fred, words cannot express my gratitude for sticking with me through this five-year roller coaster ride. Thank you for picking up the slack when I was too busy or too tired to help around the house. Thank you for always believing I could get to this point, even when I was convinced it would never happen. Thank you for listening and truly trying to understand when I would ramble about fibronectin, integrins, and EMT after a few too many beers. I am certain you know more about pulmonary biology than any other computer programmer! Most of all thank you for your love, positive attitude, and constant support. You always find a way to make me smile even on the worst of days. I would not be the person I am today without you. You are truly my best friend and I am forever grateful to have you by my side.

TABLE OF CONTENTS

LIST OF TABLES

LIST OF FIGURES

LIST OF SYMBOLS

α	alpha
β	beta
k_a	kinetic association rate constant
k_d	kinetic dissociation rate constant
K_d	equilibrium dissociation rate constant

LIST OF ABBREVIATIONS

α-SMA	alpha smooth muscle actin
AFM	atomic force microscopy
ATI	alveolar epithelial type I
ATII	alveolar epithelial type II
ECM	extracellular matrix
EMT	epithelial to mesenchymal transition
Fn	fibronectin
FnIII9-10	fibronectin 9^{th} and 10^{th} type III domain
FnIII9*10	fibronectin 9^{th} and 10^{th} type III domain with stabilizing point mutation
FnIII9p10	fibronectin 9^{th} and 10^{th} type III domain with mutation in PHSRN site
$FnIII9^{2G}10$	fibronectin 9^{th} and 10^{th} type III domain with 2-glycine insertion
$FnIII^{4G}10$	fibronectin 9^{th} and 10^{th} type III domain with 4-glycine insertion
IPF	idiopathic pulmonary fibrosis
LAP	latency associated peptide
Ln	laminin
NAC	N-acetyl cysteine
P4H	prolyl-4-hydroxylase
PM	particulate matter
PM2.5	fine particulate matter with a diameter < 2.5 microns
ROS	reactive oxygen species
SPR	surface plasmon resonance
TGFβ	transforming growth factor beta
TNFα	tumor necrosis factor alpha

SUMMARY

The extracellular matrix (ECM) is a dynamic environment that provides important cues for directing intermediate and terminal cell fate. Cells are able to respond to and actively remodel their ECM. This dynamic remodeling of the ECM is essential for processes including development, normal tissues homeostasis, as well as wound healing. However, many different severe pathologies can arise when ECM remodeling becomes uncontrolled. Dysregulation of both the biochemical and biophysical properties of the ECM are observed in several diseases including cancer and fibrotic pathologies such as cardiovascular disease and pulmonary fibrosis. These changes in the ECM force cell into a non-homeostatic niche, altering their normal responses to the microenvironment**.** In the case of pulmonary fibrosis, the ECM is known to shift biochemically from a predominantly laminin and elastin matrix to a provisional matrix that is predominantly composed of fibrin and fibronectin (Fn). Furthermore, the elasticity of tissue from patients with pulmonary fibrosis has been shown to increase approximately nine-fold, drastically changing the biophysical properties of the matrix. For example, many studies have shown that cells adjust their internal stiffness to match their surroundings in response to increases in substrate stiffness. This mechanical homeostasis between the cell and its increasingly stiff surrounding environment results in increased activation of several contractile signals including Rho and Rho associated kinase (ROCK). This increased contractile signaling results in many diverse secondary effects, such as increased forces applied by cells to their underlying ECM. As a consequence of increased forces on the matrix, proteins that comprise structural proteins, for example Fn, can

undergo conformational changes including partial unfolding, which further changes the biochemical nature of the ECM. Specifically, changes in the conformation of Fn have been shown to have major consequences on cell phenotype and fate by the ability to alter integrin binding. These alterations in the ECM as well as changes in mechanical properties of the ECM are hypothesized to contribute to pathological processes such as epithelial to mesenchymal transition (EMT).

EMT, the differentiation of cells from an epithelial to mesenchymal phenotype, has been highly implicated in several disease including cancer metastasis and the onset and progression of pulmonary fibrosis. The process of EMT is necessary for many biological processes such as embryonic development and adult wound healing. However, when dysregulated, EMT can lead to tissue and organ deficiencies. EMT is a highly regulated process that integrates biochemical signals from ECM receptors known as integrins as well as growth factor receptors like transforming growth factor – β (TGFβ) receptor. TGFβ is of particular interest in the onset and progression of pulmonary fibrosis because it has been shown to be a potent inducer of EMT in several different cell types and tissues. TGFβ must be activated in order to bind to its receptors. This activation can occur through several different mechanisms, including but not limited to a mechanical activation process as a result of cell contractile forces. Given that this activation is a cell-mediated process, mechanical activation of TGFβ will be greatly influences by both the aforementioned changes to the biochemical and biophysical properties of the ECM. Previous work has shown that increases in substrate stiffness as well as changes in integrin engagement can modulate cell contractility, leading to TGFβ activation and ultimately EMT.

Adding the complexity of studying the mechanisms that contribute to the onset and progression of pulmonary fibrosis is the continual exposure of the lung to insults of injury from day to day activity. For example, pollution and particulate matter (PM) have been linked with adverse pulmonary health effects and increased mortality. Environmental PM is capable of depositing in the airways of the pulmonary system, penetrating into the alveoli, increasing respiratory distress and exacerbating pre-existing pulmonary conditions such as pulmonary fibrosis. Specifically, PM has been shown to have secondary effects that can induce cellular damage resulting in additional fibrotic remodeling events. This additional remodeling stands to further contribute to biochemical and biophysical changes of the surrounding matrix. Previous studies to date have focused on either biochemical changes or biophysical changes of the matrix on cell phenotype. In addition no studies to date have explored how injury events, e.g. exposure to environmental pollutant particulate matter, contributes to pathological processes such as EMT. This dissertation seeks to first, connect the biochemical and biophysical changes observed in the ECM during fibrosis to the pathologic process of EMT and second, determine how exposure to physiologically relevant levels of environmental pollutants affects the process of EMT during remodeling events.

First, the role of alterations in Fn conformation on cell binding and phenotype were explored. Recombinant Fn fragments were created that model different conformational states of the molecule and integrin specific binding to the fragments as well as downstream cell phenotypes were investigated to confirm our model system. Next, to explore simultaneous alterations in the biochemical and biophysical properties commonly seen during pulmonary fibrosis, a model system was created that utilized the

aforementioned Fn fragments cross-linked to polyacrylamide gels of varying substrate stiffnesses mimicking healthy to fibrotic tissue stiffnesses. EMT responses were characterized and the role of TGFβ activation was investigated. Finally, the role of exposure to PM in conjunction with the established model accounting for biochemical and biophysical changes to the microenvironment was explored for EMT responses, TGFβ activation, and the presence of reactive oxygen species.

The results presented here show that both biochemical and biophysical state of the ECM contribute to the pathological progression of EMT, and that there is a delicate balance between the two. Specifically, the work shows that, biochemical changes which facilitate cell binding through α5β1 and α3β1 integrins, can maintain an epithelial phenotype, and activate low levels of TGFβ even on stiffer substrates that alone drive EMT. Conversely, we show that biochemical changes that facilitate cell binding through αv integrins lead to enhanced activation of TGFβ and EMT even on softer substrates that alone maintain epithelial phenotype. Furthermore, we find that exposure to environmental particulates on intermediate substrate stiffness, modeling a "pre-fibrotic" state, drive epithelial cells to completely undergo EMT and activate significantly increased levels of TGFβ. In addition, this work shows that a *partial* recovery of epithelial phenotype and decreased levels of TGFβ are observed when cells exposed to PM are cultured in conjunction with Fn fragments that force cell binding predominantly through α5β1 and α3β1 integrin. Finally, the presence of reactive oxygen species (ROS) was explored, and we conclude that the presence of ROS is a possible contributor to the increased levels of TGFβ and EMT seen with the addition of PM. These results taken together show that there is a delicate balance between both the biochemical and biophysical components of

the ECM, TGFβ, and EMT, that these responses can be altered by exposure to injury adjuvants such as PM, and that these changes to the cellular microenvironment can be significant contributors to the emergence of pathological phenotypes that are associated with the progression of pulmonary fibrosis.

CHAPTER 1

INTRODUCTION

Fibrosis is a potentially deadly pathology that is characterized by excessive deposition of extracellular matrix, which leads to increased stiffness of the tissue and ultimately loss of tissue structure and function. Many lung diseases, including pulmonary fibrosis, COPD, and lung cancer are thought to be driven by changes in the ECM that drive the pathological phenotypes that contribute to the disease. Mounting evidence suggests that the lung "precursor" cell, the alveolar type II (ATII) epithelial cell is a key player in the initiation and progression of pulmonary fibrosis. Although the exact mechanism has yet to be elucidated, it is generally accepted that in response to changes in the extracellular environment, altered signaling events result in the ATII cell undergoing an epithelial to mesenchymal transition, which leads to secretory fibroblasts, that lay down increased matrix and stiffen the lung tissue (1-5).

During pulmonary fibrosis, cells experience many changes to their microenvironment at both the biochemical and biophysical level, resulting in a stiffer underlying ECM (6-12), and a change in the ECM composition from a predominantly laminin and elastin matrix to a provisional ECM composed predominantly of fibrin and fibronectin (Fn) (13). The mechanisms of the biophysical changes in the matrix have been widely studied, and are thought to occur through a combination of changes in the ECM composition by means of changes in gene expression, increased glycosylation, and increased cross-linking of the matrix through tissue transglutaminases or lysyl oxidase (14, 15). Furthermore, much of the cell population in fibrotic tissue has been shown to

shift to a more contractile phenotype, which can further contribute to mechanical changes in the ECM. This increased contractility of cells further regulates the state of the matrix not only by stiffening the surrounding tissue, but also by altering the biochemical state of fibrillar ECM proteins, notably Fn (13). Fn is highly sensitive to force-mediated unfolding, where only small inputs of force can lead to expansion of the cell binding domain, resulting in the separation of the major integrin binding sites, RGD and PHSRN (13, 16, 17). The positioning of these two sites is crucial to determining which integrins cells use to bind their ECM. Specifically, the relative positioning of these two sites has been shown to influence α5β1 integrin binding, resulting in changes in integrin engagement based on positioning, and ultimately driving differential cell phenotypes (1, 18-20).

A major process that has been implicated in the onset and progression of pulmonary fibrosis is the epithelial to mesenchymal transition (EMT) (2, 21-24). EMT is the de-differentiation of an epithelial cell into a mesenchymal cell, and is characterized by a loss of cell-cell contacts, decreased expression of epithelial markers such as e-cadherin, and a loss of cell polarity, while concomitantly gaining increased expression of mesenchymal markers such as alpha smooth muscle actin (α-SMA), increased ECM production, and an increase in stress fiber formation, cell contractility, and cell mobility (25-27) . Several studies have observed EMT in pulmonary fibrosis models. For example, *in-vivo,* in a bleomycin induced pulmonary fibrosis model, EMT was observed within the fibrotic regions of the lung (28). In addition, multiple studies *in-vitro,* have shown that ATII cells undergo EMT in response to their exposed underlying matrix. Specifically, ATII cells cultured on laminin matrices (Ln) maintain an epithelial phenotype, while

ATII cells cultured on provisional Fn matrices undergo EMT (29, 30). Although the exact mechanisms which stimulate the onset and progression of EMT are still unclear, it is under agreement that transforming growth factor beta (TGFβ) is a major player and a potent inducer of EMT (29-37). TGFβ must be activated in order to bind to its receptor(s), which can be performed through several different mechanisms including specific integrin binding, the presence of reactive oxygen species (ROS), proteolytic cleavage, and increases in pH (38-43). In addition, increased cell contractile forces can result in a mechanical activation of TGFβ. This increase in cell contractile events can be a result of biophysical changes of the matrix, such as increased tissue stiffness, or biochemical changes, such as the binding of αv integrin to the altered provisional Fn matrix (29, 44-46) .

Although it is known that both the biochemical and biophysical properties of the ECM have dramatic effects on cell phenotype and the progression of fibrotic pathologies, no studies to date have explored how cell phenotype is affected when several different dynamic remodeling events occur simultaneously. In addition, the presence and activation of TGFβ is a crucial factor shown to be upregulated from both changes in biochemical and biophysical nature of the ECM. However, these changes are certainly not the only factors which can induce TGFβ activation; notably, studies have shown that increased ROS can lead to the activation of TGFβ (39, 47-51). This is of particular interest in the initiation and progression of pulmonary diseases due to the continued exposure of the lung to insults of injury, including environmental particulate matter (PM). Previous studies have shown that particles generated from numerous different sources have to ability to cause or exacerbate lung disease and that the fibrogenic potential of

these particles is due to a combination of several factors including particle size, surface area, and composition (52-56). Smaller inhaled particles, under 10 microns, can reach the distal lung and have a higher potential to cause injury due to their high surface to mass ratio (57-59). These sized particles are of particular interest in the progression of pulmonary fibrosis due to their ability to reach into the alveoli and come in contact with the ATII cells. In addition, these particles are likely able to induce an inflammatory response in the lung and result in widespread secondary effects (59-61).

Although it is known that each of these factors is critical during pulmonary homeostasis and remodeling, there is little known about how dynamic changes to the ECM work together in controlling cell viability and phenotype. Furthermore, no studies to date have focused on how environmental injury adjuvants affect the lung during notable matrix remodeling events. The *overall objective* of this thesis was to characterize how the biophysical and biochemical nature of the ECM contribute to TGFβ activation and subsequently EMT, and how further exposure to injury adjuvants alters this response. Specifically, this work aims to explore how the altered cellular environment during the initiation and progression of pulmonary fibrosis affects future insults of lung injury. The *central hypothesis* of this work is that both increases in substrate rigidity and changes in integrin engagement work together to modulate cell contractility, TGFβ activation and subsequently EMT events, and that this process is exacerbated by exposure to environmental injury adjuvants. This dissertation explores the combined influence of substrate rigidity and integrin specific interactions with or without exposure to environmental injury adjuvants, on ATII cell contractility, TGFβ activation, and downstream EMT events. Integrin-specific recombinant fragments of Fn type III repeats,

specifically the 9th and 10th type III repeats (FnIII9'10), polyacrylamide gels of varying rigidity, and different concentrations of isolated PM were used to address this hypothesis through two specific aims: 1) Determine the integrated response of ATII cells to changing biochemical (integrin specific adhesion domains) and biophysical (matrix elasticity) microenvironment cues; and 2) Once the microenvironment has been established as dynamic, determine the consequence of additional injurious environmental adjuvants on ATII cell phenotype and modulation of EMT. This work will provide insight into the pathological progression of pulmonary fibrosis and may uncover potential targets for diagnostic tools or therapeutics.

Specific Aim 1: Determine the integrated response of ATII cells to changing biochemical (integrin specific adhesion domains) and biophysical (matrix elasticity) microenvironment cues

The hypothesis of this aim was that adhesive ligands that promote α3, but not αv, integrin engagement will inhibit epithelial cell contraction in response to higher matrix elastic moduli, TGFβ activation, and EMT events. Since α3 and α5 integrins are known to play a major role in wound healing while αv integrins are implicated in fibrotic progression, a model system of varying Fn fragments that preferentially bind either α3/α5 integrins or αv integrins was developed. The system was first validated by surface plasmon resonance (SPR), cell attachment, and cell spreading studies. In addition, increased matrix rigidity was modeled by creating polyacrylamide gels of increasing stiffness exhibiting elastic moduli indicative of either healthy or fibrotic tissues. ATII cells were cultured on the polyacrylamide gels of varying rigidities with each of the Fn

fragments crosslinked to the surface or Fn or Ln coated glass as controls. EMT was investigated through western blot and immunofluorescence analysis of various epithelial and mesenchymal markers. Cell contractility was investigated through analysis of stress fiber formation, and changes in cell phenotype in the presence of the contractility inhibitor, Y-27632. Lastly, the role of TGFβ activation in response to changes in the biophysical and biochemical properties of the matrix was investigated by the mink lung epithelial cell assay.

Specific Aim 2: Once the microenvironment has been established as dynamic, determine the consequence of additional injurious environmental adjuvants on ATII cell phenotype and modulation of EMT

The hypothesis of this aim was that exposure of ATII cells to environmental fine particulate matter during altered biochemical and biophysical matrix conditions will increase TGFβ activation and exacerbate stiffness mediated EMT events. Fine particulate matter (PM2.5) was collected on Teflon filters from the Atlanta area and analyzed for major elemental composition. The total PM was isolated from the filters and serial dilutions were done to provide three different physiological concentrations indicative of high, medium, and low exposure levels. ATII cells were cultured on polyacrylamide gels of varying rigidities with Fn cross-linked to the surface or Fn or Ln coated glass as controls with or without each of the different levels of PM2.5 and analyzed for cell contractility, TGFβ activation, and EMT events. Additionally, ATII cells were cultured as described above, but with the FnIII9'10 fragments crosslinked to the polyacrylamide gels and TGF β activation analysis was compared. Finally, the presence and contribution of

reactive oxygen species was explored by an oxidation assay and TGFβ activation was measured in the presence and absence of antioxidants.

This body of work focuses on a highly significant unknown in the field of pulmonary repair, remodeling, and pathogenesis, by investigating the combined role of integrin specific binding, tissue rigidity, and environmental injury exposure in initiating and modulating EMT. Studies to date have focused on single changes to the matrix on ATII cell phenotypic differentiation; however, the pulmonary microenvironment is highly dynamic with many changes occurring simultaneously during pathogenesis. Therefore it is imperative to study how these dynamic changes work together in the control of pulmonary cell phenotype. Specifically, this study focuses on the role of increases in tissue rigidity, over a range of tissue stiffnesses observed in pulmonary fibrosis *in-vivo*, in conjunction with a model of integrin binding that utilizes domains characteristic of either healthy or fibrotic lung in exploring ATII cell phenotypic differentiation. Additionally, no studies to date have explored how these dynamic changes of the microenvironment are altered in response to additional insults of injury. This is highly significant because several other epithelial tissues, such as skin, can be isolated from further injury during the repair process, whereas the lung is continually exposed to insults of injury. Understanding how these processes interact with one another to control alveolar cell phenotype will provide insight into how the biochemical and biophysical properties of the matrix contribute to the pathological process of pulmonary fibrosis, and how these conditions alter the normal repair process of the lung in response to injury, which could uncover new potential targets for therapeutics targeted towards halting the progression of the disease. This work illustrates the importance of both the biochemical and biophysical

properties and signals from the ECM in the pathological progression of EMT. Notably, this work shows for the first time that there is a fine balance between the biophysical and biochemical properties of the matrix in regulating EMT**.** Furthermore, this delicate balance can be shifted by additional insults of injury characteristic of normal pollutant exposure. Current therapeutics for fibrotic diseases widely focus on treating the cells, but this work suggests that 1) the state of the matrix based on disease progression must be considered, and that 2) combinatorial approaches that control TGFβ activation through fine control the matrix properties and decreasing oxidative stress may be an improved approach in the development of effective therapeutics for pulmonary fibrosis.

CHAPTER 2

BACKGROUND

Epithelial to Mesenchymal Transition in Lung Fibrosis

Fibrotic pathologies are characterized by excessive ECM production, interstitial scar tissue formation, and an increase in tissue stiffness. During the course of idiopathic pulmonary fibrosis (IPF), functional lung tissue of the alveoli is replaced with collagen-rich ECM, leading to rapid and severe decreases in lung compliance and irreversible loss of lung function (62, 63). IPF is a currently untreatable and ultimately fatal condition with 3 and 5 year mortality rates of 50% and 80%, respectively (5). In addition to formation of scar tissue, another hallmark of IPF and other fibrotic conditions is the influx of extremely contractile myofibroblasts. The influx of myofibroblasts further perpetuates the disease through persistent matrix production and contraction, contributing to increased cytokine activation. Lack of effective treatment options for this disease, and many other fibrotic diseases is largely due to lack of understanding of the exact mechanisms initiating fibrosis, however many studies implicate alveolar epithelial to mesenchymal transitions (EMT) in the onset and progression of fibrosis (30, 32, 36, 64-66). EMT has been theorized to increase the number of ECM secreting mesenchymal cells, and several cell tracking studies have demonstrated that a considerable number of myofibroblasts directly arise from the process of EMT (30, 36, 64, 66, 67).

EMT is the de-differentiation of an epithelial cell into a mesenchymal cell, and is defined through the loss of apical-basolateral polarity, loss of tight cell junctions, and a marked down-regulation of e-cadherin. These changes are accompanied by a concomitant

up-regulation of α -smooth muscle actin (α-SMA), increased stress fiber formation and alignment, increased migration through filopodia and lamellopodia formation, and an increased synthesis of ECM. EMT is very important during normal cellular processes in wound healing, embryogenesis, and development, contributing to wound-closure, blastocyst implantation, gastrulation, generation of the neural crest, and palate closure (68-70). Though EMT is an important cellular transition, if not tightly regulated, EMT can lead to dysregulated wound healing and scar tissue formation in mature tissues, contributing to pathological conditions such as pulmonary fibrosis.

EMT has been shown to occur in response to several factors such as growth factors including transforming growth factor beta (TGFβ), tumor necrosis factor alpha (TNFα), epidermal growth factor (EGF), and reactive oxygen species, as well as in response to extracellular matrix proteins including fibronectin (Fn) (35, 71-74). The role of TGFβ is by far the most well defined of all these factors, and is known to be a potent inducer of EMT. TGFβ signaling is quite complex and can activate a number of different pathways, including SMAD-dependent and independent pathways (75-77). SMAD dependent signaling can lead to Snail1 activation, which plays a role in EMT by down regulating e- cadherin expression and up regulating a number of mesenchymal genes including α-SMA (78-80). Though many advances have been made in understanding factors contributing to EMT, the precise events leading to the initiation of EMT as well as how multiple regulators drive or inhibit the process are still unclear. This dissertation focuses on the role of dynamic changes of the biochemical and biophysical properties of extracellular matrix microenvironment and how these changes regulate cues involved in the onset and progression of EMT on ATII cells.

Pulmonary Homeostasis and Repair

Pulmonary remodeling and repair involves a similar process of any epithelial barrier, which includes the proliferation, migration, and differentiation of epithelial cells into the site of injury in response to provisional ECMs. Specifically, in pulmonary tissue, the underlying vasculature is damaged and results in the initiation of the clotting cascade and the creation of a fibrin rich intermediate ECM with areas of cross-linked fibronectin. This provisional matrix is eventually degraded by invading mesenchymal fibroblasts, and then replaced with an intermediate fibronectin rich ECM (81). Alveolar epithelial cells then interact with this Fn-rich intermediate ECM, through a range of different ECM-binding receptors, i.e. integrins. In humans, the program regulating pulmonary homeostasis is altered in most pulmonary disease states following injury to the mature lung. After injury, the lung epithelium may either activate the necessary repair and regeneration pathways as described above for repopulation of the damaged or lost epithelial cells, or may undergo an aberrant remodeling and differentiation process, which represents the common pathway for many different types of pulmonary diseases including emphysema, COPD, and idiopathic interstitial pneumonia. Each of these diseases involves defective epithelial-mesenchymal interactions, which lead to dysfunctional wound healing and ultimately result in abnormal lung remodeling. The events in the pathogenesis of lung disease can be divided into three main phases illustrated in **Figure 2.1:** 1) initiation, resulting from intrinsic and/or extrinsic events that cause damage to the epithelium; 2) amplification, mediated in part by the inflammatory response; and 3) the response stage, where epithelial cells make a decision to either properly repair through activation of proliferative and differentiation programs or

reprogram to a dysfunctional differentiation state. This is the critical point where either successful healthy repair occurs, or abnormal repair results in the production of a fibrotic scar (82). These processes suggest a central role for the alveolar epithelium in disease progression where chronic injury results in remodeling similar to abnormal wound repair.

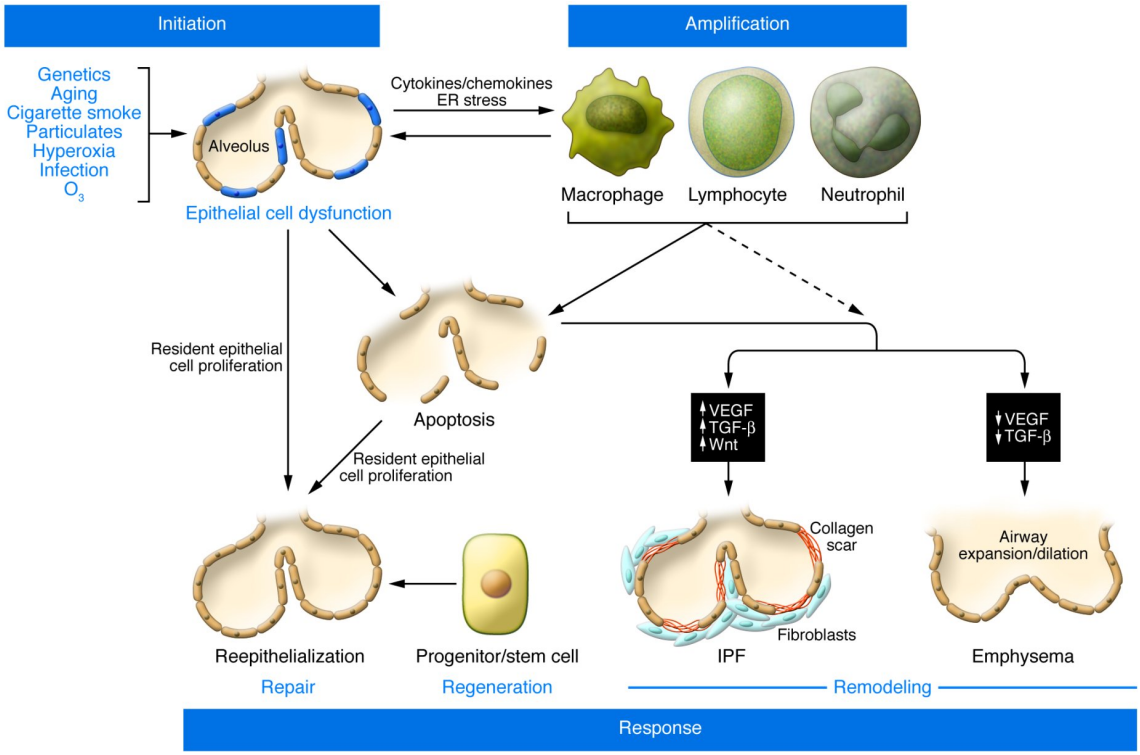

Figure 2.1 The epithelial-mesenchymal wound model for lung injury, repair, and regeneration. In the initiation stage, different microinjuries damage and activate alveolar epithelial cells. In the amplification stage, activating signals in AEC cells can promote release of chemokines/cytokines, promoting migration of inflammatory effector cells into the distal lung. Persistent activation can result in apoptosis. In the response stage, repair is attempted using local proliferation and transdifferentiation of ATII cells. In the absence of successful repair or regeneration, remodeling is initiated. In a fibrotic phenotype (e.g., IPF), the local signals (including high TGF-β levels) promotes proliferation of fibroblasts, activation of myofibroblasts, increases in basement membrane disruption, with resulting formation of a scar (82).

TGFβ Activation and Signaling in Pulmonary Repair

The TGFβ super family consists of a wide range of proteins that are able to regulate many different physiological processes including embryonic development, homeostasis, wound healing, and cell migration. Cytokines of the TGFβ superfamily are dimeric proteins with conserved structures. TGFβ1, 2, and 3 are the prototype of the TGFβ superfamily and inhibit proliferation in most cells and can induce apoptosis of epithelial cells (34, 43). In addition, these cytokines stimulate mesenchymal cells to proliferate and produce ECM and induce a fibrotic response in various tissues in vivo. Specifically, TGFβ1 has been shown to play a critical role in the onset and progression of EMT in pulmonary tissues. Since TGFβ1 is a potent inducer of EMT and many other cellular processes, its presentation needs to be tightly controlled. TGFβ1 exists in an inactive form which must be activated in order to bind to its receptor. When TGFβ1 is in its inactive form it forms a complex with the latency associated peptide (LAP), named the small latent complex. The small latent complex then proceeds to form a large latent complex by binding the latent TGFβ binding protein, which allows immobilization of the inactive TGFβ in the ECM (83-85). The latent complex of TGFβ is able to be activated in the lung through two major possible events. First, activation can occur through integrin mediated binding, specifically through binding of the latency-associated protein complex to integrin αvβ6 or αvβ8 via RGD sequences (40, 86, 87). Cell contractile forces are applied to the integrin-LAP complex and result in a separation of the LAP complex away from TGFβ. This allows for either release of the active growth factor in a soluble form (αvβ8 engagement) or exposure of it to neighboring cells (αvβ6 engagement) (45, 46). Second, activation has been proposed to occur through a similar release process of TGFβ

bound within the ECM via the large latent complex (88). Both processes of TGFβ activation have been shown to be directly related to biochemical and biophysical changes in the extracellular environment, which change integrin expression and induce cell contractility. These changes in the environment can then further regulate additional activation or inhibition of TGFβ. This dissertation specifically focuses on how dynamic changes to both the biochemical and biophysical properties of the ECM commonly associated with pulmonary fibrosis work together to control TGFβ activation and signaling.

Inflammation and Pulmonary Fibrosis

A complex set of reactions must occur for the formation and accumulation of fibrous tissue seen in pulmonary fibrosis. Recent evidence has suggested that the pathogenesis of pulmonary fibrosis may begin as an inflammatory response to injury when immune cells are excessively or improperly activated. These immune cells release toxic mediators that compromise epithelial integrity and promote further tissue injury (5, 62, 63, 66, 89). The repair process involves recruitment of mesenchymal cells, which lay down extracellular matrix, re-epithelialization, and restoration of normal lung structure. However, aberrant tissue remodeling can occur which results in excessive matrix deposition leading to pulmonary fibrosis. Although minimally studied, the inhalation of particles that are unable to be cleared from the lungs, may cause a sustained inflammatory response that can lead to abnormal tissue remodeling. This tissue remodeling may be involved in the initiation and progression of pulmonary disease such as pulmonary fibrosis (90).

Particles generated from numerous sources have the ability to cause or exacerbate lung diseases including asthma, bronchitis, and COPD (89, 91, 92). Fibrotic responses are seen in each of these diseases and involve increases in the deposition of extracellular matrix by pulmonary fibroblasts. The fibrogenic potential of these particles has been shown to be due to several factors including particle size, surface area, and composition. Smaller inhaled particles in the 1 to 10 micron range can reach the distal lung, and have a higher potential to cause injury due to their high surface to mass ratio (89, 93-95). In addition, particle composition is likely an important determinant of the effect of the particles on the progression of fibrotic diseases. Both organic and inorganic agents, such as transition metals, hydrocarbons, and endotoxins can contribute to the composition of particles (94, 96, 97). Previous studies have found that many of the components of the particles are able to activate the inflammatory response leading to widespread secondary effects. For example, several air pollution sources have been shown to stimulate the release of TNFα. Although TNFα does not directly promote fibroblast growth or the deposition of ECM proteins, it is able to stimulate the production of TGFβ, a major inducer of EMT that leads to the presence of myofibroblasts and subsequent ECM deposition commonly seen in pulmonary fibrosis (95, 98-100).

Reactive Oxygen Species and TGFβ Activation

Reactive oxygen species (ROS) are small oxygen containing molecules that contain a single high-energy electron, giving the molecule strong reactivity and contributing to cell signaling pathways and cellular immune defense (101-104). The most common ROS are superoxide anions $O2^-$, hydrogen peroxide, and hydroxide radical, HO' (102, 103). ROS can be created and used to signal the presence of acute cellular injury

and influence cell function by the activation of TGFβ. Of particular interest in the onset and progression of pulmonary fibrosis is that hydroxyl radicals can activate TGFβ by direct oxidation of methionine-253 within the LAP peptide. These redox reactions cause a rapid conformational change in the LAP, which allows for the rapid release of the homodimer. Other isoforms of TGFβ cannot be directly activated by ROS, which makes TGFβ1 an interesting sensor of extracellular oxidative stress (39, 48, 50, 51).

$O2^-$ has been implicated in the progression of pulmonary fibrosis. $O2^-$ radicals have been found to be elevated in the blood of IPF patients, suggesting a deficiency in glutathione regulation (51). $O2^-$ is able to enter cells through chloride ion receptors in lung fibroblasts and leads to the release of active TGFβ and increased collagen and fibronectin expression. Interestingly, excessive $O2^-$ is known to breakdown into hydroxyl radicals, which can activate TGFβ directly in the ECM (105). Interestingly, hydrogen peroxide produced by IPF fibroblasts in response to TGFβ signal to alveolar epithelial cells to induce apoptosis, which may be an important link to the progression of pulmonary fibrosis. Furthermore TGFβ enhanced production of ROS is thought to cause a further activation of more TGFβ residing in the tissue by directly activating methionine-253. This suggests that this redox sensing system of TGFβ causes a positive feedback loop resulting in chronic fibrosis (47, 48, 105).

Approaches targeting ROS, such as treating with high doses of the antioxidant N-acetyl-cysteine (NAC) have significantly delayed the progression of pulmonary fibrosis but do not result in improvements in lung function (93). These outcomes indicate that although oxidative stress in the lung is a contributor to the progression of pulmonary fibrosis, it is likely that other modes of TGFβ activation contribute to drive fibrogenesis.

Alveolar Type II Epithelial (ATII) Cells

Adult pulmonary tissue is composed of over 40 different cell types and possesses over 300 million alveoli, the primary functional structure of lung. Two primary epithelial cells populate the alveolus, Type I and II alveolar epithelial cells (ATI and ATII). ATI cells, separated from capillaries by only a thin basement membrane, are the primary gas-exchange cells and comprise 90% of the alveolar surface yet only 10% of the epithelial cell number (106, 107). ATII cells are pseudo-cuboidal, multifunctional cells that are considered the "protector of the alveolus" due to their central role in defense and repair. ATII cells act as the primary surfactant-secreting cell, precursors to ATI cells, and in many instances as non- professional antigen-presenting cells (107). ATII cells also contribute significantly to the fluid balance across the epithelial barrier through sodium transport functions(108). These various functions underscore the vital importance of these cells in maintaining pulmonary function. The importance of ATII cells in alveolar repair and regeneration is further supported by animal models that show that, in bleomycin induced lung injury, intratracheal delivery of a purified population of ATII cells is sufficient to block fibrotic lung remodeling. During normal repair, ATII cells are thought to proliferate, migrate onto a provisional matrix and differentiate into ATI cells. Despite their obvious beneficial effects, evidence has suggested that perturbation or repeated injury of ATII cells may result in several undesirable outcomes such as increased apoptosis and trasnsdifferentiation to a contractile myofibroblastic phenotype resulting in the onset and progression of pathologies such as pulmonary fibrotic disorders **(Figure 2.2)** (106, 109-111).

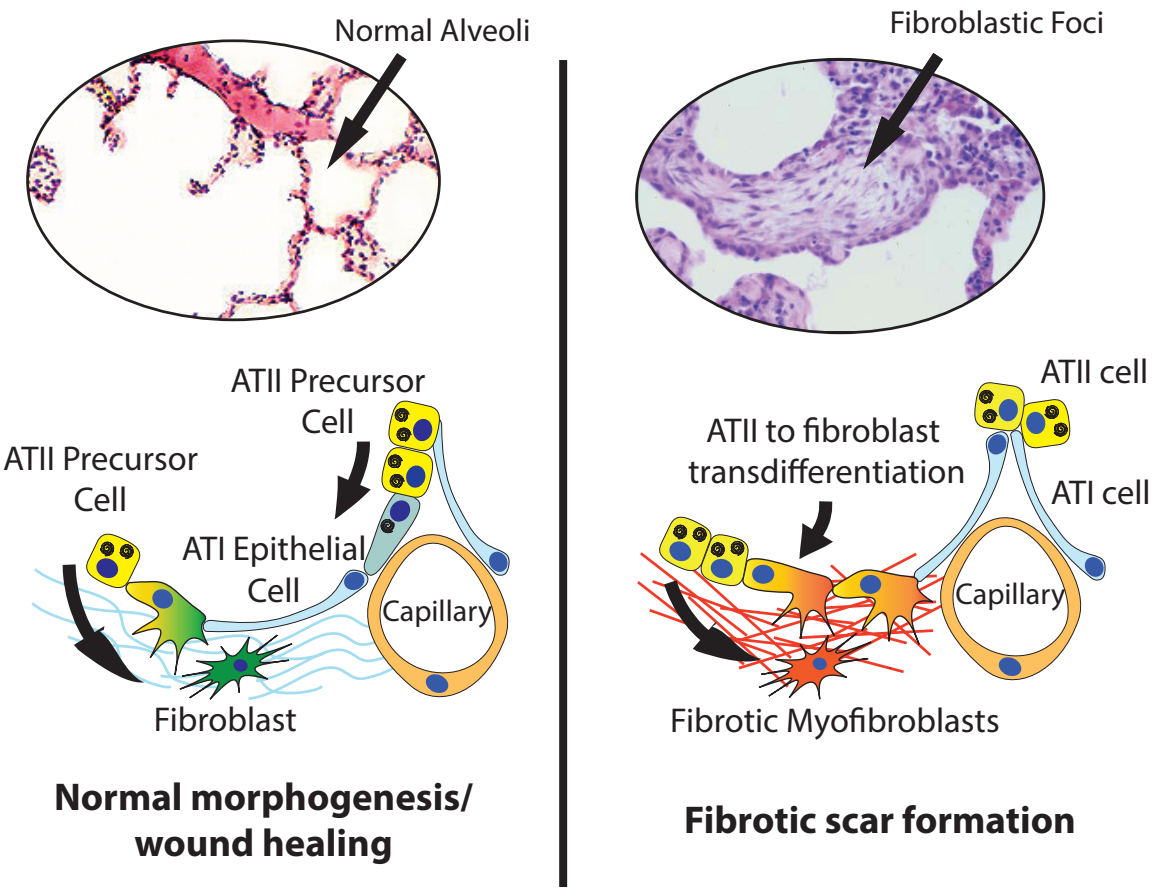

Figure 2.2 Healthy epithelial pulmonary morphogenesis vs. formation of fibrotic tissue. During healthy morphogenesis and repair, ATII precursor cells differentiate into, and repopulate ATI cells, fibroblasts repair damaged matrix, and then apoptose, returning the environment to a homeostatic state. In dysregulated wound healing, ATII cells transdifferentiate into contractile myofibroblasts that secrete excess matrix leading to increased tissue stiffness and the formation of a fibrotic scar.

ATII Cell Integrins

ATII cells are known to express a wide variety of integrins. There are several major integrin pairs expressed in healthy adult ATII cells including α2β1, α3β1, α6β4, α9β1, αvβ5, αvβ6, and αvβ8. In addition, α5β1 integrin expression is rapidly increased in response to pulmonary injury, and is therefore critical in wound healing responses (112). Each of these integrins are known to have critical roles in pulmonary epithelial homeostasis, repair, and pathologic responses, including the maintenance of epithelial integrity and phenotype (α3β1) (112), regulating wound healing (α5β1) (19), and activation of the critical EMT mediator, TGF-β (αvβ6 and αvβ8) (17, 29, 40).

Many studies have stressed the importance of α3β1 integrin in the maintenance of alveolar epithelial integrity. α3β1 integrin expression has regularly been shown to be decreased in patients with cancer metastasis and is associated with a more malignant phenotype (113). Furthermore, a reduction in α3β1 has also been shown in response to TGF β, highly implicating it in the progression of EMT in the lung (114). Typically, integrin α3β1 binds laminin as its ligand (112, 115). However, integrin α3β1 has also been shown to have the ability to bind other ECM ligands such as collagen and fibronectin (116-118). Fibronectin is a provisional matrix protein and is of interest because it has the ability to bind many of the integrins that are expressed by ATII cells including α3β1, αvβ3, αvβ6, as well as α5β1 during injury (19, 116, 118, 119). The binding of α3β1 of Fn has been shown to occur in an RGD dependent manner (119). In addition, its binding to Fn can be affected by the presence of α5β1 integrin, notably that cells that express comparable levels α3β1 and α5β1 have significantly decreased binding of α3β1 (19). This is of particular interest because α5β1 is only expressed in response to

injury, indicating that α3β1 likely binds Fn with great affinity under normal, healthy conditions. Integrin blocking studies have indicated that α5β1 is the main Fn receptor during wound healing, but that α3 blocking antibodies also resulted in significantly decreased wound repair (19). These studies highlight that ATII cells have competitive binding of these different integrins and that differential binding of these integrins is a major factor that drives cell phenotype leading to healthy repair or pathological EMT events that result in fibrosis. This work specifically utilizes this fact to create a model system where ATII cells will preferentially bind α3/α5 integrins versus αv integrins.

Biochemical Cues: Fibronectin

Fibronectin is a soluble dimeric glycoprotein that is composed of two 230-270 kDa monomers that are linked together covalently by a pair of disulfide bonds 47 56. Each of the monomers consists of three repeating modules, names type I, type II, and type III. These modules contain functional domains that are able to mediate interactions with cell surface receptors, other ECM components, and Fn itself (116). The type I and type II repeats are structurally stabilized by two intra-chain disulfide bonds in each repeat. Interestingly, the type III repeats have no disulfide bonds subjecting them to be highly sensitive to force-mediated unfolding.

The protein fibronectin is of particular interest in the initiation and progression of fibrotic diseases due to its capacity to bind multiple different integrins and initiate many different intracellular signals that drive cell phenotype and ultimately the state of the tissue. The most studied integrin recognition sequence is the RGD (Arg-Gly-Asp) site, which is located on the 10^{th} type III repeat. The recognition of this site is very complex and depends of many factors including its three dimensional presentation. For example,

binding to RGD along with a second recognition sequence, the synergy site (PHSRN), in the adjacent 9th type III repeat is known to promote α5β1 integrin binding to Fn, highlighting the importance of these sites in homeostasis vs. wound healing (120-122).

As previously mentioned these type III repeats are subject to force-mediated unfolding, which can lead to changes in integrin engagement and subsequently cell phenotype. Due to this elasticity of the 9th and 10th type III repeats, many different conformations can arise, resulting in differential integrin specificity in the region (17). Of particular interest is the synergy site, which is located on the 9th type III repeat, only 32Å from the RGD site on the 10th type III repeat. In this folded conformation, the two sites act together to bind α5β1 integrin. However, when exposed to small forces from cells (<10 pN) the 10th type III repeat is separated away from the 9th type III repeat. When this occurs the distance between these two binding domains are separated by an additional 20Å (from 32Å to 55Å). This additional separation results in a lack of ability for both sites to co-bind a single receptor, and studies have shown that this increased separation results in significantly decreased α5β1 integrin binding (123). This is of particular interest because it suggests that α5β1 binding can be inhibited by changing the conformation of these sites of Fn. In addition, several studies have shown that increasing the stability of the 9th and 10th type III repeats modulates integrin accessibility of the RGD site. For example, a Leu to Pro point mutation at amino acid 1408, within the 9th type III repeat results in increased affinity for α3β1 and α5β1 integrins over αvβ3 integrins (124, 125). Numerous studies have highlighted the importance of integrin specificity on cell proliferation, differentiation, and ultimate fate. Some examples of this include the correlation of αv integrins with increased cell adhesion and proliferation (126, 127),

while the β1 subunit has been shown to enhance differentiation (128, 129). Therefore, it is clear that changes in the conformation of Fn in diseased state likely has a major impact on the integrin specificity with which cells bind, and therefore modulate cell phenotype.

Biophysical Cues: Mechanics in tissue homeostasis and repair

The composition of the extracellular matrix surrounding a cell has great consequences on cell fate; however, evidence is mounting that, in addition, cells sense and respond to the mechanical properties of the ECM, particularly the rigidity of the matrix. The process of cellular sensing of the underlying properties of the ECM has been termed mechanotransduction. Matrix rigidity has been shown to influence many aspects of cellular behavior including stem cell, myoblast, and breast epithelial cell differentiation; cellular motility; contractility; and focal adhesion formation, and it has also been shown to contribute or prevent a malignant phenotype (6, 7, 9-12, 130-132). Previous work has shown that stem cell differentiation can be guided by underlying matrix mechanics, with mesenchymal stem cells on hard substrates differentiating down an osteoblastic lineage and mesenchymal stem cells on soft substrates differentiating down a neuronal lineage, which suggests a potential mechanism through which stem cells "match" their differentiation based on the surrounding tissue (7). Interestingly, as previously described, changes in tissue rigidity, specifically an increase in rigidity and hardening of tissue, is associated with the pathological progression of fibrotic responses. Recent atomic force microscopy (AFM) analysis of fibrotic tissue from mice with bleomycin-induced pulmonary fibrosis shows a nine-fold increase in rigidity of fibrotic tissue compared to that of normal tissue (133).

Interestingly, it has recently been shown that mesenchymal cells respond to

substrate stiffness by engaging their action-myosin contractile machinery in a manner that facilitates cell-ECM compliance matching. This has been demonstrated by AFM analysis of single cell stiffness, showing fibroblasts become increasingly stiff on increasingly rigid substrates, indicating a cell may adjust its internal stress through contraction to "match" its external environment (131). As a consequence of this mechano-homeostasis between the cell and its ECM, cells in increasingly rigid, or stiff, environments display increased activation of contractile signals like Rho and Rho associated kinase (ROCK), resulting in multiple and diverse secondary effects. An elegant example of this is shown by Wipff *et. al.* who demonstrate that fibroblast activation of TGFβ increases on increasingly rigid substrates, leading to greater myofibroblast differentiation on stiff, but not compliant, substrates (45, 46). Because fibrotic diseases are characterized by increased tissue rigidity, and because of TGFβ's prominent role in the onset of EMT, we hypothesized that a similar mechanism of increased TGFβ activation with increasing rigidity would contribute to EMT on increasingly rigid substrates.

While the precise mechanism of cell rigidity sensing remains still remains unclear, it likely involves the transduction of stiffness-mediated signaling via increased cell contractility. This dissertation explores the role of mechanotransduction events in the onset and progression of EMT by studying the role of biophysical changes of the matrix such as substrate rigidity in Fn - mediated EMT. These studies provide insights into the role of mechanotransduction in altering the pulmonary microenvironment further and in the onset and progression of fibrotic pathologies.

CHAPTER 3

CHARACTERIZATION OF FIBRONECTIN 9-10 VARIANTS: DEVELOPMENT OF BIOCHEMICAL MODEL SYSTEM

Introduction

Cells interact with their surrounding ECM via transmembrane cell surface receptors, known as integrins. Integrins are heterodimeric proteins consisting of one α subunit and one β subunit, which are known to form at least 24 unique heterodimers (119). Integrin interactions with their extracellular matrix (ECM) ligands facilitate a host of cellular responses, including cell spreading, migration, proliferation, and differentiation, and can contribute to more orchestrated cellular events, such as development and wound healing, by contributing to epithelial to mesenchymal transitions (29, 134, 135). Integrin binding to ECM ligands occurs through specific binding sequences, the most notable of these sequences being Arg-Gly-Asp (RGD), which is found on a large number of ECM proteins, including fibronectin, laminin, and several others. (136) Furthermore, integrin heterodimers can interact with multiple ECM ligands and bind to multiple binding sequences (137, 138).

Fibronectin is a widely expressed extracellular matrix protein during epithelial tissue repair and regeneration and is known to bind at least 16 integrins. Biochemically, Fn exists as a soluble dimeric glycoprotein composed of two nearly identical 230-270 kDa monomers linked covalently near their C- termini by a pair of disulfide bonds (116, 139). Each monomeric subunit consists of three types of repeating modules, type I, II, and III. These modules comprise functional domains that mediate interactions with other

ECM components, cell surface receptors, and Fn itself (116). Whereas type I and II repeats are structurally stabilized with two intrachain disulfide bonds in each repeat, type III repeats have no disulfide bonds and, therefore, are highly sensitive to force-mediated unfolding, resulting in alterations of conformation of the molecule (16, 139, 140). This is of particular interest in pathological states where cells become more contractile and increase their force exerted on the underlying matrix. Interestingly, a large number of Fn-integrin interactions occur through the RGD site, which is located on the 10th type III repeat. The recognition of this simple tripeptide sequence can be quite complex and greatly depends on flanking residues, its three dimensional presentation, and individual features of the integrin-binding pockets. This is most well characterized in α5β1 integrin binding to Fn, in which RGD in combination with a second recognition sequence (PHSRN), the so-called "synergy" site, in the adjacent 9th type III repeat is known to promote the specific interaction of α5β1 integrin binding to Fn through interactions with the α5 subunit (120, 122). The synergy site is located approximately 32 Å from the RGD loop on the 10^{th} type III repeat. The type III repeats show great elasticity in the loops between their F- and G-β strands, known as the FG loop, which allows the 9^{th} and 10^{th} type III repeats to present multiple conformations. Under small applied forces (on the order of 10 pN) Fn's 10th type III repeat is susceptible to partial unfolding, resulting in an intermediate state in which the RGD loop within the 10^{th} type III repeats begins to translocate away from the 9^{th} type III repeat, resulting in an increase in the distance between the RGD and synergy sites from approximately 32 Å to approximately 55 Å (17). This capacity to present multiple spatial orientations of the 9^{th} and 10^{th} type III repeats has great implications on cell binding and subsequent cell phenotype because the

relative positioning of these two domains has been shown to influence integrin α5β1 binding. Integrin α5β1 binds by simultaneously engaging the RGD and synergy sites and is known to be highly involved in epithelial tissue repair. As these sites translocate away from one another, they can no longer be bound simultaneously, and integrin α5β1 no longer binds resulting in changes in the normal tissue repair process. These results suggest that the conformation of these two domains may be used to drive which integrins cells use to bind Fn. For example, by stabilizing the 9th type III repeat by a Leu-Pro mutation at amino acid 1408, there is an increased affinity for α5β1 over integrin αvβ3. Alternatively, by increasing the linker region between the RGD and synergy sites there is a reduction in α5β1 binding. Furthermore, α3β1 integrin binding to Fn, which is associated with epithelial cell homeostasis, may also be promoted by the 9th type III repeat (44). Using recombinant Fn fragments displaying the RGD and synergy sites with a stabilizing (L_{1408}-P) point mutation (FnIII9*10) or RGD alone (FnIII10), it was previously demonstrated that the presence of Fn's synergy site enhances epithelial cell integrin specificity; epithelial cell binding to FnIII9*10 was significantly inhibited by anti-α3 and anti-α5 antibodies ($p<0.01$), while their inhibition of cell binding to RGD only Fn fragments was negligible. Additionally, epithelial cells seeded on FnIII9*10, but not FnIII10, formed α3 and α5 integrin clusters.

Though the classical ligand for integrin α3β1 is laminin (Ln) (112, 115) it has been reported to bind collagen and Fn (116-118) and facilitate cell-cell interactions through both homophillic binding and binding to e-cadherin (141-143). Integrin α3β1 plays a critical role in maintaining epithelial integrity and facilitating wound repair responses, and, if not bound to its extracellular matrix ligands, it can contribute to

pathologies such as EMT (30, 113). Furthermore, αv integrin engagement has been shown to play a major role in the activation of TGF β and the onset and progression of EMT. These previous data indicate that stabilization of the synergy and RGD sites on the 9^{th} and 10^{th} type III repeats increases the specificity for α3 and α5 integrins which are associated with healthy tissue and proper repair and regeneration programs. Furthermore, these data suggest that separation of these two binding sequences will inhibit α3 and α5 integrins, and preferentially bind the ECM through αv integrins, which are associated with pathological pulmonary conditions.

Therefore, since integrin binding is highly dependent on the conformation and stability of the 9^{th} and 10^{th} type III repeats of Fn, a variety of recombinant FnIII9'10 variants were created that preferentially bind α3 and α5 integrins or αv integrins. These variants display i) a stabilization of the 9^{th} type III repeat by a Leu-Pro mutation at amino acid 1408 (9*10), ii) a dominant negative R-A mutation in the synergy site ($FnIII^{9p}10$), iii) a 2xG insertion in the linker region ($FnIII9^{2G}10$), or iv) a 4xG insertion in the linker region ($FnIII9^{4G}10$). It was hypothesized that these Fn fragments would display a graded loss of affinity for α3 and α5 integrins with increasing decoupling of RGD and synergy and display increasing affinity for αv integrins. First, surface plasmon resonance (SPR) was utilized to determine binding kinetics of integrin α3β1, α5β1, and αvβ3 to the Fn fragments. Next, cell attachment and cell spreading assays were performed to validate differences in cell phenotype based on the differences in integrin binding based on each of the Fn fragments.

Materials and Methods

Construction of mutant pGEX4T1-FnIII9-10 clones

Cloning of the wild type FnIII9-10 was performed as previously described. A Leu1408 to Pro mutation (FnIII9*10) was made using the pGEX4T-1-FN III9-10 plasmid as previously described (44, 125, 144). FnIII9*10 variants displaying i) a dominant negative R-A mutation in the synergy site (FnIII^{9P}10), ii) a 2xG insertion in the linker region (FnIII9^{2G}10), or iii) a 4xG insertion in the linker region (FnIII9^{4G}10) were then created using the QuikChange® II-E Site-Directed Mutagenesis Kit (Stratagene, La Jolla, CA). Sequences are presented in **Table 3.1**. All plasmids were introduced to and maintained in the electro-competent XL-1 Blue *E.coli* strain provided and cultured in LB + ampicillin plates at 37°C. Plasmids were extracted from cultures using the QIAquick Spin Miniprep Kit (QIAGEN, Valencia, CA) and verified via sequencing (Johns Hopkins Synthesis & Sequencing Facility, Baltimore, MD)

Table 3.1. FnIII9-10 variants produced and function

Fragment	Sequence 1373-1423 of FnIII9-10	Role
FnIII9*10	DRVPHSRNSITLTNLTPGTEYVVSIVALN GREESP**P**LIGQQSTVSDVRPD	Leu1408 to Pro; Stabilizes relative positions of FnIII9 and FnIII10
FnIII^{9P}10	DRVPHS**A**NSITLTNLTPGTEYVVSIVALN GREESP**P**LIGQQSTVSDVRPD	Arg to Ala point mutation in PHSRN site
FnIII^{2G}10	DRVPHSRNSITLTNLTPGTEYVVSIVALN GREESP**P**LIGQQSTVS**GG**DVRPD	Increased distance between FnIII9 and FnIII10
FnIII^{4G}10	DRVPHSRNSITLTNLTPGTEYVVSIVALN GREESP**P**LIGQQSTVS**GGGG**DVRPD	Increased distance between FnIII9 and FnIII10

Expression and purification of recombinant FnIII9-10 proteins

Recombinant Fn fragments were produced as previously described (44, 144). Briefly, the expression vectors described above were transformed into BL21 *E.coli*, cells were grown to the exponential growth phase and treated with IPTG for 3 hours. Cells were then lysed by the addition of 10mg/ml lyzozyme and sonication, followed by incubation with 1% triton X-100 and 10U/ml of DNAse I. Fn fragments were purified by GST affinity chromatography (AKTA Purifier, GE Healthcare, Piscataway, NJ, USA). GST tags were removed using bovine thrombin (Sigma–Aldrich, St. Louis, MO, USA). A second round of purification was performed using GST and serine protease affinity chromatography to remove cleaved GST tags and thrombin. Proteins were verified as >98% pure by SDS-PAGE.

Surface plasmon resonance studies

The Biacore 2000 (Biacore Lifesciences, GE Healthcare) was used to investigate kinetic binding constants (k_a and k_d) of Fn fragments variants for integrins α3β1, α5β1, and αvβ3. Briefly, integrins α3β1, α5β1, or αvβ3 (R&D Systems, Minneapolis, MN, USA) were covalently immobilized to gold-coated SPR sensor chips via self-assembled monolayer surface chemistry to generate a non-fouling surface with a controlled density of reactive carboxylic acid groups. Mixed self-assembled monolayers were generated on gold-coated chips as previously described (145, 146) by incubating with a 10:1 mixture of 1-mM of tri(ethylene glycol)–terminated alkanethiols (HS-(CH2)11–(OCH2CH2)3–OH (ProChimia, Gdansk, Poland) and carboxylic acid–terminated alkanethiols (HS-(CH2)11–(OCH2CH2)6–OCH2COOH) overnight. The sensor chip was then loaded into the Biacore 2000 and the carboxylic acid–terminated alkanethiol surfaces was activated

by flowing 200mM 1-ethyl-3-(3-dimethylaminopropyl) carbodiimide (Sigma-Aldrich) and 50mM N-hydroxysuccinimide (Sigma-Aldrich; 5μL/minute for 10 minutes). Immediately after activation, α3β1, α5β1, or αvβ3 integrins (100μg/ml) were immobilized at a flow rate of 5μL/minute for 10 minutes to achieve approximately 1500 resonance units (1 resonance unit ~ 1 pg/mm2). An additional channel was immobilized with BSA to serve as a reference channel; BSA (100ug/ml) was immobilized to achieve approximately 1500 resonance units. Immobilization of integrins and BSA were performed in 0.1M sodium acetate, pH4.5. Unreacted N-hydroxysuccinimide groups were quenched in all flow cells with 1M ethanolamine, pH 8.5 (10 μL/minute for 10 minutes). Upon stabilization of the baseline signal, kinetic binding experiments were run in duplicate with Fn fragments, full length Fn, or Ln as the flow analytes. Various concentrations for each Fn fragment (10μM-1nM) were flowed at 30μL/minute for 5 minutes immediately followed by a 10-minute dissociation phase. Binding experiments were performed in 10mM HEPES, 150mM NaCl, 0.0001% Triton-X 100, and 2mM each $MgCl_2$ and $MnCl_2$, pH 7.4.

SPR analysis and evaluation

SPR sensorgrams were analyzed with the aid of Scrubber 2 and ClampXP software (Center for Biomolecular Interactions Analysis, University of Utah). (147-149) Reference cell responses were subtracted from corresponding active response curves. Double-referenced curves were acquired by further subtracting the reference cell blank buffer injections from each reference-subtracted response curve. (150) The resulting curves were then analyzed and fitted to the kinetic model. Kinetic modeling and simulations were performed with ClampXP software; globally fitted parameters were determined for

each kinetic dataset per Fn fragment. Equilibrium binding constants were calculated from fitted kinetic constants. Goodness of fit for each model was determined by evaluating the residual plots and residual sum of squares.

Cell spreading and α3β1 integrin binding

In order to determine the role of Fn fragments in epithelial cell spreading, RLE-6TN cells were cultured on FnIII9*10 (2μM), FnIII^{9P}10 (2μM), FnIII9^{2G}10 (2μM), FnIII9^{4G}10 (2μM), Fn (0.1μM), or Ln (0.1μM) coated, hd-BSA blocked coverslips in serum-free DMEM/F12 media for 3 hours and fixed with 4% formaldehyde. The concentration of Fn was chosen based on previous studies showing similar binding of an antibody specific to the 7-10 type III repeats of Fn (clone HFN7.1a1) (144) to Fn coated at 0.1μM and the Fn fragments at 2μM concentrations. The concentration of Ln was chosen based on ELISAs showing saturation of the surface using 0.1μM. Cells were washed with PBS, fixed with 4% formaldehyde, permeabilized with 0.2% Triton-X 100 and then blocked with 10% goat serum. Integrin α3 (Ralph 3.2) antibodies were incubated overnight at 4°C then washed thoroughly with PBS + 0.2% Tween-20. Secondary antibodies (Alexa-Fluor-488 goat-anti-mouse, Invitrogen; FITC-conjugated goat anti-Armenian hamster, Santa-Cruz Biotech) were incubated for 1 hour then washed thoroughly with PBS + 0.2% Tween-20. Actin was stained with Texas-red phalloidin (Invitrogen) and nuclei were stained with Hoescht stain (Invitrogen). Coverslips were mounted and images acquired with a Nikon Eclipse (TiE) inverted fluorescence microscope at 100X magnification (PlanApo 100X, 1.4 NA oil-immersion objective) with a CoolSNAP HQ2 Monochromatic CCD camera. Representative images are presented.

Area and perimeter of individual cells was determined for each condition using Image J (NIH Freeware) image processing software, and circularity was determined using the equation circularity = $4\pi(\text{area}/\text{perimeter}^2)$. Three independent images were analyzed for each condition, and at least 10 cells were analyzed per image. Data is pooled from all 3 images analyzed per condition. Statistical analysis was performed by multi-variate ANOVA using Prism (Graphpad Software Inc., La Jolla, CA, USA). Statistical significance was achieved for $p<0.05$.

Cell attachment assays

Wells of a 96 well plate were coated with each of the purified Fn fragments, Fn, or Ln overnight at 4°C then blocked with heat denatured BSA. RLE-6TN cells were incubated in microcentrifuge tubes at a concentration of $3x10^6$ cells/ ml in DMEM media with or without the addition of α3, α5, or αv antibodies or combinations of the three for 30 minutes at 37°C. In order to determine 100% attachment, RLE-6TN cells were plated on poly-L-lysine coated tissue culture plastic wells. Cells with or without the addition of antibodies were then plated on each of the Fn fragment, Fn, or Ln coated wells for 30 min, then all control and treated wells were fixed with 5% gluteraldehyde, and stained with 0.1% crystal violet stain. The dye was solubilized in 10% acetic acid and absorbance measured on a Biotek Synergy H4 Multi-Mode Plate Reader. Results are pooled from three independent triplicate experiments and presented as percent of 100% attachment.

Results

Fitted α3β1 binding affinity parameters

SPR with soluble recombinant integrin immobilized to the surface of the sensor chip was utilized to determine the role of FnIII9-10 in integrin α3β1 interactions with Fn. (**Figure 3.1**)

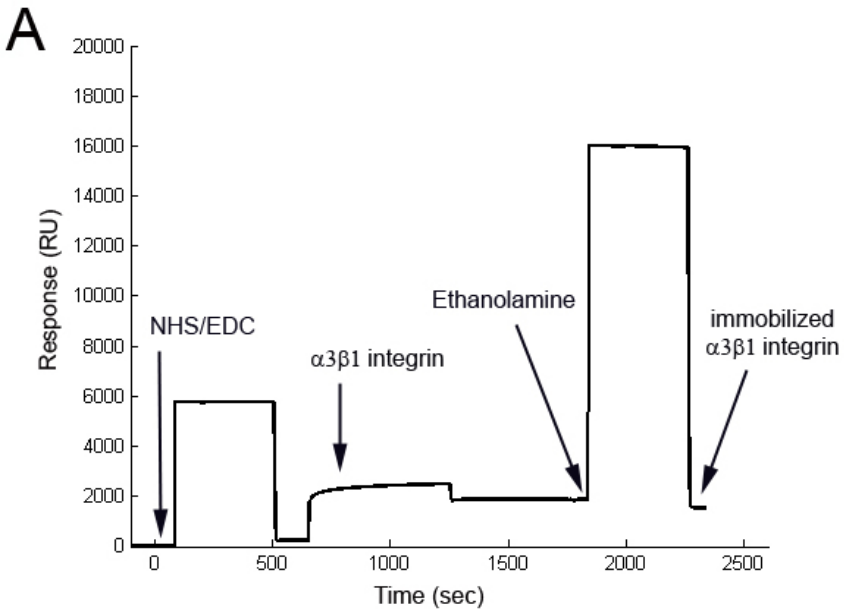

Figure 3.1: Integrin immobilization: To analyze integrin binding to FnIII9-10 variants, recombinant soluble integrin was immobilized onto a Biacore sensor chip to achieve approximately 1500 resonance units.

Response curves obtained from all FnIII9-10 variants binding to integrin α3β1 were fit to both a 1:1 Langmuir binding model. The fitted parameters k_a ("on rate") and $k_{d,}$ ("off rate"), calculated Kd and residual sum of squares of the fit of each FnIII9-10 variant, Fn, and Ln using a Langmuir 1:1 model are displayed in **Table 3.2 and Figure 3.2**.

Table 3.2: K_d values: α3β1: Langmuir 1:1 model

Analyte	k_a*10^{-4}	k_d*10^4	$Kd*10^9$	RSS
FnIII9*10	4.3+/- 0.3	7.1+/- 0.29	**32**	1.7
$FnIII^{9P}10$	0.49+/- 0.44	59+/- 8.4	**172**	2.56
$FnIII^{2G}10$	1.12+/- 1.12	10.8+/- 5.2	**97**	2.52
$FnIII^{4G}10$	0.311+/- 0.19	27.5+/- 1.7	**855**	5.85
Fn	1.0+/- 0.81	2.5+/- 0.9	**24**	2.5
Ln	3.47+/- 1.8	4.87+/- 2.46	**14**	0.223

Comparing k_d values obtained from the model, FnIII9*10 was found to have the lowest k_d of all FnIII9*10 variants analyzed at 7.1 x 10^{-4} s^{-1}. Increasing the linker region between the 9th and 10th type III repeats with either 2 Gly residues or 4 Gly residues resulted in an increase in the k_d to 10.8 x 10^{-4} s^{-1} and 27.5 x 10^{-4} s^{-1}, respectively, indicating that increasing the space between the PHSRN and RGD sites disrupts the interactions between FnIII9-10 domains and integrin α3β1. Furthermore, an Arg to Ala point mutation within the PHSRN site results in an eight-fold increase in k_d to 59 x 10^{-4} s^{-1}. Equilibrium dissociation constants, which take k_d and k_a values into account, were calculated for each analyte. FnIII9'10 was found to have the lowest K_d, 32nM. Direct disruption in the PHSRN site resulted in a fivefold increase in K_d to 172nM, while increasing the spacing between the 9th and 10th type III repeats by either 2 or 4 Gly residues resulted in a three and 26-fold increase to 97nM and 855nM, respectively. The K_d value for Ln was the lowest for all analytes, 14nM, which was expected, as Ln is thought of as the dominant ligand for integrin α3β1; however, Fn was found to have a high affinity for the integrin, with a K_d of 24nM. These results indicate that Fn does bind

integrin α3β1 with a high affinity, and this binding is dependent on the positioning and spatial orientation of the PHSRN and RGD sites.

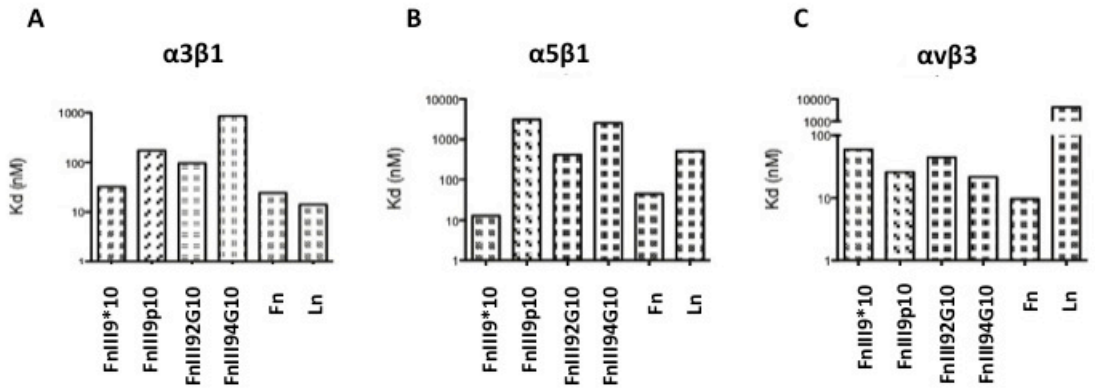

Figure 3.2: FnIII9-10 variants bound to α3β1, α5β1, and αvβ3. Calculated Kd values for FnIII9-10 variants, Fn, and Ln interactions with immobilized α3β1 integrin (A), α5β1 integrin (B), or αvβ3 integrin (C) were determined using a Langmuir 1:1 model.

K_d values for integrins α5β1

The role of the PHSRN site, as well as the relative orientation with respect to the RGD site, is known to be critical for α5β1 binding to Fn, while binding to αvβ3 only requires the RGD site. To confirm these previous reports, binding of FnIII9*10, FnIII^{9p}10, FnIII9^{2G}10, FnIII9^{4G}10, Fn, and Ln to immobilized integrin α5β1 and αvβ3 was investigated. Curves were fit to a simple Langmuir 1:1 model. Calculated K_d values are shown in **Figure 3.2**. As expected, α5β1 binding was found to depend on the presence and spatial orientation of the PHSRN site. Equilibrium dissociation constants were calculated for each analyte, and FnIII9*10 was found to have the lowest K_d of all

FnIII9'10 variants, with a value of 12.9 nM. FnIII^{9p}10, FnIII9^{2G}10 , FnIII9^{4G}10 were found to have K_d values of 3100 nM, 417 nM, and 2530 nM, respectively. Fn and Ln were found to have K_d values of 44 nM and 519 nM, respectively. Though Ln is not typically regarded as a ligand for α5β1, there have been previous reports demonstrating interactions between these molecules. (151)

K_d values for integrins αvβ3

Evaluation of FnIII9*10 binding to integrin αvβ3 was not dependent on the presence or spatial orientation of the PHSRN site, which was expected as αvβ3 interactions occur through the RGD site alone. Equilibrium dissociation constants were calculated for each analyte, and K_d values were within the same range for all FnIII9*10 variants **(Figure 3.2).** FnIII9*10, FnIII^{9P}10, FnIII9^{2G}10, and FnIII9^{4G}10 were found to have K_d values of 59.6 nM, 25.9 nM, 44.5 nM, and 21.5nM, respectively. Though all values were comparable, minor differences in binding were observed, and, interestingly, an opposite trend from α5β1 binding was observed, such that affinity for FnIII9*10 < FnIII9^{2G}10 < FnIII^{9P}10 < FnIII9^{4G}10. Fn was found to have a K_d value of 9.59 nM, while only minimal binding was observed to Ln.

Epithelial cell spreading on FnIII9-10 variants

To characterize α3β1 binding to FnIII9*10 variants in a cell system and subsequent changes in cell spreading, RLE-6TN cells, an alveolar epithelial cell line, were cultured on Fn fragments, Fn, and Ln for a period of 3 hours and then stained for integrin subunits α3 and actin. This cell type highly expresses α3β1 and also expresses α5β1 and several αv integrins. Cells cultured on Ln and FnIII9*10 displayed staining for α3, while cells cultured on Fn and all other FnIII9-10 variants displayed minimal staining

for α3 integrins (**Figure 3.3**). Cells cultured on FnIII9*10 displayed a rounded, cuboidal morphology and diffuse staining for actin, which was similar to cellular responses on Ln. Cells cultured on Fn and all other FnIII9-10 variants displayed were more spread and began to display aligned actin filaments. Cell shape was further characterized through analysis of circularity, with values closer to 1 indicating a more rounded cell. Cells cultured on FnIII9*10 exhibited a circularity value of 0.79, which was similar to cells cultured on Ln, with a circularity value of 0.73. Cells cultured on Fn and all other FnIII9-10 variants were found to have significantly lower circularity values compared to cells cultured on FnIII9*10 and Ln ($p < 0.001$), with values ranging from 0.65 to 0.61.

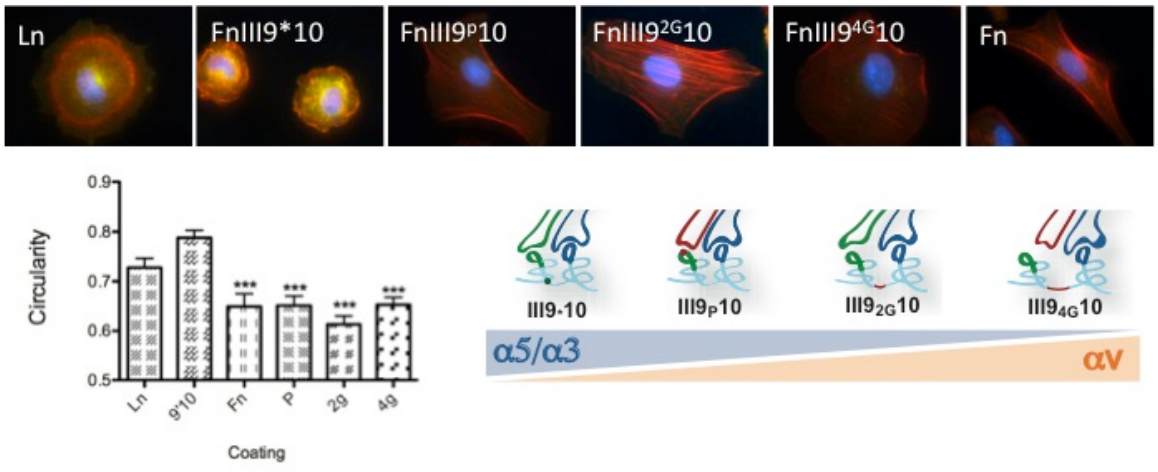

Data from Ashley Brown

Figure 3.3: Cell spreading on FnIII9-10 variants. To evaluate cell-surface integrin binding to FnIII9-10 variants and control surfaces and cell spreading responses, RLE-6TN cells were cultured on FnIII9*10, FnIII^{9p}10, FnIII^{2G}10, FnIII^{4G}10, Fn, or Ln coated surfaces for 3 hours. α3β1 integrin binding was visualized through immunofluorescence staining (green), and actin (red) was visualized through staining with Texas-red-X conjugated phalloidin. Circularity was calculated to measure differences in cell spreading/shape. *** represents $p<0.001$ compared to FnIII9*10.

Epithelial cell attachment to FnIII9-10 variants is integrin dependent

To characterize how epithelial cells attach to different FnIII9-10 variants, RLE-6TN cells were incubated with α3, α5, or αv antibodies or combinations of the three for 30 minutes, then plated on each of the FnIII9-10 fragment, Fn, or Ln and allowed to attach for 30 minutes. The attached cells were fixed to the surface, stained, and absorbance measured. The results shown are presented as percent of 100% attachment. These data coincide closely with the SPR results, indicating that cell attachment to Ln and FnIII9*10 surfaces is highly dependent on α3 integrin, while cell attachment to FnIII9^{2G}10, FnIII9^{4G}10, and Fn was predominantly mediated by αv integrin **(Figure 3.4).** Interestingly, cells cultured on the FnIII9p10 surface, appear to mediate attachment through both α3 and α5 integrins. Previous studies have suggested that the RGD and PHSRN sites serve as an on/off switch for α5β1 binding to Fn such that destabilization of the PHSRN and RGD sites may turn the switch off for α3β1/α5β1 binding and on for αv integrin binding. Although this is supported by our results with the 2-glycine and 4-glycine insertion variants, it appears that a mutation in the synergy site is not sufficient to drive epithelial cells to predominantly attach through αv integrin over α3 and α5 integrin.

Overall, these results indicate that stabilization of the RGD and synergy sites in the FnIII9*10 variant facilitate cell attachment predominantly through α3 and α5 integrins which is typical of epithelial cell homeostasis and healthy repair, while destabilization of the two binding sites through an increased linker region in FnIII9^{2G}10 and FnIII9^{4G}10 drives cell attachment predominantly through αv integrins, typically seen during abnormal epithelial repair processes.

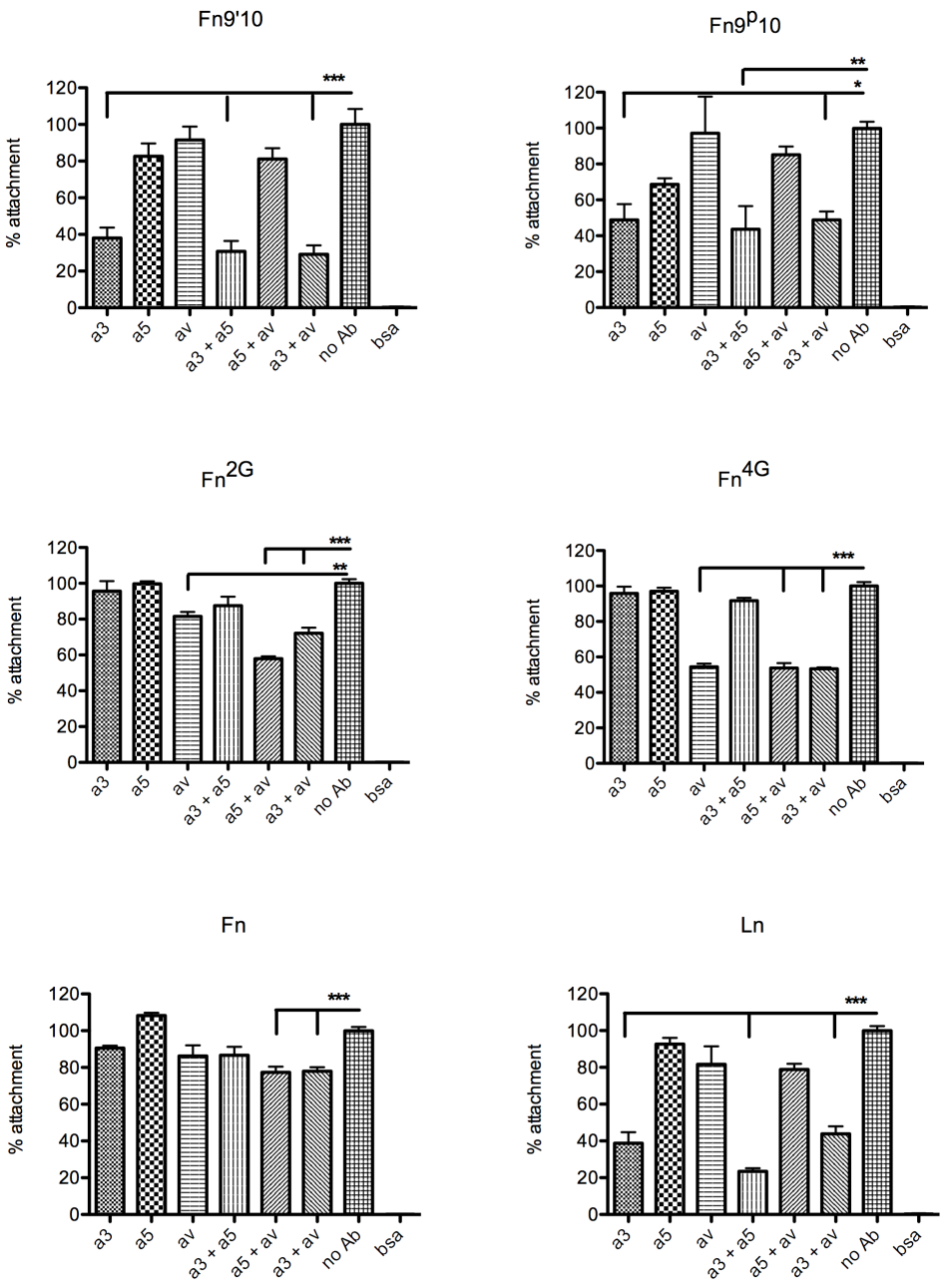

Figure 3.4: Alveolar epithelial cells attach to FnIII9-10 variants through α3, α5, and αv integrins. RLE-6TN cells were incubated with α3, α5, or αv blocking antibodies, and cultured on each of the FnIII9-10 variants, Fn, or Ln. Results are pooled from three independent triplicate experiments and are reported as percent of 100% attachment.

Discussion

These results show that Fn binds integrin α3β1 in cell-free system, and this binding is dependent on the presence of the PHSRN site and is dependent on the spacing relative to the RGD site. These findings have implications in dynamic epithelial tissue wound healing responses since integrin α3β1 is highly expressed by many epithelial cells, which interact with Fn predominantly during wound healing. In addition, studies suggest that the PHSRN site acts to stabilize the high affinity conformation of the RGD site required for α5β1 integrin binding. The results presented here confirm these studies and also show that α3β1 integrin binding to Fn is also dependent on the relative positioning of the RGD and PHSRN sites.

Because α3β1 and α5β1 integrin are involved in epithelial wound repair, these findings that α3β1 integrin, like α5β1 integrin, binds to Fn in a synergy dependent manner have implications in cell interactions during wound healing. Alveolar epithelial type II cells (ATII) only express α5β1 integrin in response to injury; (19) therefore, it is likely that integrin α3β1 binds Fn with great affinity in this cell type in early wound repair before α5β1 integrin is highly expressed. Though α5β1 appears to be the main Fn receptor during alveolar wound repair, integrin blocking experiments with airway epithelial cells showed that in addition to α5, β1, and Fn blocking antibodies, α3 blocking antibodies also resulted in a significant decrease in wound repair (19). Interestingly, it has been shown that integrin α3β1 binding to Fn can be affected by the presence of α5β1 integrin such that α3β1 binding is low in cells expressing α3β1 and α5β1 at comparable levels, but α3β1 binding to Fn is greatly enhanced in cells that

highly express α3β1 compared to other integrins (118). These reports, along with the results of these studies, suggest that α3β1 binding to Fn may modulate wound repair by facilitating binding to ECM in a wound healing environment as the ECM composition transitions from predominantly Ln to high levels of Fn.

SPR experiments demonstrate similar affinities of all FnIII9-10 variants for integrin αvβ3, with all FnIII9-10 variants showing affinities in the 10s of nM range. However, small variations were observed, with a trend of increasing affinity opposite of those observed with PHSRN-dependent integrins α3β1 and α5β1, such that affinity of FnIII9*10 < FnIII9^{2G}10 < FnIII^{9P}10 < FnIII9^{4G}10. This indicates that increasing the linker region between the 9th and 10th type III repeats or mutations in the PHSRN site may make the RGD site more accessible to αvβ3. The RGD and PHSRN sites have previously been described as an on/off "switch" for α5β1 binding to Fn. These findings shown that in the context of epithelial cells, destabilizing the PHSRN and RGD sites may turn the switch off for α3β1/α5β1 binding and on for αv integrin binding. Highlighting the significance of such an integrin switch, binding of α3β1/α5β1 integrins have markedly different effects on epithelial phenotype compared to αv integrin binding. Integrin α3β1 epithelial cell interactions are associated with maintenance of epithelial phenotype and wound healing, while interactions with αv integrins have been associated with abhorrent wound healing, scar tissue formation, epithelial to mesenchymal transitions, and even tumor metastasis (17, 24, 26, 44). Functionally, these interactions were validated through cell attachment assays showing that alveolar epithelial cells bind to each of the FnIII9-10 variants through different integrin profiles based on the location and stabilization of the RGD and synergy sites. Finally, the physiological relevance of

these interactions were confirmed by demonstrating differences in cell spreading in epithelial cells cultured on FnIII9*10 compared to cells cultured on FnIII9*10 with mutation in the PHRSN site or alterations in the spatial orientation of RGD and PHSRN. These studies provide insights into how Fn interactions can contribute to normal vs. pathological wound healing and provide a model system for use in studying the affects of biochemical changes of the ECM in the onset and progression of epithelial cell pathogenesis associated with pulmonary fibrosis.

CHAPTER 4

INTEGRIN SPECIFIC RESPONSES TO FIBRONECTIN TYPE III DOMAINS MODULATE STIFFNESS INDUCED EPITHELIAL TO MESENCHYMAL TRANSITIONS (EMT)

Introduction

The extracellular matrix (ECM) is essential in directing numerous cellular processes including spreading, proliferation, and differentiation. Cells adhere and interact with their underlying ECM through specific transmembrane receptors known as integrins, which are intracellularly linked to the cell cytoskeleton via macromolecular assemblies known as focal adhesions. The physical binding of the ECM to integrins to the cytoskeleton represents the primary mechanotransductory axis of the cell and enables cells to both apply forces to the ECM and to sense mechanical perturbations emanating from the ECM microenvironment.(6, 131, 152) Recent evidence suggests that only specific integrins are mechanosensory and therefore cells may be more or less sensitive to the mechanics of their environment depending on the ECM ligands presented.(153-155) Integrins bind to ECM molecules through specific sequences on the ECM proteins. There exist numerous ECM proteins have several binding sites for multiple integrins. Additionally, some individual integrin binding sequences can bind multiple integrins, resulting in the possibility for multiple cellular responses from the same ECM molecule, thus the interplay between integrin selectivity of the ECM and the cell's responsiveness to mechanical stimuli are quite complex.(155, 156)

ECM-integrin interactions play a major role in directing cell processes critical to tissue development, regeneration, as well as pathology and thus are of great interest in biomaterials research. Epithelial to mesenchymal transition (EMT), the differentiation of cells from an epithelial to mesenchymal phenotype, is one such cell behavior controlled in part by the ECM. (69, 70) EMT is critical in normal embryonic development of complex tissues, tissue repair and regeneration, as well as several pathologies like fibrosis and cancer metastasis.(30, 69) Understanding ECM-cell interactions that regulate EMT and how to control them are critical for tissue engineering applications. In particular, by finely controlling ECM-integrin interactions through biomaterials design, directed EMT could significantly impact regenerative medicine approaches.

EMT has been shown to occur in response to numerous different factors, including transforming growth factor beta (TGFβ), tumor necrosis factor alpha (TNFα), and epidermal growth factor (EGF).(65, 71-73) EMT can also take place in response to extracellular matrix proteins including fibronectin (Fn) binding to certain integrins. While the exact molecular mechanisms for ECM-mediated EMT are still unclear, data from our lab and others has established that engagement of specific integrins, such as α3β1, play a strong EMT-inhibitory role whereas others, like αvβ3, may serve to promote EMT.(30, 44, 143)

Integrin binding to ECM ligands on proteins, including fibronectin and laminin, occurs through specific binding sequences, such as the well-documented Arg-Gly-Asp (RGD) sequence. Many Fn-integrin interactions occur through the RGD sequence, which is located on the 10^{th} type III repeat of Fn. In addition to the RGD sequence, few integrins are known to engage a second recognition sequence (PHSRN), or the "synergy" site,

found on the adjacent 9th type III repeat.(17, 116, 122, 139) Previous reports suggest that under small, physiologically relevant forces the 10th type III repeat can partially unfold, thus present multiple conformations that result in the graded decoupling of RGD and synergy.(13, 16, 17) These different conformations of the 9th and 10th type III repeats can greatly influence specific integrin binding.(122, 125) We previously found that stabilization of the 9th type III repeat of Fn increases α5β1 integrin affinity resulting in enhanced MSC osteodifferentiation, and inhibition of the early EMT program in epithelial cells.(44, 144) Therefore, engineering the conformation of the cell adhesive 9th and 10th type III repeats of Fn may serve as a way to control EMT for complex tissue engineering applications.

In addition to integrins, the physical properties of the ECM, such as the matrix stiffness, contributes to the process of EMT. (Unpublished data, (7, 9, 131, 132, 157, 158)) Specifically, cells are capable of sensing the underlying matrix stiffness via specific integrin-focal adhesion complexes, and will attempt to match their internal stress to the external environment.(131, 132) Mechanistically, it has been shown that cells cultured on increasingly rigid substrates increase the activation of actinomyosin contractile signaling molecules such as Rho GTPase, Rho associated kinase (ROCK), and myosin light chain kinase. Increased cell contractility has been established as a primary mechanism for TGFβ activation.(12, 37, 46, 65) Specifically, αvβ6 integrin binds RGD sequences on the latent TGFβ complex. The application of cell contractile forces on the integrin TGFβ complex results in mechanoactivation of the potent growth factor. (31, 32, 36, 159) The consequence of this elegant system is cell differentiation on stiff substrates but not soft substrates. In the case of EMT, TGFβ receptor engagement results in the down

regulation of epithelial genes such as E-cadherin and cytokeratins and up regulation of mesenchymal genes including α-smooth muscle actin (α-SMA).(36, 46, 160)

Since both biochemical and mechanical stimuli have been shown to affect EMT events, we sought to explore how these two factors may synergistically control EMT. We hypothesized that epithelial cell activation of TGFβ and subsequent EMT would only be supported on stiff substrates presenting adhesive ligands that preferentially bind αv integrins. The hypothesis was tested using a variety of recombinant variants of the 9th and 10th type III repeats (FnIII9-10) created in our lab including i) a stabilizing (L_{1408}-P) point mutation (FnIII9*10), ii) a dominant negative R-A mutation in the synergy site (FnIII9p10), iii) a 2xGly insertion in the linker region between the 9th and 10th type III repeats (FnIII9^{2G}10), and iv) a 4xGly insertion in the linker region (FnIII9^{4G}10). These fragments have been shown to display a graded loss of affinity for α3 and α5 integrins with increasing decoupling of RGD and synergy and display constant affinity for αv integrins. Understanding the effects of orthogonal biochemical and mechanical cues on EMT will allow us to better mimic in-vivo environments and may be a first step to engineering biomaterials with exceptionally high levels of control for tissue regeneration and replacement applications.

Materials and Methods

Production and purification of FnIII9-10 variants

Cloning of the wild type FnIII9-10 into the pGEX4T bacterial expression vector was performed as previously described. A Leu1408 to Pro mutation (FnIII9*10) was made using the parent pGEX4T-FnIII9-10 vector as described previously. FnIII9*10 variants displaying i) a dominant negative R-A mutation in the synergy site (FnIII9p10), ii) a 2xG insertion in the linker region (FnIII9^{2G}10), or iii) a 4xG insertion in the linker region (FnIII9^{4G}10) were then created using the QuikChange® II-E Site-Directed Mutagenesis Kit (Stratagene, La Jolla, CA). All plasmids were introduced to and maintained in the electro-competent XL-1 Blue E.coli strain provided and cultured in LB + ampicillin plates at 37°C. Plasmids were extracted from cultures using the QIAquick Spin Miniprep Kit (QIAGEN, Valencia, CA) and verified via sequencing (Johns Hopkins Synthesis & Sequencing Facility, Baltimore, MD).

Expression vectors were transformed into BL21 E.coli and individual clones picked for subsequent expansion and protein production. Transformed BL21 were grown in LB with ampicillin (100 μg/ml) and protein production was induced by addition of IPTG. Following 3-4 hours of protein production cultures were centrifuged and lysed by freeze thaw cycling. Recombinant GST-FnIII9-10 proteins were purified on a GST-Prep column (GE Healthcare) and the GST tag subsequently cleaved with thrombin. Purity of the FnIII9-10 variants was established by SDS-PAGE analysis as previous reported.(44, 144)

Poly-acrylamide gel production:

Poly-acrylamide (PA) gels of varying bisacrylamide concentrations were created on amino-silanated coverslips as previously described.(161) PA gel solutions were produced by combining acrylamide and bisacrylamide to final concentrations of 8% acrylamide (Biorad, Hercules, CA, USA) and 0.048%, 0.208%, or 0.391% bis (Biorad) to obtain gels with final elastic moduli of 2 kPa, 16 kPa, or 32 kPa respectively. 60 μl of each solution was polymerized by the addition of ammonium persulfate (VWR, West Chester, PA, USA) and N,N,N',N'-tetramethylethylenediamine (Biorad, Hercules, CA, USA) (1% and 0.1% final concentration respectively). The gels were allowed to polymerize for approximately 30 minutes, then washed three times with PBS. FnIII9-10 variants were covalently attached to the surface using the heterobifunctional crosslinker sulfosuccinimidyl-6- (4'-azido-2' nitrophenyl-amino) hexanoate (sulfo-SANPAH; Pierce Chemical Co., Rockford, IL., USA). Following an overnight incubation with the Fn fragments, gels were washed three times with PBS.

Cell Culture:

RLE-6TN cells, an alveolar epithelial cell line were obtained from ATCC, and grown in DMEM/F12 media supplemented with 10% fetal bovine serum and 1% penicillin / streptomycin (P/S). To determine the combined affect of different Fn fragments and substrate rigidity on epithelial cell fate, cells were plated at a density of 100,000 cells/cm^2 on polyacrylamide gels with Fn fragments cross linked onto the surface with the following rigidities: E = 2kPa, 16kPa, 32kPa, or on glass coverslips coated with Fn or Ln as controls. For experiments utilizing the different Fn fragments, cells were plated on FnIII9-10-immobilized (2 μM) gels placed in 1% bovine serum albumin

(BSA)- blocked plates and cultured in DMEM/F12 media supplemented with 10% Fn-depleted serum for five days. Media was changed every 48 hours.

Immunofluorescence staining and circularity analysis:

Following culture for 5 days, cells were washed with PBS, fixed with 4% formaldehyde, permeabilized with 0.2% Triton-X 100 and then blocked with 10% goat serum. Primary mouse anti-α-SMA (1A4, Sigma-Aldrich) or mouse anti-E-cadherin (36/E-cadherin, BD Transduction Laboratories) antibodies were incubated overnight then washed thoroughly with PBS + 1.5% goat serum. Alexa-Fluor-488-conjugated goat-anti-mouse (Invitrogen) was used as the secondary antibody for both markers in separate staining experiments. To characterize cell shape, actin was stained with Texas-red phalloidin (Invitrogen) and nuclei were stained with Hoechst (Invitrogen). Images were acquired with a Nikon Eclipse (TiE) inverted fluorescence microscope at 20X magnification (PlanFluor 20X, 0.5 NA objective) with a CoolSNAP HQ2 Monochromatic CCD camera. Experiments were performed in triplicate, and images presented are representative from 5-10 random fields for each independent experiment. To characterize circularity, area and perimeter of individual cells stained for actin were determined for each condition using Image J (NIH Freeware) image processing software, then circularity was determined using the equation circularity = $4\pi(\text{area}/\text{perimeter}^2)$. Three independent images were analyzed for each condition, and at least 10 cells were analyzed per image. Data is pooled from all 3 images analyzed per condition.

Immunoblot:

RLE-6TN cells were cultured for 5 days as described above then washed with PBS and cells lysed directly in Laemmli buffer containing protease inhibitors (Roche Applied

Sciences). Total protein concentration was determined using the BCA protein quantification kit (Pierce Chemical Co.). Forty μg of total protein was separated by electrophoresis on a 4-15% gel, then transferred to a nitrocellulose membrane using a semi-dry transfer system, blocked with 5% nonfat dry milk in TBS, then incubated with E-cadherin (36/E-cadherin), α-SMA (1A4), or GAPDH (14C10, Cell Signaling Technologies, Boston, MA, USA) antibodies overnight at 4° C. Following washing with TBS + 0.1% Tween 20, membranes were incubated for 2 hours with IR secondary antibody (Licor), washed, and then imaged using the Odyssey IR scanner. Western blots were quantified using Image J image processing software, using GAPDH as the endogenous control.

TGFβ activation assay:

RLE-6TN cells were cultured on Fn fragment-PA gels, Fn-coated glass, or Ln-coated glass in Fn depleted growth media as described above. TGFβ activation was determined by a mink lung epithelial cell (MLEC) assay as previously described (162). MLECs stably transfected with an expression construct containing a truncated Pai-1 promoter fused to the firefly luciferase reporter gene respond in a dose dependent manner to active TGFβ, but are incapable of activating TGFβ. After 5 days of RLE-6TN culture on the various substrates, MLECs were added at a density of 50,000 cells/cm^2 on top of the RLE-6TN cells in serum free DMEM/F12 media + 1% BSA. Cells were co-cultured for 16 hours, lysed and luciferase activity was determined via the One-Glo luciferase assay (Promega). Luminescence was measured with a Synergy H4 Multi-Mode Plate Reader (BioTek, Winooski, VT, USA). TGFβ activation is presented as pg/mL calculated from normalized luminescence compared to MLEC only (unstimulated) wells.

Results presented are pooled from 3 independent triplicate experiments.

Statistical Analysis:

All statistical analysis for 3 or more experimental groups was performed by two-way ANOVA using Prism (GraphPad Software Inc., La Jolla, CA, USA). Statistical significance between groups was determined by performing Tukey's post hoc analysis. All data is presented as mean +/- SEM and statistical significance is achieved for $p<0.05$.

Results

Alveolar epithelial cells maintain an epithelial phenotype when engaging the stabilized FnIII9*10 fragment.

Utilizing PA gels and surface immobilized Fn mutants and varying stiffness from 2 to 32 kPa, alveolar epithelial cells were cultured for 5 days and then analyzed for different EMT responses. EMT was characterized through analysis of cell circularity/spreading, and expression of different epithelial and mesenchymal markers by immunofluorescence staining and western blots. Alveolar epithelial cells have been shown to undergo EMT on Fn-coated glass coverslips but maintain an epithelial phenotype on Ln-coated glass coverslips. Therefore, these conditions were used as controls and, as expected, EMT was observed on Fn-coated glass as indicated by high expression of α-SMA and low levels on E-cadherin at cell-cell contacts. Contrary, cells cultured on Ln-coated glass exhibited an epithelial phenotype as indicated by low levels of α-SMA and maintenance of E-cadherin expression at cell-cell contacts.

Cells cultured on 2kPa and 16kPa gels with the FnIII9*10 fragments maintained an epithelial phenotype with positive staining for E-cadherin at cell-cell contacts and

minimal staining for α-SMA as well as high cell circularity. At 32kPa, staining for E-cadherin decreased and staining for α-SMA slightly increased showing a slight shift to a more mesenchymal phenotype. In contrast, cells cultured on gels presenting the FnIII9p10, FnIII9^{2G}10, or FnIII9^{4G}10 mutants all showed an up-regulation of mesenchymal markers, a loss of cell-cell contacts, and decreased cell circularity at all substrate stiffness values (**Figure 4.1**). In addition, EMT was monitored by analyzing cell spreading and cytoskeletal organization / stress fiber formation. Alveolar epithelial cells were once again cultured on combinations of different Fn fragment mutants and substrates of varying stiffness for 5 days. They were then stained with Texas Red-X conjugated phalloidin to visualize the actin cytoskeleton. Cells cultured on the stabilized FnIII9*10 mutant displayed the typical rounded epithelial morphology and diffuse cortical staining for actin. In contrast, cells cultured on all other mutants displayed an elongated morphology and thick, aligned actin filaments indicative of stress fibers. Despite previous reports indicating the inability of cells on soft substrates to generate stress fibers, we observed that epithelial cells cultured on FnIII9p10, FnIII9^{2G}10, FnIII9^{4G}10 all showed of the formation of a few stress fibers even on low stiffness (2kPa) gels. Cell circularity was calculated to quantify differences in observed cell shape. Values closer to 1 indicate a more rounded, epithelial-like cell. (**Figure 4.2**)

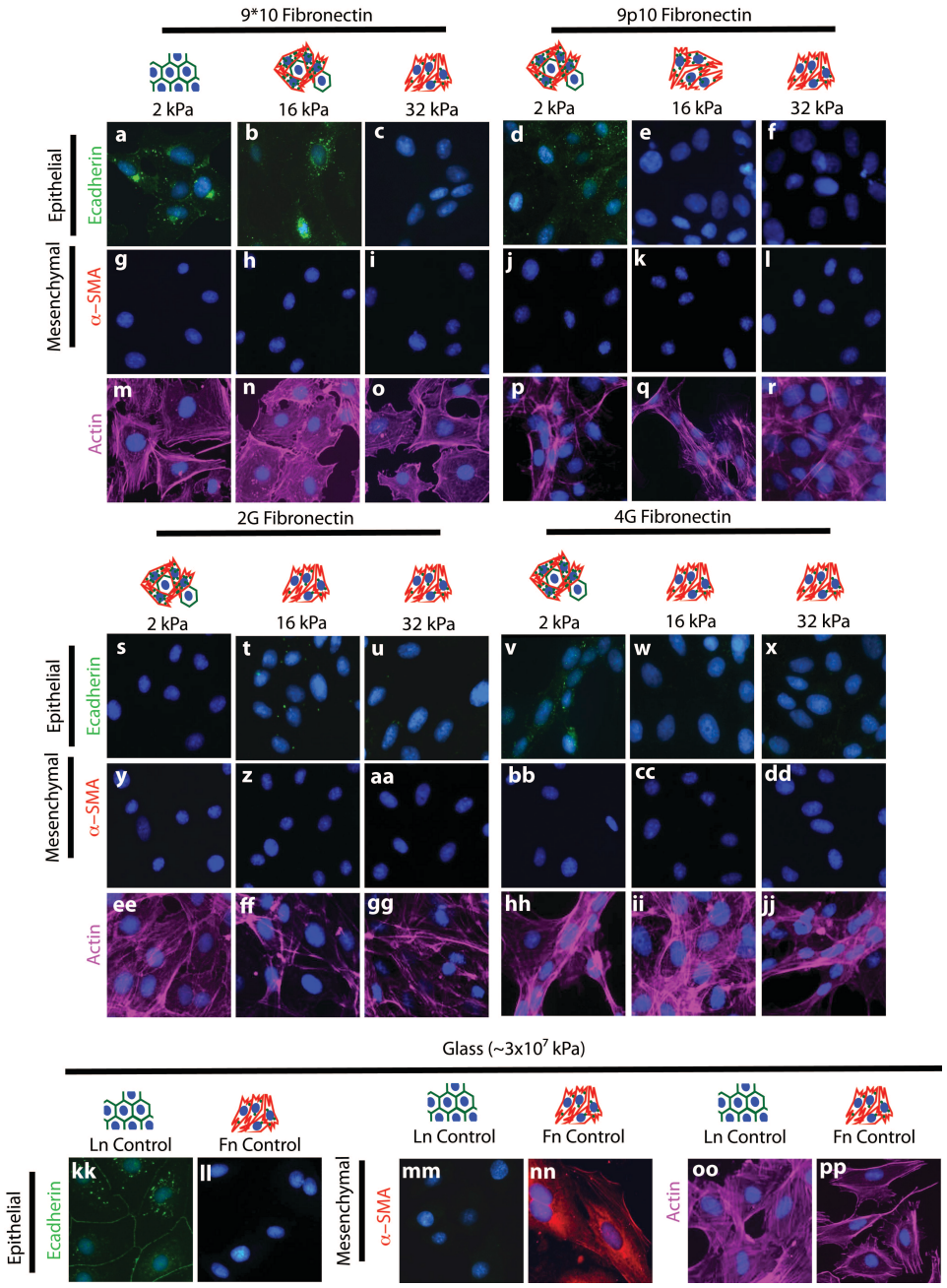

Figure 4.1: Analysis of epithelial and mesenchymal markers of RLE-6TN cells cultured on differing Fn fragment-substrate stiffness combinations. RLE-6TN cells were cultured on differing fragment-stiffness combinations for 5 days then analyzed for epithelial and mesenchymal protein expression through immunofluorescence staining for E-cadherin **(a-f, s-x, kk-ll)** and α-SMA **(g-l, y-dd, mm-nn).** The actin cytoskeleton was visualized by staining with Texas-red phalloidin and the nuclei stained with Hoechst **(m-r, ee-jj, oo-pp).** Fluorescent images were acquired with a Nikon Eclipse (TiE) inverted fluorescence microscope at 20X magnification. Experiments were performed in triplicate, and images presented are representative from 5-10 random fields for each independent experiment.

The shift from an epithelial to mesenchymal phenotype was further quantified by western blots for E-cadherin (epithelial) and α-SMA (mesenchymal). Western blots were quantified and expressed as fold change compared to expression on 2kPa gels, normalizing for protein loading differences with the GAPDH signal. Higher expression of E-cadherin was seen on the 2kPa gels for each of the fragments compared to higher substrate stiffnesses, while expression of α-SMA was higher on the stiffer substrates. Although some E-cadherin expression was observed on higher substrate stiffnesses and on the destabilized mutants, it was lost from cell-cell contacts. This corroborates observations that E-cadherin is lost from cell-cell contacts early in the progression of EMT but is still observed intracellularly. The loss of E-cadherin protein levels occurs well into the EMT program. This fact accentuates the relevance of the magnitude of E-cadherin loss on the destabilized Fn mutants. Differences in protein expression, in general, correspond with the immunohistochemistry results, indicating that stabilization of the RGD and PHSRN synergy by the FnIII9*10 mutation supports an epithelial phenotype (inhibits EMT) at higher stiffnesses concomitant with its ability to bind α3 and α5 integrins. On the contrary, the decoupled (FnIII9p10) and destabilized (FnIII9^{2G}10, FnIII9^{4G}10) mutants, which decreasingly bind α3 and α5 integrin, still support EMT, even on soft substrates. (**Figure 4.3**)

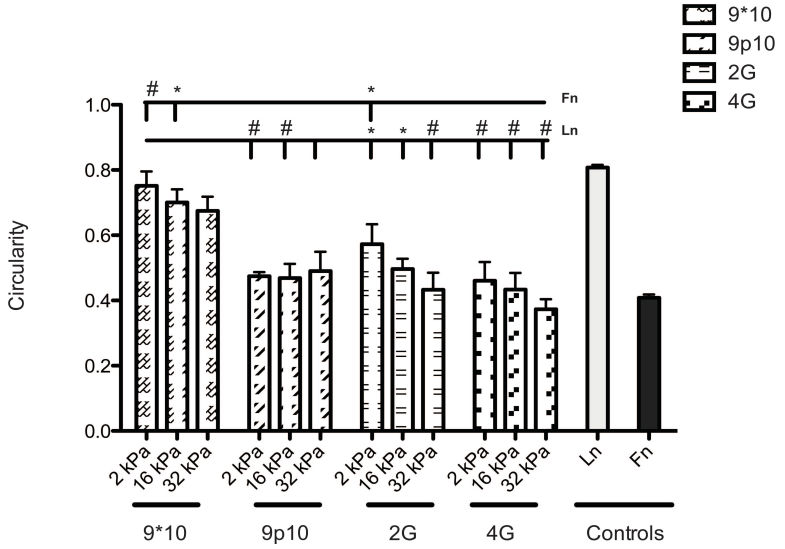

Figure 4.2: Analysis of circularity of cells cultured on various fragment-stiffness combinations. Cells were cultured for 5 days, lysed and responses were analyzed through changes in actin cytoskeleton alignment and cell circularity. Experiments were performed in triplicate and significance is reported compared to either Fn or Ln at either $p < .05$ (*) or $p < 0.01$ (#).

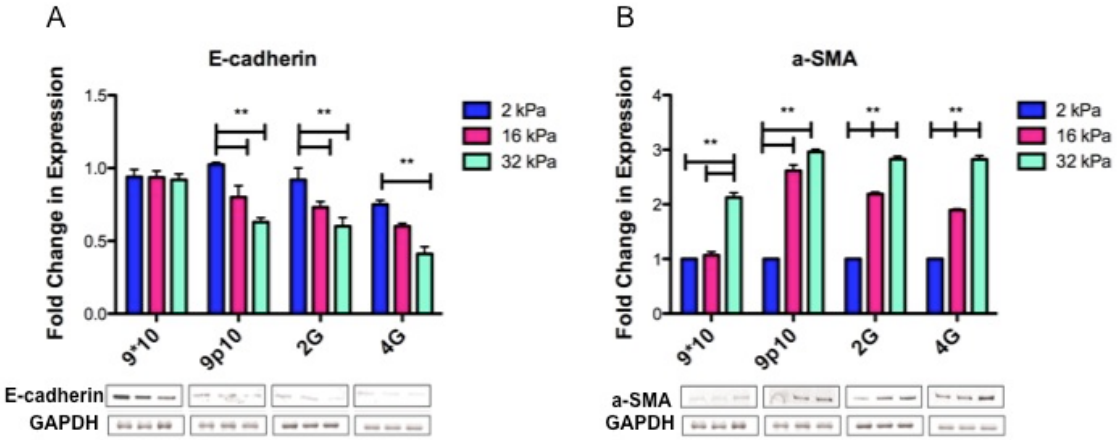

Figure 4.3: Analysis of epithelial and mesenchymal protein expression of cells cultured on various fragment-stiffness combinations. Cells were cultured for 5 days, lysed and EMT responses were analyzed through changes in epithelial and mesenchymal protein expression western blotting for E-cadherin (epithelial) **(A)** and α-SMA (mesenchymal) **(B)**, and GAPDH (endogenous control). Western blots were quantified and expressed as fold changed compared to expression on the 2kPa gels using GAPDH as the endogenous control **(A, B)**.

EMT events are dependent on cell contractility

Based on previous observations that epithelial cell stiffness increases with increasing matrix rigidity, we investigated if the observed EMT on the Fn fragment-stiffness combinations maintained this dependency. Alveolar epithelial cells were again cultured for 5 days on differing Fn fragment mutant-substrate stiffness combinations in the presence or absence of the ROCK inhibitor, Y-27632, and EMT events characterized as previously described. In the presence of the ROCK inhibitor, cells on all substrates displayed positive staining for E-cadherin at cell-cell contacts and minimal staining for α-SMA (**Figure 4.4**). In addition, cells on all substrate combinations maintained a round, epithelial morphology as indicated by quantitative circularity analysis **(Figure 4.5).** Finally, protein expression for E-cadherin and α-SMA remained unchanged in cells culture on each fragment and stiffness combination (**Figure 4.6**). These results strongly indicate that blocking epithelial cell contractility is able to overcome matrix/substrate effects and implicates activation of the cell contractile machinery as a primary target mechanism for the observed substrate-mediated EMT.

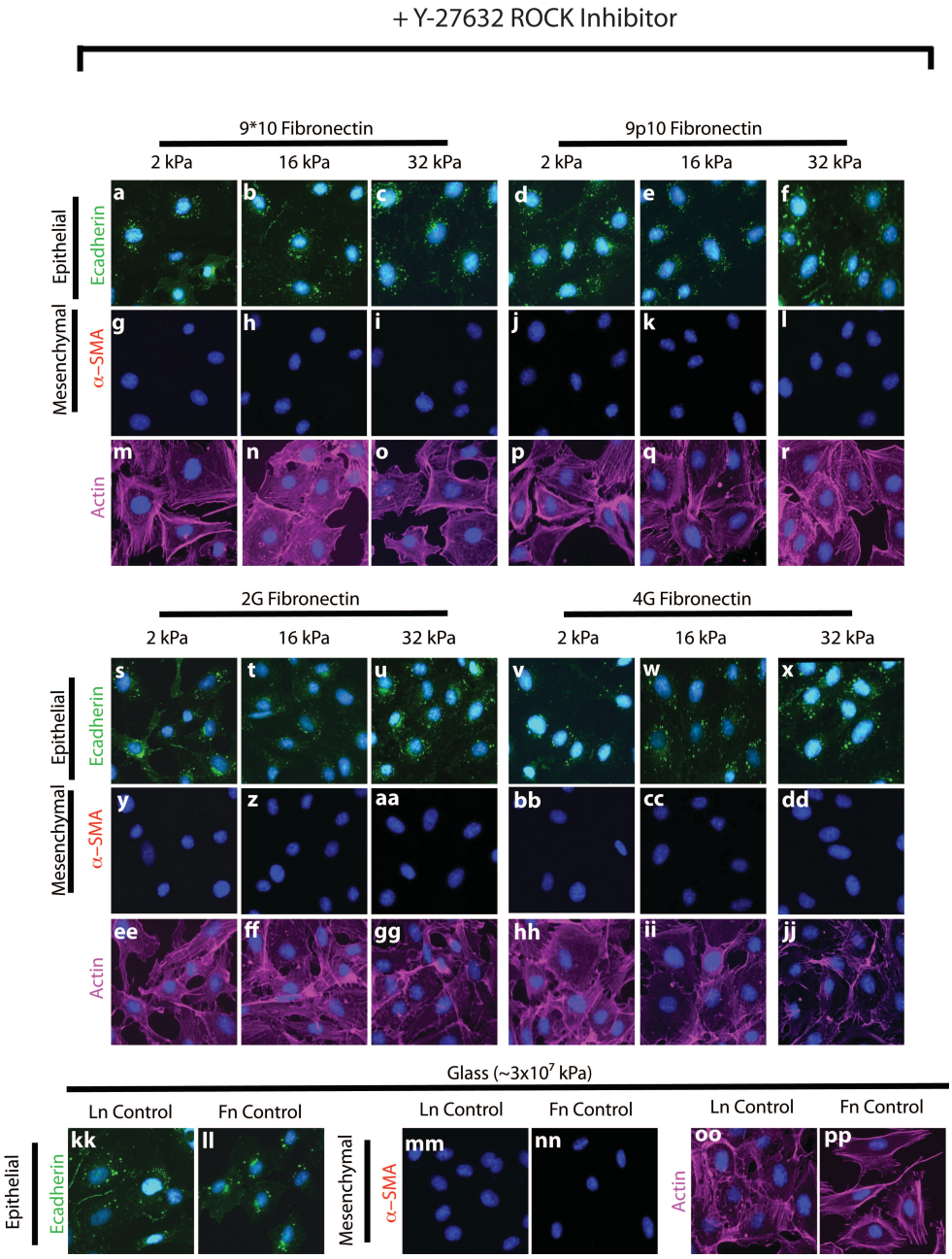

Figure 4.4: EMT events are dependent on cell contractility. RLE-6TN cells were cultured on fragment-stiffness combinations in the presence or absence of 10 μM Y-27632 ROCK inhibitor for 5 days and then EMT responses were analyzed through changes in epithelial and mesenchymal protein expression through immunofluorescence staining for E-cadherin **(a-f, s-x, kk-ll)** and α-SMA **(g-l, y-dd, mm-nn)**. The actin cytoskeleton was visualized by staining with Texas-red phalloidin and the nuclei stained with Hoechst **(m-r, ee-jj, oo-pp).**

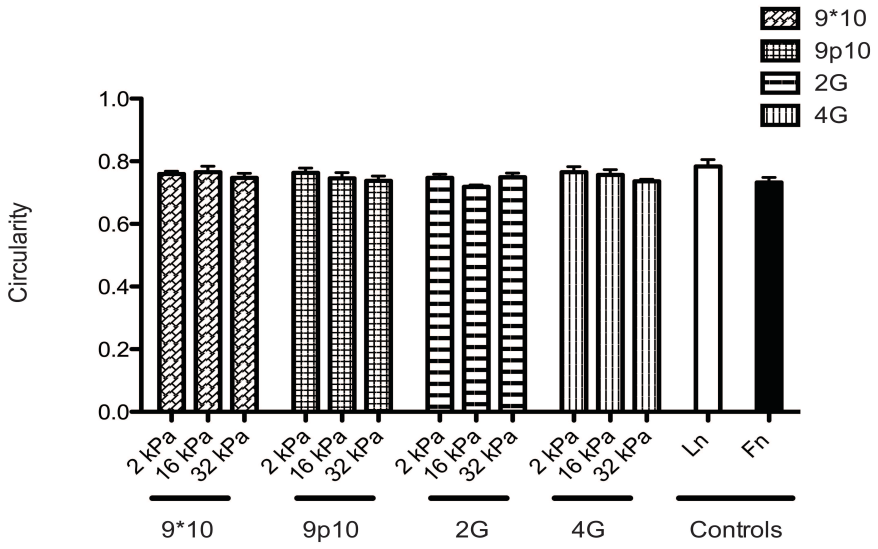

Figure 4.5: Fn fragment -- substrate stiffness circularity is dependent on cell contractility. RLE-6TN cells were cultured on fragment -- stiffness combinations in the presence or absence of 10 μM Y-27632 ROCK inhibitor for 5 days and then responses were analyzed through changes in actin cytoskeleton alignment and cell circularity. Experiments were performed in triplicate, and data was collected from 5-10 random fields for each independent experiment.

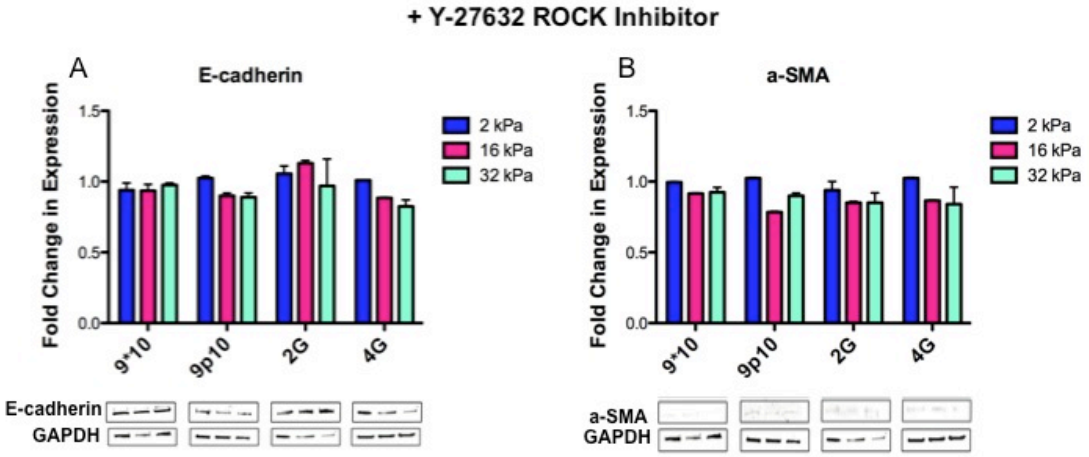

Figure 4.6: Fn fragment-substrate stiffness EMT is dependent on cell contractility. RLE-6TN cells were cultured on fragment - stiffness combinations in the presence or absence of 10 μM Y-27632 ROCK inhibitor for 5 days and EMT responses were analyzed through changes in epithelial and mesenchymal protein expression by western blot for E-cadherin (epithelial) **(A)** and α-SMA (mesenchymal) **(B)**, and GAPDH (endogenous control). Western blots were quantified and expressed as fold change compared expression on the 2kPa gels using GAPDH as the endogenous control **(A, B)**.

Alveolar epithelial cells display enhanced TGFβ activation in conjunction with cell contractility and EMT

Previous studies have shown that elevated levels of cell contractile forces enable the activation of TGFβ, a potent EMT inducer, from its matrix associated latent form. Since inhibition of contractile forces eliminated the substrate-dependent EMT responses, we investigated if differences in TGFβ activation on Fn fragment -- substrate stiffness combinations could explain, in part, the observed substrate-mediated EMT events. To determine if differences in fragment-stiffness combinations induced changes in TGFβ activation, the mink lung epithelial reporter cell (MLEC) bioluminescence co-culture assay was performed (**Figure 4.7**). Generally, alveolar epithelial cells were found to increasingly activate TGFβ in response to increased substrate compliance. Furthermore, epithelial cells cultured on the destabilized Fn mutants activated significantly greater amounts of TGFβ compared to the stabilized mutant (FnIII9*10) or Ln. Statistical comparisons were made across all sample groups. The following samples were statistically different from the Ln control: FnII9p10 (32kPa), FnIII9^{2G}10 (2, 16, 32kPa), and FnIII9^{4G}10 (2, 16, 32kPa). The following samples were statistically different from the Fn control: Fn9*10 (2, 16, 32kPa) and FnIII9p10 (2kPa). The FnIII9p10 (16kPa) sample was not statistically different from either control. As predicted, the control groups cultured on Fn-coated glass showed high levels of TGFβ activation, while those cultured on Ln-coated glass showed significantly less ($p < 0.01$) levels than Fn that were comparable to the negative (no stimulation MLEC) control.

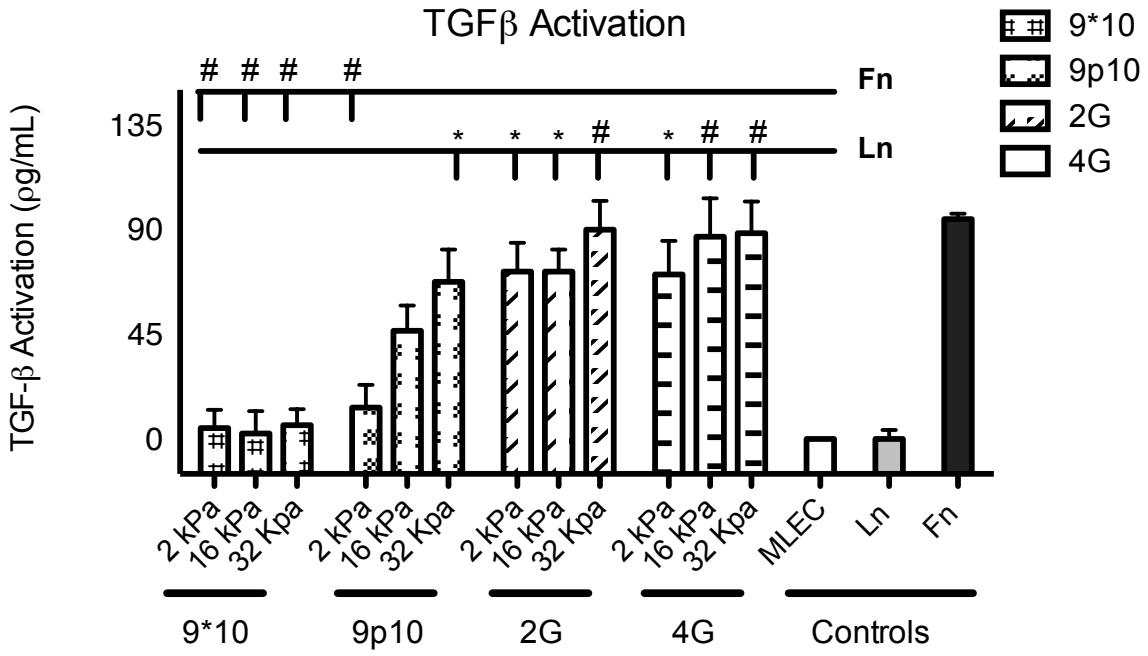

Figure 4.7: TGF-β activation is necessary for EMT. RLE-6TN cells were cultured for 5 days on differing fragment -- stiffness combinations and then levels of TGFβ activation was determined using the MLEC bioluminescence co-culture assay. TGFβ activation is reported as pg/mL, and results shown are pooled from 3 independent triplicate experiments. Significance is reported compared to either Fn or Ln at either $p < .05$ (*) or $p < 0.01$ (#).

Discussion

Cell-integrin interactions play a major role in directing cellular processes that drive tissue regeneration. Understanding these interactions and how to control them at the biomaterial-cell interface is critical for tissue engineering applications that aim to direct cell fate in vitro, or direct tissue regeneration in vivo after injury. Although much effort has been made to prevent biomaterial-associated pathologically related cell behaviors, like EMT, these transitions are necessary for proper repair and regeneration of most complex tissues. As such, there is a growing need for new biology that informs biomaterials design. Cell-integrin interactions are central to directing EMT events, and if uncontrolled lead to pathological conditions. However, if finely controlled, directed EMT could have significant potential for regenerative medicine applications, such as directing complex tissue formation from a single cell population, like stem or progenitor cells. Here we show for the first time that EMT-related responses can be controlled, in part, through cell adhesive Fn fragments which have been engineered to differentially engage specific integrins. These fragments, or similarly designed integrin-specific ECM adhesive polypeptides, may in the future be used in three-dimensional synthetic biomaterials to direct complex epithelial cell responses, e.g. EMT and branching morphogenesis, facilitating tissue regeneration.

The work presented here is based on previous data illustrating that $\alpha 3\beta 1$ and $\alpha 5\beta 1$ integrin engagement has markedly different effects on epithelial phenotype compared to αv integrin engagement. Specifically, $\alpha 3$ integrins are associated with maintenance of an epithelial phenotype while αv interactions are associated with EMT. In addition, the RGD and PHSRN sites of Fn's cell binding domain have been described

as a possible integrin 'mechanoswitch' for α5β1 binding to Fn.(30, 44, 142, 143) Unpublished data from our lab strongly suggests that α3β1 integrin shares this binding behavior to Fn's cell binding domain. Therefore, destabilization of this critical region, as achieved through our FnIII9p10, FnIII9^{2G}10, and FnIII9^{4G}10 mutants, should turn the switch 'off' to α3 and α5 integrin thus pushing the Fn fragments toward binding predominately αv integrins, and ultimately driving EMT. Our results strongly support this hypothesis. In particular, the Fn fragment variants that display higher αv to α3/α5 binding affinities enable epithelial cells to undergo EMT even on extremely soft substrates that are inherently inhibitory to the process. Likewise, structural stabilization of FnIII9-10 is capable of supporting epithelial phenotypes even on substrate stiffness values that we have previous shown as promoting EMT (>8kPa). Taken together, our results indicate that both the biochemical and mechanical signals from the microenvironment play a role in activation of the EMT program. Perhaps not unexpected, the data suggest that neither the conformation of Fn nor the substrate compliance is a dominant effector. In other words, it appears that either the ligand or the compliance is capable of overcoming the effect of the other. The response of epithelial cells to the array of conditions tested also suggests that cells have an integrated response to combinations of integrin engagement and compliance matching (the notable exception being Ln). Of particular interest is the finding that while FnIII9*10 prevented significant cell spreading and TGFβ activation, the epithelial cells still display some indications of EMT on the stiffest substrate (32kPa). On the opposite end of the spectrum, we found our original hypothesis to be only partially correct. Specifically, epithelial cells engaging Fn fragments that predominately support αv integrin engagement actively initiated the

EMT program despite being cultured on substrates with stiffness values that do not support cell contraction. Future studies elucidating the molecular details of these varied responses will no doubt provide interesting insights into the complexity of EMT.

In conclusion, we demonstrate for the first time, that different combinations of substrate compliance and integrin-specific engagement can be used to guide different epithelial cell phenotypes directed through the process of EMT **(Figure 4.8).**

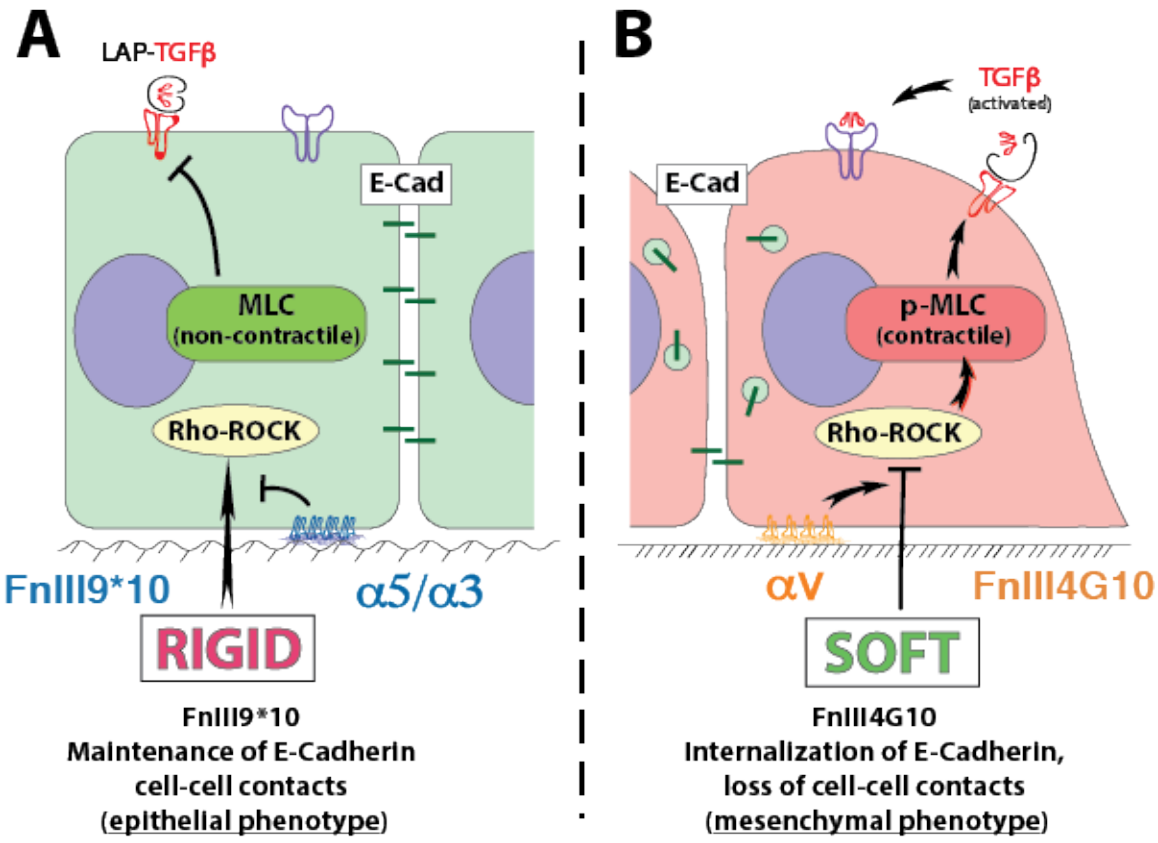

Figure 4.8. Combined substrate compliance and integrin specific engagement drive differential epithelial cell phenotypes. Epithelial cells cultured on rigid substrates normally facilitate pro-contractile signals. However engagement of α3 integrins by utilizing the FnIII9*10 variant can modulate this response and maintain an epithelial phenotype (A). Alternatively, epithelial cells on soft substrates normally inhibit pro-contractile signals, but with engagement of αv integrin by utilizing the FnIII^{4G}10 variant cells become contractile and acquire a mesenchymal phenotype **(B).**

These responses appear to be partially regulated through the cell's ability to activate TGFβ, likely via integrin-mediated mechanoactivation. This work further illustrates that altered biophysical states of Fn's cell binding domain that alter the integrin binding profile to this domain are capable of regulating the maintenance of epithelial phenotypes or driving EMT and show translational promise in biomaterials-based regenerative medicine approaches.

CHAPTER 5

EXPOSURE TO ENVIRONMENTAL PARTICULATE MATTER ALTERS STIFFNESS MEDIATED ALVEOLAR EPITHELIAL CELL EMT EVENTS

Introduction

Over the past decade, several studies have linked deteriorating pulmonary conditions to exposure to air pollution and particulate matter (PM). Epidemiological studies have linked exposure to particles with diameters less than 10 um with increased pulmonary morbidity and mortality. It is estimated that the annual number of premature deaths due to particle exposure is approximately one million worldwide(57-59, 61). Several different pulmonary effects have been associated with PM exposure, including decreased lung development and function, exacerbation of asthma, chronic obstructive pulmonary disease (COPD), and pulmonary fibrosis (52, 54, 56). Despite numerous epidemiological studies that associate PM with adverse pulmonary conditions, the underlying biological mechanisms are not fully understood.

Ambient PM is a complex mixture consisting of solid particles and liquid droplets of varying size and composition. The size of the particles is defined by its aerodynamic diameter, which can range from a few nanometers to tens of micrometers, and is highly dependent of characteristics such as shape, density, and structure (53, 55, 163). When studying biological health effects of PM, particles with aerodynamic diameters of less than 10 microns are broken into three subcategories: coarse particles (aerodynamic diameters of 2.5um – 10um), fine particles (aerodynamic diameters of 0.1um – 2.5um)

and ultrafine particles (<0.1 um), and these are generally referred to as PM10, PM2.5, and PM0.1.

The adverse effects of inhaled PM are highly dependent on the deposition and retention of particles within the lung, and this deposition is dependent on the aerodynamic properties. In general, large particles primarily deposit in the large airways of the respiratory tract, while smaller particles pass directly through the upper airways and are able to deposit in the bronchiolar and alveolar regions (54, 56-58, 61). Ciliated cells clear most particles deposited in the upper airways in less than 24 hours from deposition. However, smaller particles that reach the alveoli cannot be cleared in this manner. Particle clearance in the distal lung is attempted by phagocytosis by alveolar macrophages, although this process is less efficient for ultra-fine particles. Smaller particles that cannot be cleared go on to interact directly with alveolar epithelial cells (54, 56, 58).

These smaller particles have been suggested to be more detrimental to progression of lung pathologies due to their high surface to mass ratio. Although size is a critical factor in reaching the distal lung, previous studies have shown that several components of PM are able to activate an inflammatory response and that there are secondary effects that can induce cellular damage, which stimulate fibrotic remodeling pathways (95, 98-100). A variety of characteristics that contribute to inflammation in the lung have been identified both in-vivo and in-vitro, including the content of endotoxins, transition metals, and hydrocarbons. Therefore, both the surface area and the surface reactivity of particles are potential mediators in the onset and progression of pulmonary pathogenesis (54, 56, 58).

Of particular interest, is that alveolar macrophages, which are recruited in response to PM deposition in the lung, store large quantities of latent TGF β that can be released upon stimulation. In response to tissue damage, the latent TGF β is released into the site of injury, and can be inserted into the matrix of the provisional wound. Furthermore, it has been suggested that PM exposure may exert oxidative stress on alveolar cells by presenting or stimulating the cells to produce reactive oxygen species (48, 49, 60, 102). These reactive oxygen species in turn have the ability to activate stores of latent TGF β by direct oxidation of methionine-253 within the LAP peptide. The redox reactions cause a rapid conformational change in the LAP, which allows for the rapid release of the TGF β homodimer (24, 48, 49, 60, 101, 102).

As shown in Aim 1 of this work, TGF β is a potent inducer of EMT, which has been highly linked with the onset, and progression of pulmonary fibrosis. Furthermore, in Aim 1 we show that both the dynamic biochemical and biophysical properties of the ECM work together to control TGF β activation, and that this activation initiates the progression of EMT. Therefore, we sought to explore if exposure of physiologically relevant concentrations of PM2.5, to alveolar epithelial cells alters the activation of TGF β and ATII cell phenotype normally seen in response to varied matrix stiffnesses. This is of great significance because the lung is exposed to particulate matter on a daily basis. Therefore, it is important to explore how processes driving pulmonary fibrosis are affected in this highly physiologically relevant condition. Furthermore, exploration of the combination of PM and matrix stiffness will give insight into how these processes are altered in a pre-fibrotic or fibrotic environment compared to a healthy environment. The hypothesis for this work was that exposure of alveolar epithelial cells to PM2.5 would

exacerbate the induction of stiffness mediated EMT. The consequence of this combined effect would lead to the rationale that exposure to fine particulate matter can further drive a fibrotic state leading to increased progression of lung disease. Furthermore, it was hypothesized that the intensified EMT response with exposure to PM2.5 could be mediated by inhibition of ROS and / or engagement of an epithelial-maintaining Fn conformation.

Materials and Methods

Poly-acrylamide gel production:

Poly-acrylamide (PA) gels of varying bisacrylamide concentrations were created on amino-silanated coverslips as previously described.(161) PA gel solutions were produced by combining acrylamide and bisacrylamide to final concentrations of 8% acrylamide (Biorad, Hercules, CA, USA) and 0.048%, 0.117%, 0.208%, or 0.260% bis (Biorad) to obtain gels with final elastic moduli of 2 kPa, 8kPa, 16 kPa, or 24 kPa, respectively. 50 µl of each solution was polymerized by the addition of ammonium persulfate (VWR, West Chester, PA, USA) and N,N,N',N'-tetramethylethylenediamine (Biorad, Hercules, CA, USA) (1% and 0.1% final concentration respectively). The gels were allowed to polymerize for approximately 30 minutes, then washed three times with PBS. Fibronectin was covalently attached to the surface using the heterobifunctional crosslinker sulfosuccinimidyl-6- (4'-azido-2' nitrophenyl-amino) hexanoate (sulfo-SANPAH; Pierce Chemical Co., Rockford, IL., USA). Following an overnight incubation with the fibronectin or fibronectin variants, gels were washed three times with PBS.

Production and purification of FnIII9-10 variants

Cloning of the wild type FnIII9-10 into the pGEX4T bacterial expression vector was performed as previously described. A Leu1408 to Pro mutation (FnIII9*10) was made using the parent pGEX4T-FnIII9-10 vector as described previously. FnIII9*10 variants displaying i) a dominant negative R-A mutation in the synergy site (FnIII9p10), ii) a 2xG insertion in the linker region (FnIII9^{2G}10), or iii) a 4xG insertion in the linker region (FnIII9^{4G}10) were then created using the QuikChange® II-E Site-Directed Mutagenesis Kit (Stratagene, La Jolla, CA). All plasmids were introduced to and maintained in the electro-competent XL-1 Blue E.coli strain provided and cultured in LB + ampicillin plates at 37°C. Plasmids were extracted from cultures using the QIAquick Spin Miniprep Kit (QIAGEN, Valencia, CA) and verified via sequencing (Johns Hopkins Synthesis & Sequencing Facility, Baltimore, MD).

Expression vectors were transformed into BL21 E.coli and individual clones picked for subsequent expansion and protein production. Transformed BL21 were grown in LB with ampicillin (100 μg/ml) and protein production was induced by addition of IPTG. Following 3-4 hours of protein production cultures were centrifuged and lysed by freeze thaw cycling. Recombinant GST-FnIII9-10 proteins were purified on a GST-Prep column (GE Healthcare) and the GST tag subsequently cleaved with thrombin. Purity of the FnIII9-10 variants was established by SDS-PAGE analysis as previous reported.(44, 144)

Cell Isolation and Maintenance:

RLE-6TN cells were purchased from ATCC and maintained in DMEM/F12 media with 10% FBS and 1% penicillin/streptomycin at 37°C and 5% CO2. Media was

refreshed every 2 to 3 days and cells were split upon reaching 95% confluency.

LIVE/DEAD Assay of cell viability

RLE-6TN cells were cultured for 24 hours with increasing concentrations of PM2.5 ranging from .01ug/cm^2 to 50ug/cm^2 and cell viability was determined by staining with trypan blue. Cells were trypsinized and then resuspended in a 1:1 suspension using 0.4% trypan blue. The cell suspension was analyzed by counting dead cells (stained blue) vs. total cells using a hemacytometer. Each concentration of PM2.5 was tested in triplicate and results are presented as % viable cells for each PM concentration.

Fine Particulate Matter Isolation and Cell Culture Experiments

Fine particulate matter samples were collected on Teflon filters from the Atlanta area (Dekalb county) as part of a study for the Georgia Tech Civil and Environmental Engineering department. The samples were collected daily using multichannel particle composition monitors (PCM). The specific area of collected PM is located near two major highways (I20 and I285), and near a school, both of which can lead to increased levels of mobile source generated particulate matter [8]. In each channel of the PCM, air first passes through a cyclone separator to remove particles that are greater than 10um. In one channel, the air next passes through a WINS impactor to remove particles that are greater than 2.5um. Finally, the remaining particles (i.e. the PM2.5 fraction) is collected on a Teflon filter. In channel two, after passing though the cyclone, the air passes through an annular denuder to remove acidic and alkaline gases. Then the air passes through the WINS impactor and the remaining particles are captured on a nylon filter in order to analyze the ionic species. In the third channel, the air passes through a denuder in order to remove organic gases, flowed by the WINS impactor, and the particles are collected in a

quartz filter for organic and elemental carbon analysis [8, 9]. After collection in the particle composition monitors, the filters are stored at -20°C for later chemical analysis. The Teflon filter is stored for exploratory analyses, such as this study.

In order to prepare the PM2.5 fraction for cell culture experiments, five different PM containing Teflon filters were weighed to determine the total particulate mass on each filter. Five samples were pooled together to minimize variation based on the day collected, and placed in sterile 50 ml centrifuge tubes fully covered with 5ml of diH_20, and sonicated 5 times for 10 minutes to release the particles captured on the filters. The samples were filtered through a 5um diameter pore size filter to remove any larger particle debris. The pooled sample was resuspended in DMEM/F12 culture media to a final concentration of 100ug/ ml. Serial dilutions were then performed to prepare experimental groups of 1:100, 1:1000, and 1:10000 which correspond to physiologically relevant concentrations of approximately 10ug/cm2, 1ug/cm2, and 0.1ug/cm2 respectively. RLE-6TN cells were maintained and passaged in DMEM/F12 media supplemented with 10% FBS + 1%P/S. The particulate containing media was made fresh for each experiment, keeping total PM mass from the pooled filters consistent for each preparation. The fresh particulate containing media was then added directly to cell culture wells of varying substrate stiffnesses for subsequent different studies.

TGFβ activation assay:

RLE-6TN cells were cultured on Fn or Fn variant coated PA gels, Fn-coated glass, or Ln-coated glass with addition of particulate matter as described above. TGFβ activation was determined by a mink lung epithelial cell (MLEC) assay as previously described. MLECs stably transfected with an expression construct containing a truncated

Pai-1 promoter fused to the firefly luciferase reporter gene respond in a dose dependent manner to active TGFβ, but are incapable of activating TGFβ. After 5 days of RLE-6TN culture on the various substrates, MLECs were added at a density of 50,000 cells/cm2 on top of the RLE-6TN cells in serum free DMEM/F12 media + 1% BSA. Cells were co-cultured for 16 hours, lysed and luciferase activity was determined via the One-Glo luciferase assay (Promega). To determine total levels of TGFβ, samples were heated to 85°C for 10 minutes prior to plating of MLEC cells. To ensure PM alone did not activate TGF β, soluble TGF β was added along with PM as a control. Luminescence was measured with a Synergy H4 Multi-Mode Plate Reader (BioTek, Winooski, VT, USA). Luminescence values were normalized to MLECs cultured in the absence of TGFβ. Levels of active or total TGFβ activation were then calculated through interpolation using a standard curve. Results presented are from 3 independent triplicate experiments.

$DCFH_2$-DA Oxidation Assay for measuring ROS

Following culture for 5 days, cells were washed with HBSS, and incubated with 10uM $DCFH_2$-DA for 30 minutes at 37C to measure oxidation. Controls wells were included that were not incubated with any dye. After incubation, cells were washed in sterile HBSS and CM-$DCFH_2$ fluorescence was measured (excitation of 485/20nm filter and emission of 528/20nm filter). Cells were then washed again and incubated with 5ug/ml Hoescht 33342 for 30 minutes at 37C. The Hoescht fluorescence was measured (excitation of 350nm and an emission of 461nm). The CM-$DCFH_2$ fluorescence was normalized to the Hoescht reading to account for cell number.

Immunofluorescence staining for EMT markers and cell shape analysis:

Following culture for 5 days, cells were washed with PBS, fixed with 4% formaldehyde, permeabilized with 0.2% Triton-X 100 and then blocked with 10% goat serum. Primary anti-a-SMA (1A4, Sigma-Aldrich) or anti-E-cadherin (36/E-cadherin, BD Transduction Laboratories) antibodies were incubated overnight then washed thoroughly with PBS + 1.5% goat serum. Alexa-Fluor-488-conjugated goat-anti-mouse (Invitrogen) was used as the secondary antibody. To characterize cell shape, actin was stained with Texas-red phalloidin (Invitrogen) and nuclei were stained with Hoescht stain (Invitrogen). Images were acquired with a Nikon Eclipse (TiE) inverted fluorescence microscope at 20X magnification (PlanFluor 20X, 0.5 NA objective) with a CoolSNAP HQ2 Monochromatic CCD camera. Experiments were performed in triplicate, and images presented are representative from 5-10 random fields for each independent experiment. To characterize circularity, area and perimeter of individual cells stained for actin were determined for each condition using Image J (NIH Freeware) image processing software, then circularity was determined using the equation circularity = 4π(area/perimeter2). Three independent images were analyzed for each condition, and at least 10 cells were analyzed per image. Data is pooled from all 3 images analyzed per condition.

Immunoblot for EMT marker protein levels:

RLE-6TN cells were cultured for 5 days as described above then washed with PBS and cells lysed directly in Laemmli buffer containing protease inhibitors (Roche Applied Sciences). Total protein concentration was determined using the BCA protein quantification kit (Pierce Chemical Co.). Forty mg of total protein was separated by

electrophoresis on a 4-15% gel, then transferred to a nitrocellulose membrane using a semi-dry transfer system, blocked with 5% nonfat dry milk in TBS, then incubated with E-cadherin (36/E-cadherin), pan cytokeratin (5D3 + LP34, abcam, Cambridge, MA, USA), α-SMA (1A4), prolyl-4-hydroxylase (P4H; 1D3, Santa Cruz Biotechnology, Santa Cruz, CA, USA), or GAPDH (14C10, Cell Signaling Technologies, Boston, MA, USA) antibodies overnight at 4° C. Following washing with TBS + 0.1% Tween 20, membranes were incubated for 2 hours with IR secondary antibody (Licor), washed, and then imaged using the Odyssey IR scanner. Western blots were quantified using Image J image processing software, using GAPDH as the endogenous control.

AFM nanoindentation analysis:

RLE-6TN cells with or without the addition of each of the three concentrations of PM2.5 were cultured on 8kPa gels in a 0.17 mm thick glass-bottom petri dish (World Precision Instruments, Inc.). Using the Asylum MFP-3D-BIO AFM, single force points were measured from at least 5 peri-nuclear regions that were greater than 300 nm in height by force spectroscopy using contact mode at a scan rate of 1.2 Hz. The silicon nitride AFM tip (Veeco) was customized with a 4.74 μm diameter polystyrene bead to allow for imaging at appropriate resolution scales and for elastic modulus determination using the Hertz-contact model. Single cantilever's unique spring constants were determined using the thermal resonance frequency method, with values typically ranging 0.1 – 0.3 N/m. To determine the Young's modulus of each contact point, the Hertz-contact model for determining the elastic forces between two spheres was used (Eq. 1). Using known values from the AFM measurement (xs is scanner displacement; xc is the cantilever displacement; c.p. is the contact point) and predetermined values for the

cantilever spring constant (k) and beaded-tip radius, the elastic modulus can be solved for (E) (bead force, FB, is equal to k* xc). The assumption of an isotropic material or that Poisson's ration (ν) is equal to 0.5 is valid for the small indentation depths under operation.

$$\frac{E}{1-\nu^2} = \frac{3}{4}\frac{kx_c}{\sqrt{R}(x_s - x_c - c.p.)^{3/2}}$$

Eq. 1

Statistical Analysis:

All statistical analysis for 3 or more experimental groups was performed by two-way ANOVA using Prism (GraphPad Software Inc., La Jolla, CA, USA). Statistical significance between groups was determined by performing Tukey's post hoc analysis. All data is presented as mean +/- SEM and statistical significance is achieved for $p<0.05$.

Results

Particle Composition Monitor Set up

Particulate matter to be used in future analyses was collected from 1-March-2004 to 30-June-2004 using a filter based particle composition monitor (PCM) as part of the longer term ASACA program (164). The PCM is a 3 - channel system that collects 24 hour integrated samples for analysis of ionic, carbonaceous, and metallic species in the PM2.5 size range. The monitor is controlled by a data acquisition system (DAS) that activates sampling, sequences the filters and controls sample flow to a flow rate of 16.7 L/min through each channel. Filters were installed approximately one day prior to sampling and removed one day following exposure to ambient air. Ambient air was drawn through each channel of the monitor and then flowed through denuders for selective removal of gases, a WINS impactor for providing a 2.5um size cut, and finally

the sampling media. The PCM was mounted approximately 2.5 meters above ground (164).

In channel 1, the sampled air was passed through onto a single Teflon filter. PM2.5 captured on the Teflon filter is archived for exploratory analyses, such as this. Ionic species including sulfate, nitrate, and ammonium were collected on a nylon filter using channel 2. Finally, channel 3 was used for quantification of elemental and organic carbon. Regular maintenance of the PCM was performed over the collection period.

Particulate Matter Sample Analysis

The average PM over the period during which the filters were used in this analysis was 14.2 $\mu g/m^3$. Concentrations of water-soluble sulfate, nitrate and ammonium, as well as elemental and organic carbon were determined from filter samples collected using the ASACA PCM. In addition, data on these species, as well as from elemental analyses, were available from the nearby (approximately 30 m) monitoring site run by the Georgia Environmental Protection Division (GaEPD), which is also reported as part of the US EPA Air Quality System. While the ASACA data (and the filters used) are available every day during the period, the GaEPD samping is done every third day. **Table 5.1** summarizes the composition of these components from our filters as well as the data reported in AQS. The ionic and carbonaceous composition of the PM obtained from the nylon and Teflon filters shows that the bulk of the PM was sulfate and organic carbon **(Table 5.1),** with a significant fraction being elemental carbon. It is important to note that both our collected data and the reported data are highly similar and show approximately a 1:1 relationship as seen in **Figure 5.1**.

Table 5.1: Average Comparison of AQS and ASACA Particle Composition for Species of Interest

	SD AQS Data (ug/m3)					ASACA Data (ug/m3)				
	NH4	NO3	SO4	OC	EC	NH4	NO3	SO4	OC	EC
Average	1.22	0.73	3.86	4.70	0.95	1.40	0.65	4.12	4.92	0.80

A more complete presentation of the PM composition, including elemental concentrations observed at the GaEPD site and a comparison of the average ionic and carbonaceous PM concentrations for daily (e.g., corresponding to the samples used in the cellular exposure study) versus 1-in-3 day sampling (as used for the source apportionment) is contained in Appendix A.

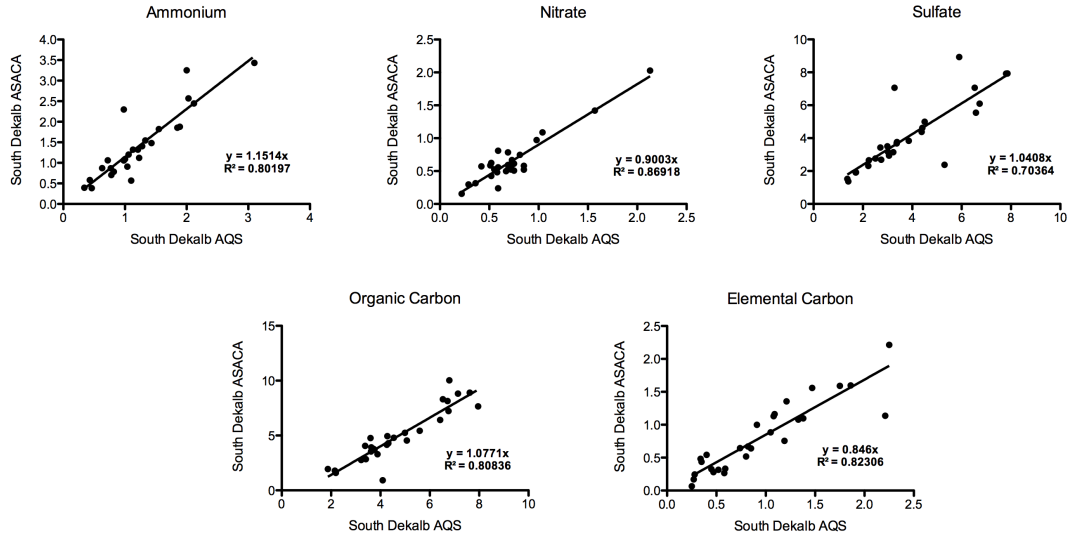

Figure 5.1: Major studied components of particulate matter are in agreement with previously reported measurements. Teflon filters from the South Dekalb area were collected and analyzed for ammonium, nitrate, sulfate, organic carbon, and elemental carbon. These results were compared to data from the Air Quality System for a similar sampling region. Our composition shows a nearly 1:1 agreement with the AQS data.

Source Apportionment Modeling of PM2.5

Measurements were used to conduct Chemical Mass Balance (CMB) source apportionment for the days that coincided with the samples used in this analysis as previously described (165) and where GaEPD data was available (i.e., every third day). The reason for conducting source apportionment when the GaEPD data is available is the need to have elemental species concentrations. The good agreement between the ASACA and GaEPD sampling, and their close proximity, suggest they are sampling from very similar air masses, and that the source apportionment conducted using the concentrations observed at the GaEPD site are applicable for the filters collected as part of the ASACA monitoring. On average, the most prominent sources for the resulting particulate matter were ammonium sulfate and bisulfate, largely due to coal burning in the region, which together comprised 38%, biomass burning at 20%, gasoline-fueled vehicles at 8%, and diesel vehicles at 9%. These results are summarized in **Table 5.2**. This source distribution is expected as coal is a major fuel-stock for electricity generation, the sampling site is near two freeways and the March-April months are when prescribed fires are most common in the Southeast.

Table 5.2: Average Source Apportionment for South Dekalb PM2.5 Collection

	GV	DV	DUST	BURN	COAL	AMSULF	AMBSULF	AMNITR	SOC
AVERAGE	10.01%	6.86%	4.70%	11.06%	0.83%	18.65%	26.64%	9.06%	12.19%

Results from the particle analysis show that the composition was primarily sulfate, related ammonium, and organic carbon, with smaller amount of elemental carbon, and that the primary sources were those leading to sulfate, biomass burning and mobile sources.

RLE-6TN cells are viable up to a concentration of 10ug/cm^2 of PM2.5

RLE-6TN cells were plates in 6 well plates at a density of 100,000 cells / cm^2 and allowed to attach for 24 hours, then treated with increasing concentrations of isolated PM2.5 for 24 hours. PM2.5 was isolated from the Teflon filters and diluted in cell culture media to concentrations of 0.01ug/cm^2, 0.1ug/cm^2, 1ug/cm^2, 5ug/cm^2, 10ug/cm^2, 25ug/cm^2, and 50ug/cm^2. These concentrations were picked based on previous literature suggesting these concentrations are generally within physiologically relevant ranges and that anything over 100ug/cm^2 has been shown to be toxic to cells **(cite).** After culture for 24 hours, the cells from each PM2.5 concentration group were trypsinized and resuspended in a 1:1 suspension with trypan blue. The suspension was analyzed by counting dead cells, which were stained blue, and normalizing to the total number of cells in each group.

As shown in **Figure 5.2**, over 99% of cells were viable up to a concentration of 10ug/cm^2. When the concentration was increased to 25ug/cm^2 and 50ug/cm^2, cell viability began to decline rapidly to only 83% and 56% of viable cells, respectively. From these viability results, a low, medium, and high concentration of PM2.5 exposure were chosen to explore in further studies. PM2.5 was isolated from the Teflon filters and added to cell culture media at 0.1ug/cm^2, 1ug/cm^{2,} and 10ug/cm^2 for all of the following described experiments.

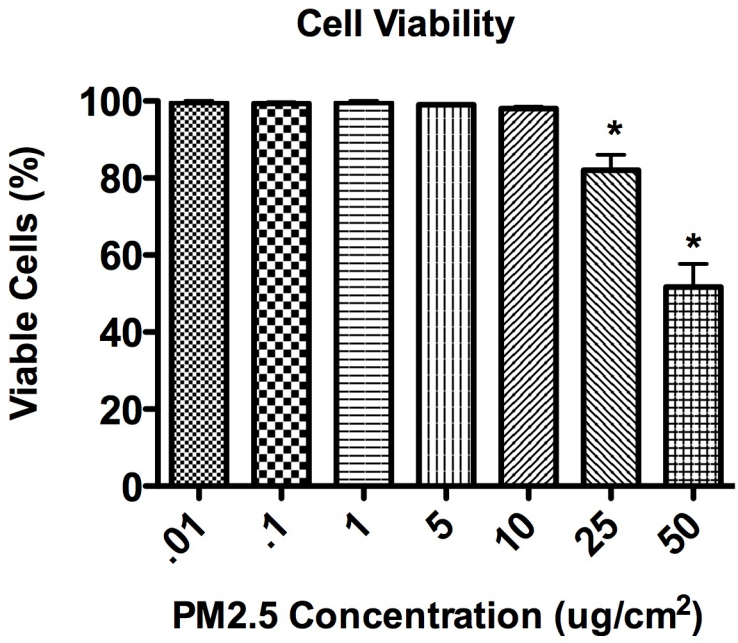

Figure 5.2: RLE-6TN cells are viable up to a concentration of 10ug/cm^2. RLE-6TN cells were cultured with increasing concentrations of isolated PM2.5 for 24 hours and analyzed using the trypan blue assay. Approximately 100% of cells were viable through a concentration of 10ug/cm^2. Treatment with concentrations above 10ug/cm^2 resulted in significant cell death. * ($p < .01$)

Addition of PM2.5 results in elongated cells and decreased circularity

In order to explore how exposure of RLE-6TN cells to PM2.5 in a range of different elastic moduli environments affects cell morphology, cells were cultured of polyacrylamide gels of varying substrate stiffness (2-24kPa) with or without the addition of PM2.5 at 10ug/ cm^2, 1ug/ cm^2, or 0.1ug/ cm^2 for five days. The cells were then fixed and stained with Texas Red-X conjugated phalloidin to visualize any changes in the actin cytoskeletal organization. Cells cultured on soft substrates and on Ln-coated glass without the addition of PM2.5 displayed the typical rounded epithelial morphology and diffuse cortical staining for actin **(Figure 5.3).**

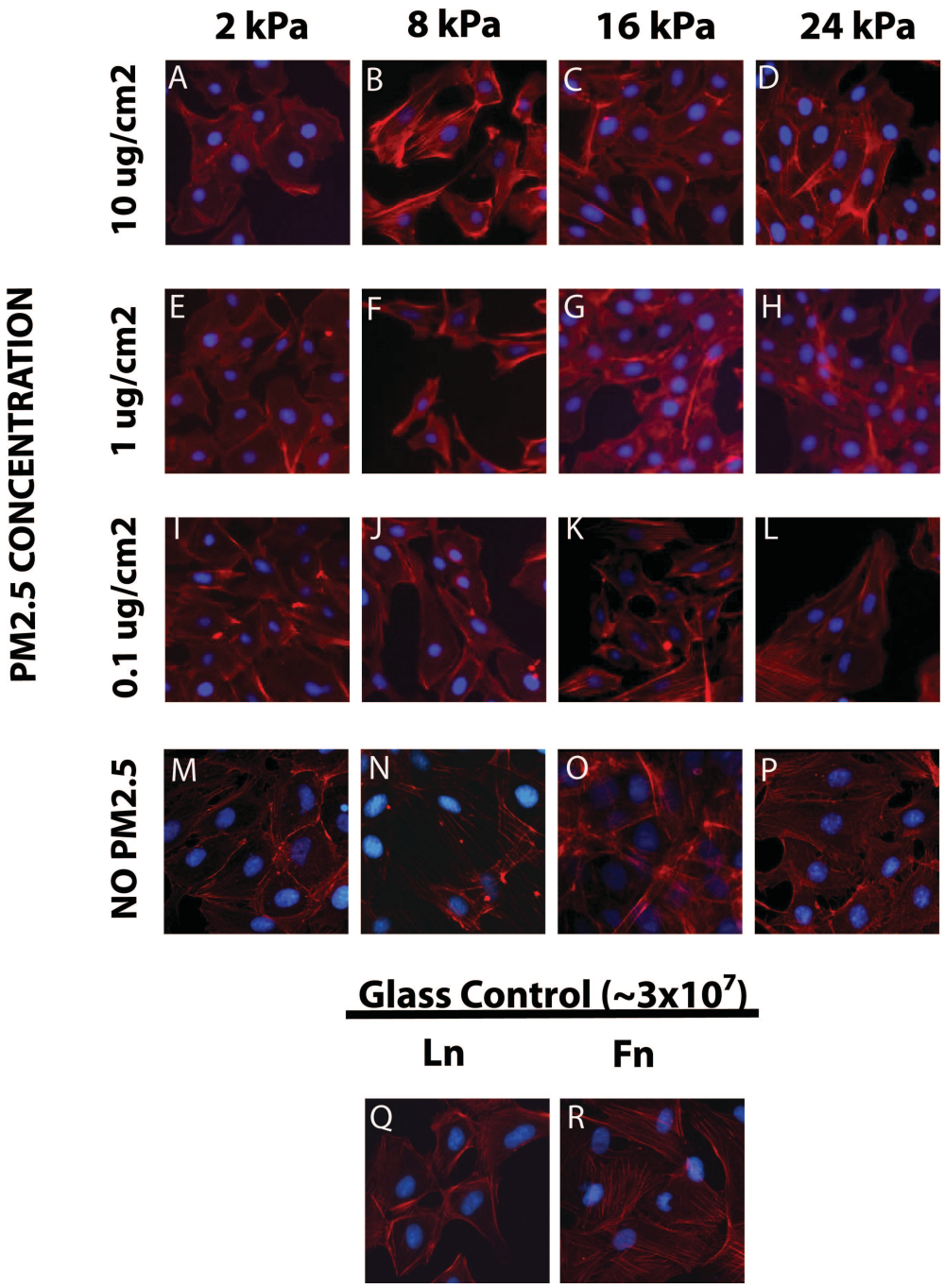

Figure 5.3: Addition of PM2.5 results in elongated cells and staining for stress fibers. RLE-6TN cells were cultured on Fn-PA gels or Fn- or Ln-coated glass for 5 days with the addition of 10ug/cm^{2,} 1ug/ cm^{2,} or 0.1ug cm^2 concentrations of PM2.5, and changes in the actin cytoskeleton were analyzed by staining actin filaments. Experiments were performed in triplicate, representative images are presented.

As substrate stiffness was increased, cells displayed a subsequent elongated morphology and thick, aligned actin filaments indicative of stress fibers. In addition, when PM2.5 was added to the cultures, most notably at the 10ug/ cm^2 concentration, cells exhibited enhanced staining for actin filament stress fibers. Notably, cells cultured on 8 kPa gels showed a considerable increase in actin fibers and cell elongation with the addition of PM2.5 when compared with matched substrate-stiffness controls **(Figure 5.3, panel B).** This substrate stiffness is of particular interest because it most closely matches that of slightly fibrotic lung tissue, indicating that PM2.5 may have more marked effects on a lung that is undergoing fibrotic remodeling. In addition, this increase appeared to be concentration dependent, with a slightly more cell elongation and stress fiber formation seen at the 10ug/ cm^2 concentration compared to 1ug/cm^2 and 0.1ug/cm^2 concentrations.

Finally, cell circularity was calculated to quantify differences in the observed cell shape. Values closer to 1 indicate a more rounded, epithelial like cell ***(*Figure 5.4*).*** Statistical significance is shown for each experimental group in comparison to its same substrate stiffness group with no PM2.5 added. These results show that the addition of PM2.5, most notably at the 10ug/cm^2 concentration result in decreased values of cell circularity.

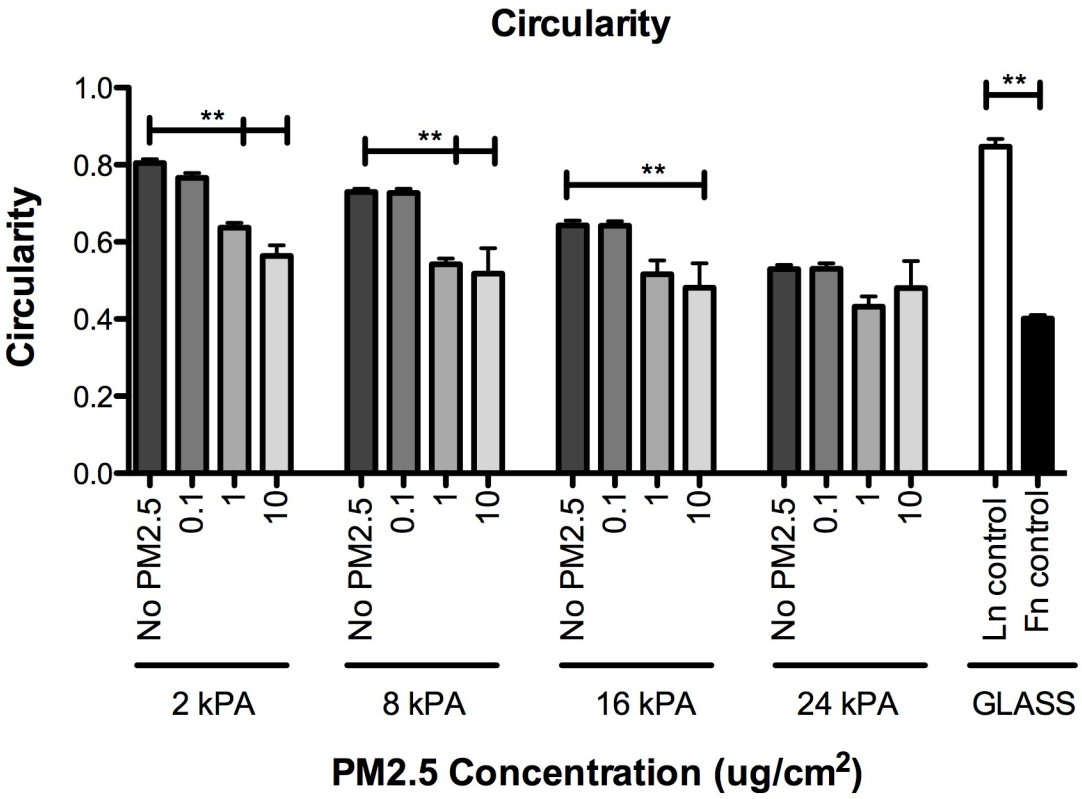

Figure 5.4: Cell circularity decreases when cultured with the addition of PM2.5. RLE-6TN cells were cultured on polyacrylamide gels of increasing stiffness, Fn or Ln coated glass. PM2.5 was added at varying concentrations for 5 days. Cells were fixed stained with Texas-red phalloidin to visualize the actin cytoskeleton and circularity analyzed. Values closer to 1 indicate a more rounded, epithelial like cell.

Increased cell elongation and stress fibers coincide with increased cell stiffness

Based on the observation that PM2.5 resulted in decreased cell circularity and increased stress fiber formation, most notably at the 8kPa substrate stiffness, it was investigated if these phenotypic observations coincided with an increase in cell stiffness. Previous studies have linked increased epithelial cell stiffness in increased substrate stiffnesses environments that are commonly seen during pulmonary fibrosis.

Furthermore, several studies have linked increased cell stiffness with increased cell contractility and TGF β activation (29).

Therefore, to explore if the addition of PM2.5 increased cell stiffness, RLE-6TN cells were cultured on Fn-cross-linked 8 kPa gels with the addition of 10ug/cm^2 , 1ug/ cm^2 , 0.1ug cm^2 , or no PM concentrations of PM2.5 and cell stiffness was measured by atomic force microscopy (AFM). It was observed that there was a concentration dependent increase in cell-stiffness with the addition of increasing amounts of PM2.5 when compared to the 8-kPa control. When cells were cultured with the addition of either 10ug/cm^2 or 1ug/ cm^2 concentrations of PM2.5, cortical cell stiffness was raised (average Young's Moduli of 2.8 kPa and 2.4kPa respectively) over cells that were cultured with the 0.1ug/ cm^2 concentration of PM2.5 or no addition of PM2.5 (Average Young's moduli of 1.5 kPa and 1.4 kPa respectively). Statistical significance is shown in comparison to the no PM2.5 added control **(Figure 5.5).** These results indicate that the addition of PM2.5 increases cell stiffness and agrees with the increase in cortical actin stress fibers and decreased circularity observed **(Figure 5.3, panels B, F, J, N, and Figure 5.4).**

Alveolar epithelial cells display increased TGFβ activation with the addition of PM2.5

Previous studies have shown that elevated levels on cell stiffness can lead to contractile forces by ultimately enabling the activation of latent TGFβ, a primary EMT inducer. Since we saw increases in cell-stiffness with the addition of PM2.5, we investigated if the addition of PM2.5 also resulted in differences in TGFβ activation, which could lead to further increased EMT events. To determine if addition of PM2.5 to alveolar cells on differing substrate stiffnesses induced TGFβ activation, the mink lung

epithelial reporter cell (MLEC) bioluminescence co-culture assay was performed for each PM2.5 concentration. Similar to the cell morphology experiments, RLE-6TN cells were cultured on PA gels ranging from 2-24 kPa with or without the addition of each concentration of PM2.5. In controls without the addition of PM2.5, alveolar epithelial cells were found to increasingly activate TGFβ in response to increases in substrate stiffness. As expected, the control groups cultured on Fn-coated glass exhibited high levels of TGFβ activation, while those cultured on Ln-coated glass showed significantly less levels. When PM2.5 was added to the cultures for 5 days, the cells were found to activate significantly greater amounts of TGFβ in a dose dependent manner **(Figure 5.6).**

Of particular interest was the comparison of TGFβ activation across the PM2.5 concentrations at 8 kPa, a physiologically relevant stiffness during the progression of human lung fibrosis. At this substrate stiffness with the addition of PM2.5, we observed an increase in TGFβ activation similar to what was observed on high substrate stiffness and Fn-coated glass without the PM2.5**.** PM2.5 addition to a solution of inactive TGFβ was found insufficient to activate TGFβ strongly suggesting that increases in TGFβ activation observed are mediated by the cells. Statistical significance is for each experimental group compared within its same substrate stiffness.

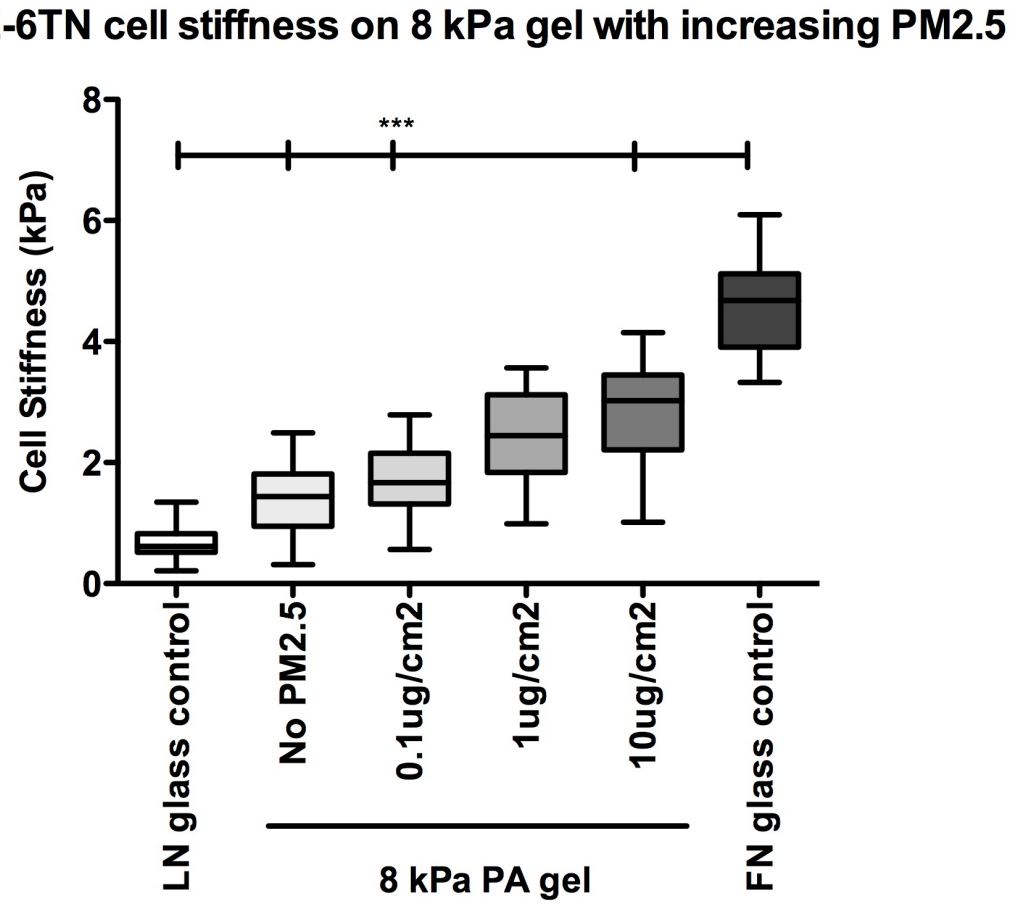

Figure 5.5: RLE-6TN cell stiffness increases on same substrate stiffness with the addition of PM2.5. RLE-6TN cells were cultured for 5 days on 8kPa polyacrylamide gels with or without the addition of PM2.5. Single cell elasticity was measured with AFM nanoindentation to characterize cell stiffening in response to substrate stiffness and PM2.5. Averages of cell stiffness for each PM2.5 concentration are presented. Significance is reported for differences shown between PM concentrations ($p < 0.01$).

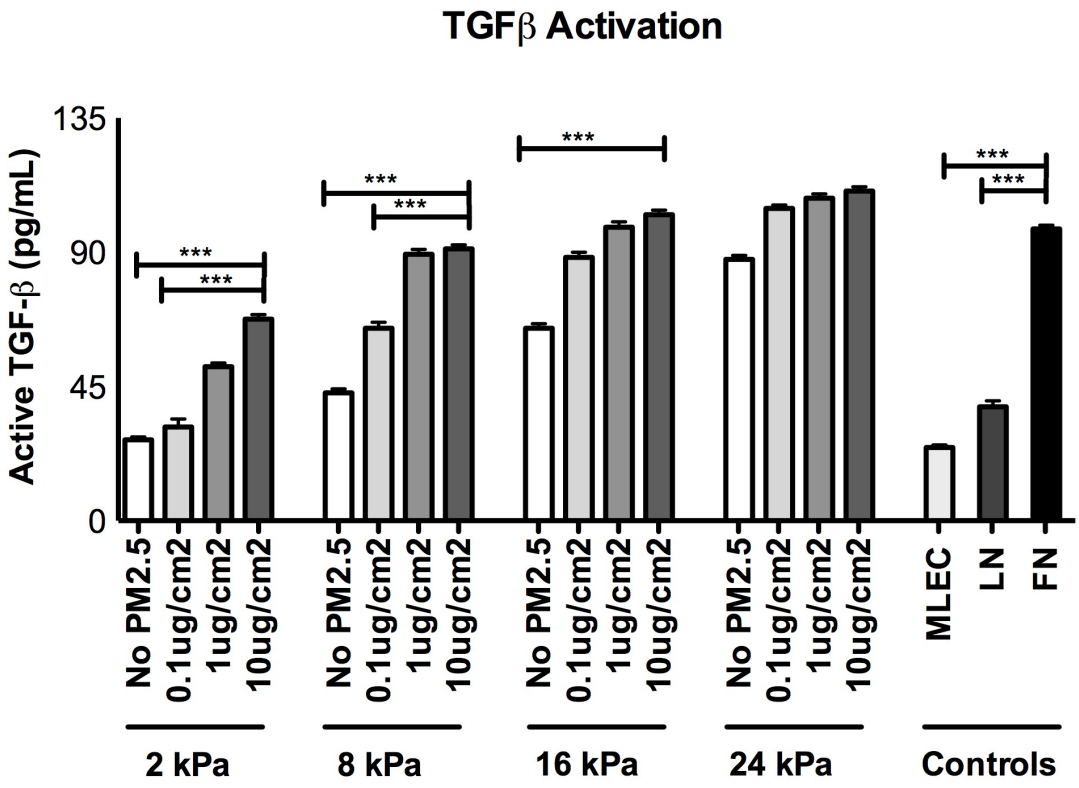

Figure 5.6: Stiffness-mediated activation of TGFβ is increased by addition of PM2.5. RLE-6TN cells were cultured for 5 days on substrates of increasing stiffness with or without the addition of each concentration of PM2.5 and levels of TGFβ activation were determined using the MLEC bioluminescence co-culture assay. Statistical significance is shown for each concentration of PM2.5 within its same substrate stiffness (*** $p < .01$).

Addition of PM2.5 exacerbates stiffness-mediated EMT

As described throughout this work, TGFβ is a potent inducer of EMT. In this work, we have shown that the addition of PM2.5 results in an elongated cellular phenotype that displays actin stress fibers, increased cortical cell stiffness, and increased TGFβ activation. Therefore, experiments were performed to confirm that these characteristics also coincide with increased EMT. As described in the previous experiments, RLE-6TN cells were cultured on increasing substrate stiffness PA gels with or without the addition of each concentration of PM2.5 for 5 days and analyzed for EMT responses by immunohistochemistry **(Figure 5.7)** and western blotting **(Figure 5.8, 5.9).** As previously mentioned, alveolar epithelial cells undergo EMT on Fn-coated glass while they maintain an epithelial phenotype on Ln-coated glass coverslips. These conditions were used as controls. As expected, EMT was observed on Fn-coated glass as indicated by high expression of alpha-smooth muscle actin (α-SMA) and low levels of e-cadherin at cell-cell contacts. Conversely, cells cultured on Ln-coated glass showed an epithelial phenotype as indicated by low levels of α-SMA and maintenance of expression of e-cadherin at cell-cell contacts **(Figure 5.7).**

Cells cultured without PM2.5 that were stained for either epithelial or mesenchymal markers after 5 days, showed a loss of epithelial markers and subsequent gain of mesenchymal markers as substrate stiffness was increased. This effect was enhanced with the addition of PM2.5. **Figure 5.9** demonstrates that when PM2.5 was added at a $10ug/cm^2$ concentration, the alveolar cells showed an increase in the expression of α-SMA at lower substrate stiffnesses when compared to stiffness-matched

controls (no PM2.5 added). In addition, there appears to be a concentration threshold of PM2.5, which is correlated with the observed increase in EMT.

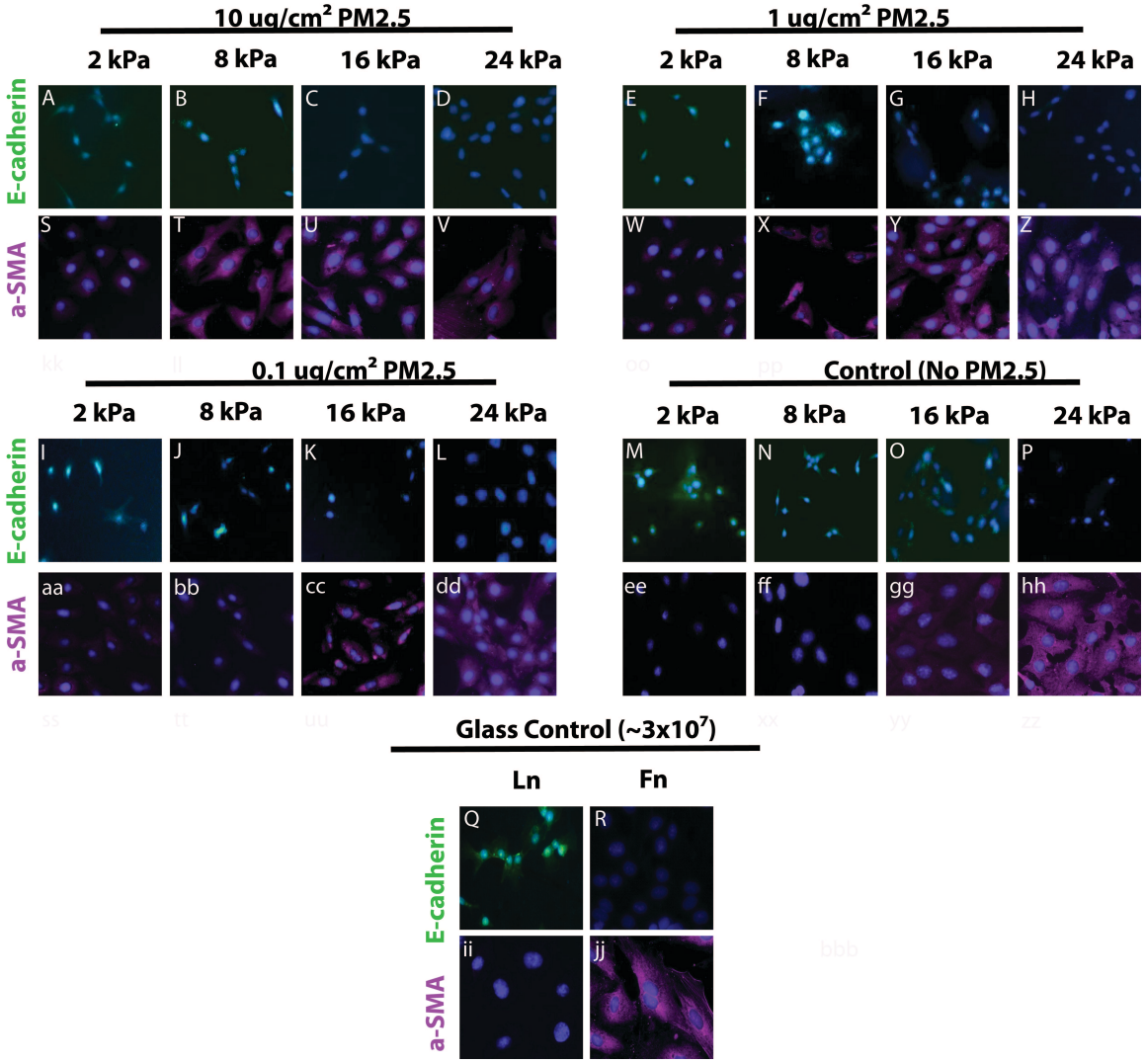

Figure 5.7. Alveolar epithelial cells show enhanced α - SMA staining in response to PM2.5 exposure. RLE-6TN cells were cultured on Fn-PA gels or Fn- or Ln-coated glass for 5 days with the addition of 10ug/cm^{2,} 1ug/ cm^{2,} or 0.1ug cm^{2} concentrations of PM2.5. Cells were fixed and immunohistochemistry for e-cadherin (epithelial) and α - SMA (mesenchymal) was performed. Experiments were performed in triplicate, representative images are presented.

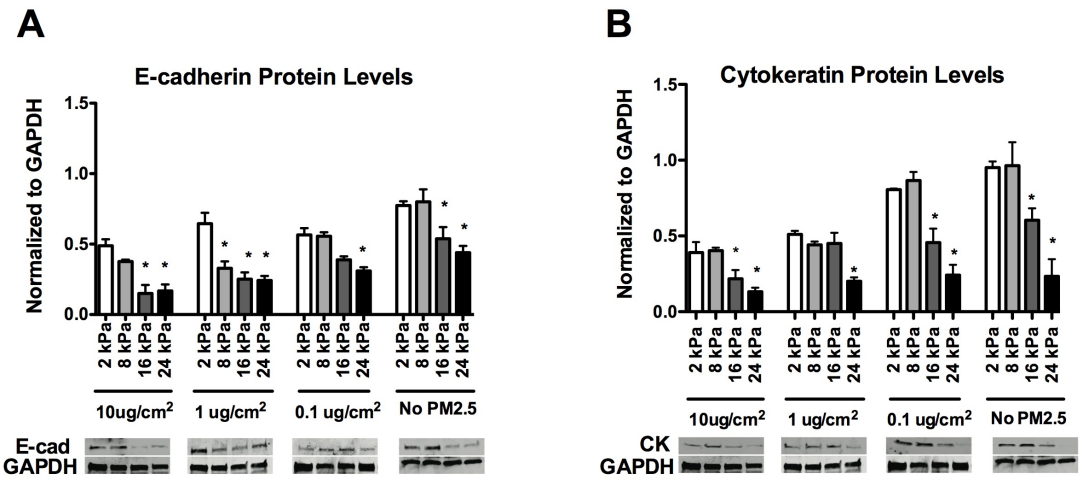

Figure 5.8. Analysis of epithelial protein markers with the addition of PM2.5. RLE-6TN cells were cultured in increasing substrate stiffnesses with or without the addition of each concentration of PM2.5 and analyzed for changes in e-cadherin (A) and cytokeratin (B) protein levels. Three independent triplicate experiments were performed and significance is shown for each group compared to the same treatment on 2kPa gel. (* p< 0.1)

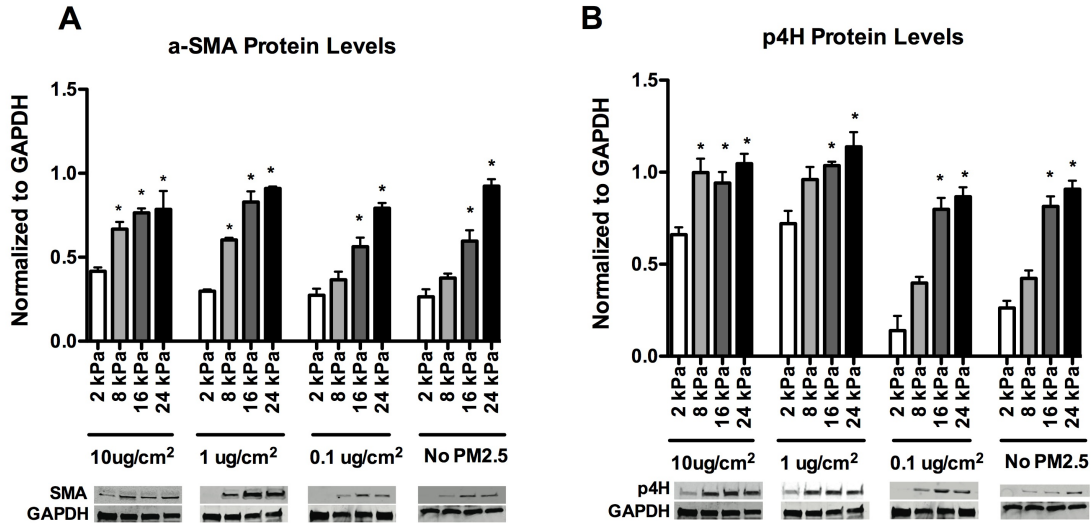

Figure 5.9. Analysis of mesenchymal protein markers with the addition of PM2.5. RLE-6TN cells were cultured in increasing substrate stiffnesses with or without the addition of each concentration of PM2.5 and analyzed for changes in alpha-smooth muscle actin (A) and prolyl-4-hydroxylase (B) protein levels. Three independent triplicate experiments were performed and significance is shown for each group compared to the same treatment on 2kPa gel. (* p< 0.1)

Exposure to PM2.5 results in increased TGFβ activation without cell contractility

The results thus far have indicated that exposure of RLE-6TN cells to PM2.5, most significantly at concentrations of 10ug/cm2, result in phenotypes consistent with EMT. Briefly, cells exhibit increase stress fiber formation, increased cell stiffness, increased TGFβ activation, and simultaneous down regulation of epithelial protein markers and up regulation of mesenchymal markers. EMT is highly dependent on cell contractility, allowing for a mechanically driven activation of TGFβ that subsequently drives EMT. Therefore, the MLEC assay that measures TGFβ activation was performed again with the same protocol but with the addition of the ROCK contractility inhibitor Y-27632 during the 5-day culture.

In the presence of the contractility inhibitor, Y-27632, cells that were not treated with PM2.5 activated low levels of TGF β despite what substrate stiffness they were cultured on. However, there were significant increases in TGF β activation with the addition of 10ug/cm2 PM2.5 on all substrate stiffnesses **(Figure 5.10).** These results suggest that inhibition of cell contractility is sufficient to inhibit substrate mediated TGF β activation, but not sufficient to inhibit TGF β activation mediated by the exposure of PM2.5. A control where PM2.5 was added to a solution of inactive TGFβ was found insufficient to activate TGFβ, again suggesting that these increases in TGFβ activation observed due to PM2.5 are still mediated by the cells, just not by cell contractility. This data indicates that there may be a second, non-mechanical mechanism of TGFβ activation that occurs when the cells are exposed to PM2.5.

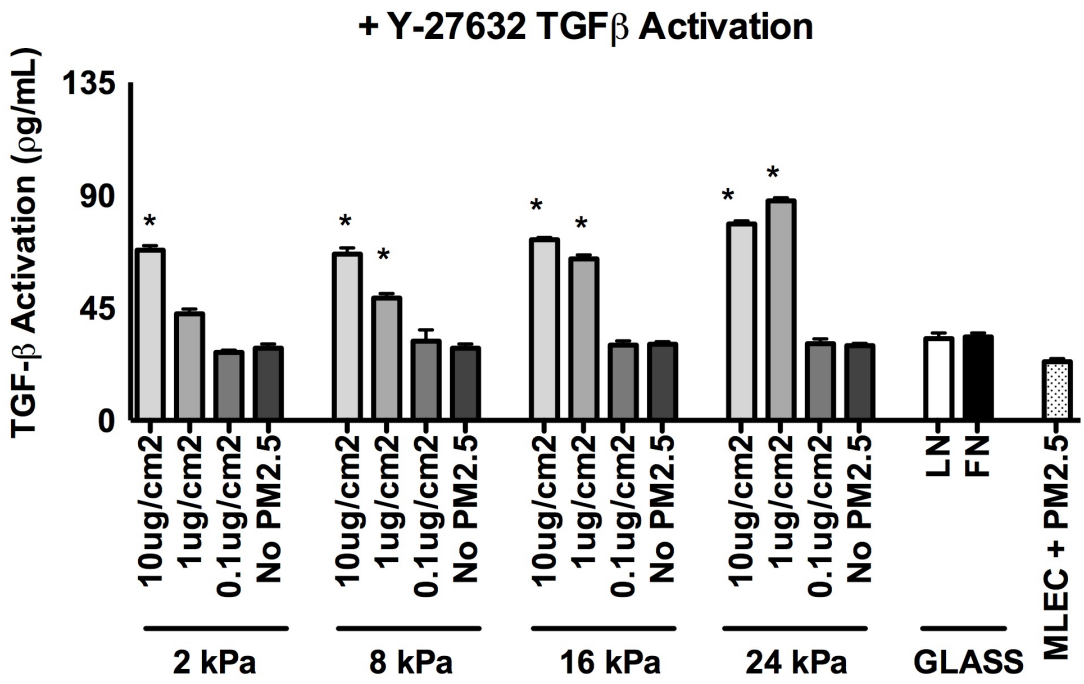

Figure 5.10: TGFβ Activation is only partially mediated by cell contractility with PM2.5 exposure. RLE-6TN cells were cultured in each condition with the addition of the ROCK inhibitor, Y-27632, for 5 days and analyzed for TGFβ activation using the MLEC assay. Statistical significance is reported for differences between same substrate stiffness conditions. (* $p < 0.01$)

FnIII9*10 reduces TGFβ activation caused to PM2.5 and substrate - stiffness

Data presented previously suggested that engagement of the matrix through α3/α5 integrins could mediate EMT events, notably TGF β activation, even on increased substrate stiffnesses. Therefore, it was investigated if this observation still held true when the cells were exposed to PM2.5. RLE-6TN cells were cultured on PA-gels ranging from 2 to 24 kPa that were cross-linked with either FnIII9*10 (predominant α3 integrin engagement) or FnIII9^{4G}10 (predominant αv integrin engagement) with or without the addition of 10ug/cm^2 PM2.5.

When RLE-6TN cells exposed to PM2.5 were also cultured on the FnIII9*10 variant, there was a partial reduction in TGFβ activation, but not to the level observed without any PM2.5 exposure **(Figure 5.11, A).** Significance is shown for comparisons between PM2.5 added groups with or without culture on the Fn variant. This further suggests that there is a secondary mechanism activating TGFβ due to exposure of cells to PM2.5. Interestingly, when cells were cultured on the FnIII9^{4G}10 variant, similar levels of TGFβ activation were observed with and without the addition of PM2.5 **(Figure 5.11, B)**. This similar activation profile suggests that there is a maximum level of TGFβ that these cells can activate, despite the mechanism of activation.

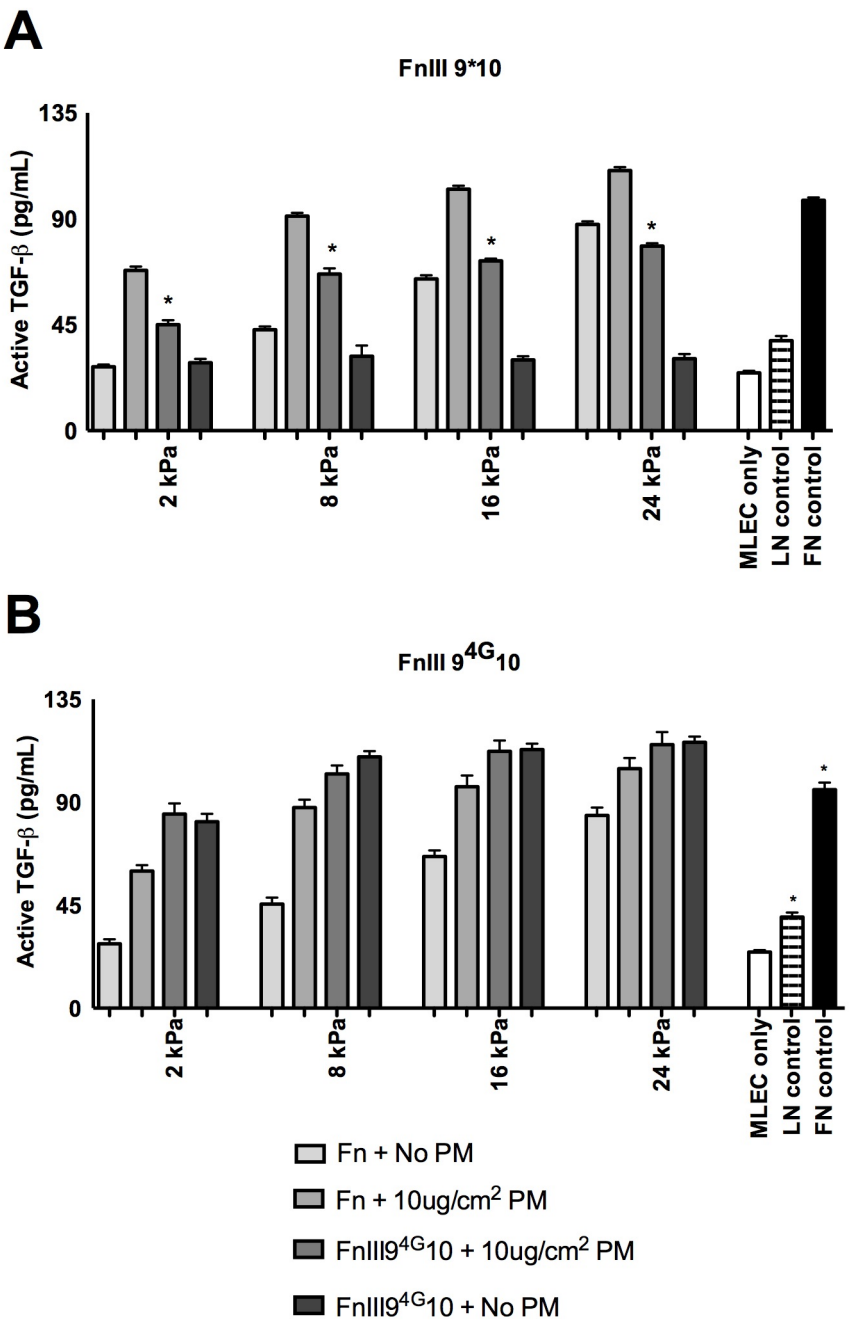

Figure 5.11: FnIII9*10 significantly reduces the effect on substrate-stiffness + PM2.5 activation of TGFβ. RLE-6TN cells were cultured on 1) Fn-coated PA gels of increasing substrate stiffness 2) Fn-coated PA gels with the addition of 10ug/cm^2 PM2.5, 3) Fn-variant coated PA gels, or 4) Fn-variant coated gels with the addition of 10g/cm^2 PM2.5 and analyzed for levels of TGFβ activation using the MLEC assay. Significance is shown for comparisons between the PM2.5 added groups with or without culture on the Fn variant. (* $p < .01$)

Exposure of RLE-6TN cells to PM2.5 results in increased levels of ROS

Finally, it was hypothesized that the observed additional activation of TGF β when cells were exposed to PM2.5 was due to intracellular production of reactive oxygen species. In order to explore this hypothesis, RLE-6TN cells were cultured on PA gels of increasing substrate-stiffness with or without exposure to 10ug/cm^2 of PM2.5 and analyzed by the DCFH$_2$-DA assay, which measures total levels of intracellular ROS. On each different group of gel stiffnesses, an increase in ROS was observed with the addition of PM2.5 **(Figure 5.12).** Interestingly, there was an increase in ROS solely due to increased substrate stiffness (no PM2.5 added). This suggests that increased tissue stiffness commonly seen in pulmonary fibrosis patients likely results in increased intracellular ROS levels and that exposure of the distal lung to PM2.5 significantly increases these levels of ROS.

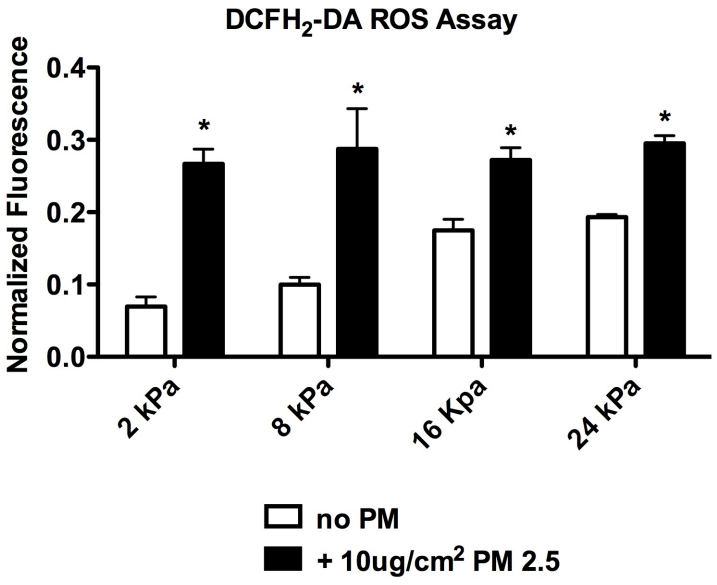

Figure 5.12: Exposure of RLE-6TN cells to PM2.5 increases intracellular ROS. RLE-6TN cells were cultured on PA gels of increasing substrate stiffness with or without 10ug/cm2 PM2.5 and intracellular ROS levels were measured by the DCFH$_2$-DA oxidation assay. * ($p < .01$)

ROS levels are mediated by treatment with antioxidants NAC and glutathione

Several studies have suggested antioxidants including N-acetyl-cysteine (NAC) and glutathione, may be effective in decreasing levels of ROS within lung tissue. Therefore, it was explored if treatment with NAC or glutathione was able to decrease the increase in ROS that was observed due to the exposure of cells to PM2.5. Similar to the previous experiment, RLE-6TN cells were cultured on increasing substrate stiffnesses with or without the addition of PM2.5 In addition, groups with PM2.5 added were either treated with NAC or glutathione. For each of the experimental groups, treatment with either NAC or glutathione drastically reduced the levels of intracellular ROS observed with exposure to PM2.5 **(Figure 5.13).** Notably, on higher substrate stiffnesses, i.e. 16 and 24 kPa, these antioxidants were able to reduce the ROS levels below the levels seen without the addition of PM2.5. This suggests that substrate stiffness alone is capable of inducing increases in intracellular ROS, and that this effect can be mitigated by treatment with these antioxidants.

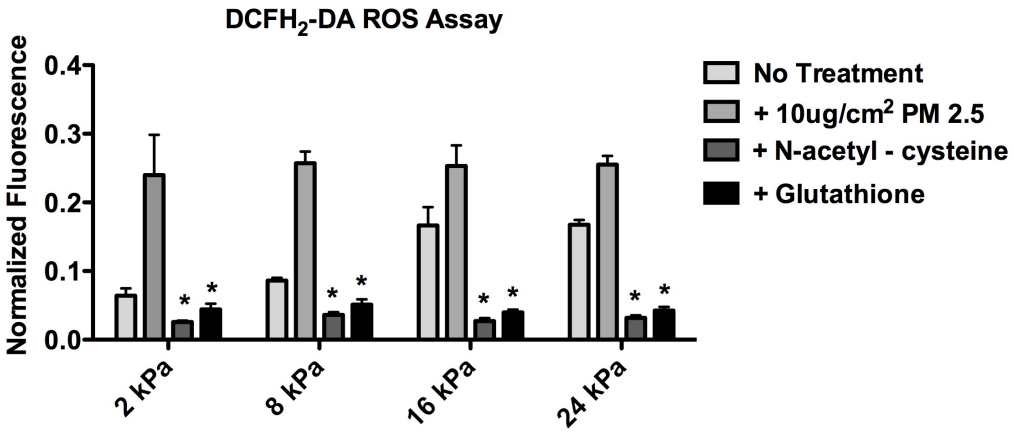

Figure 5.13: The antioxidants NAC and glutathione reduce intracellular ROS levels. RLE-6TN cells were cultured on 2-24 kPa gels with or without 10ug/cm2 PM2.5 and treatment with either NAC or glutathione. Three independent triplicate experiments were performed and significance is shown for antioxidant groups in comparison to PM2.5 treated cells at each substrate stiffness. * ($p < .01$)

α3 integrin engagement and N-acetyl-cysteine treatment abrogate increased levels of TGFβ activation due to increased substrate stiffness and PM2.5 exposure

Previous data and the experiments thus far have strongly suggested that increased substrate stiffness is able to induce cell contractility leading to mechanical activation of TGFβ and that cellular engagement of the matrix through a3 integrin can reduce this increased activation. Furthermore, when alveolar epithelial cells are exposed to PM2.5 there were even further increases in TGFβ activation than were seen on increased substrate stiffness alone. Finally, exposure to PM2.5 results in increased intracellular ROS levels, suggesting a possible second mechanism of TGFβ activation through oxidation of the LAP. It was found these increased levels of ROS could be drastically reduced with antioxidant treatments.

It was hypothesized that by altering the biochemical properties of the matrix to engage α3 integrin by utilizing the FnIII9*10 variant, while also treating the cells with NAC, TGFβ activation levels could be decreased to a level seen on laminin (i.e. levels seen from healthy epithelial cells). RLE-6TN cells were cultured on polyacrylamide gels of increasing substrate stiffness under several conditions: 1) Fn, 2) FnIII9*10, 3) Fn + 10ug/cm^2 PM2.5, 4) FnIII9*10 + 10ug/cm^2 PM2.5, 5) Fn + 10ug/cm^2 + NAC, and 6) FnIII9*10 + 10ug/cm^2 + NAC. TGFβ activation levels for the first four groups closely matched the results previously seen. Cells cultured on full length Fn with PM2.5 that were treated with NAC had decreased levels of TGFβ activation compared to cells cultured on Fn and PM2.5, but not a complete reduction to the level seen from cells cultured on Ln or 2 kPa. When cells were cultured on the FnIII9*10 and were treated with NAC, there was a complete reduction in TGFβ to levels similar to cells cultured on

Ln despite what substrate stiffness they were cultured on **(Figure 5.14).** These results taken together strongly suggest that increased tissue stiffness results in increased cell contractility and a preference to engage the matrix through αv integrin, which mechanically activates TGFβ; while exposure to PM2.5 further increases this TGFβ activation by increasing intracellular ROS and oxidizing the LAP. These events appear to have an additive effect on the activation of TGFβ and result in the significant increases observed in EMT events.

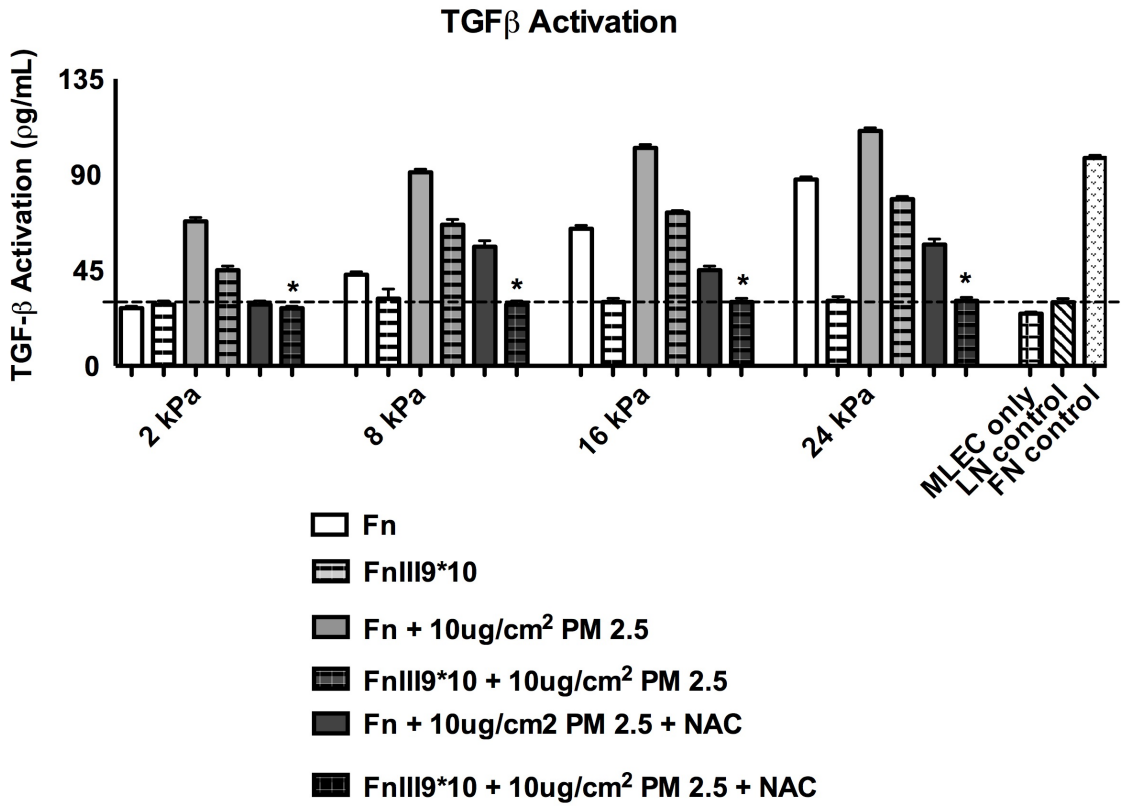

Figure 5.14: FnIII9*10 and NAC treatment restore low levels of TGFβ activation seen on epithelial maintaining substrates. RLE-6TN cells were cultured on increasing substrate stiffnesses with or without the epithelial maintaining variant FnIII9*10 cross linked to the surface and exposed to PM2.5 with or without treatment with the antioxidant NAC. Three independent triplicate experiments were performed. * ($p < 0.1$).

Discussion

EMT has been implicated as a critical process in the progression of invasive pathologies such as pulmonary fibrosis. Therefore, it is imperative that the process is fully understood in different pathological conditions in order to give insight for future therapeutic options. Several studies have previously shown that the micromechanical environment that alveolar epithelial cells interact with is a strong driving force for activating TGFβ and driving EMT by itself. Here it was shown that in addition to increased tissue stiffness, exposure to environmental stimuli, such as PM2.5, is involved in further increasing TGFβ and driving EMT events.

Immunohistochemistry, cell phenotypic analyses, and western blotting for EMT protein markers, show that at higher concentration of PM2.5 (10ug/cm2), mesenchymal markers are more highly expressed on lower substrate stiffness, which lacked mesenchymal marker expression before PM2.5 treatment. In addition, it was observed that PM2.5 was involved in the increase of epithelial cell cortical stiffness. This increase in cortical cell stiffness was hypothesized to lead to cell contraction, which can in turn mechanically activate the cytokine TGFβ, which is known to be a potent inducer of EMT. Experiments were performed where cell contractility was blocked by the ROCK inhibitor Y-27632 and TGFβ activation was measured by the MLEC assay. Interestingly, when cells were treated with 10ug/cm^2 PM2.5, inhibition of cell contractility was able to decrease TGFβ activation levels, but not to the level seen without PM2.5 exposure. This indicates that there is a second mechanism, not dependent on cell contraction and mechanical stimulus, with which TGFβ is activated in response to PM2.5 exposure. The hypothesis that a second mechanism of TGFβ activation is involved was further

confirmed by studies where alveolar epithelial cells exposed to PM2.5 were cultured on the α3 engaging matrix variant FnIII9*10. Similar results were observed to the cell contractility inhibitor study, where the FnIII9*10 variant was able to decrease TGFβ activation, but not to a level observed without the addition of PM2.5, further suggesting that PM2.5 activates TGFβ by a secondary, non-mechanical mechanism.

The alveolar epithelium forms a continuous, highly regulated physical barrier, which serves as a protector against inhaled environmental agents, including PM2.5. During EMT, the tight cell junctions and E-cadherin expression commonly seen in the epithelium are lost. This loss of structure has been implicated in the allowance of enhanced signaling between the epithelium and underlying immune cells (166). Previous studies have implicated enhanced immune cell activation and inflammation in the release of ROS that leads to the activation of TGFβ, (89, 98, 99, 167) and TGFβ itself is known to be able to induce ROS production as part of its signal transduction pathway. Therefore, ROS were determined to be a likely culprit for the further increase in TGFβ activation that was observed that could not be abrogated by the inhibition of cell contractility. First, total levels of intracellular ROS with or without the addition of 10ug/cm2 PM2.5 were measured on substrate stiffnesses ranging from 2 to 24 kPa. Significant increases in ROS were observed on each substrate stiffness when cells were exposed to PM2.5 Interestingly, as substrate stiffness was increased, there was a decreased difference between the non-treated and PM2.5 added groups. This indicated that substrate stiffness alone likely has an effect on increasing ROS levels. Next, it was explored if treatment with common antioxidants could decrease the levels of ROS observed with PM2.5 exposure. When the cells were treated with either NAC or glutathione in conjunction with

PM2.5 exposure, ROS levels were significantly decreased. Notably, on stiffer substrates, the antioxidant treatment decreased intracellular ROS to levels lower than seen on the matched substrate stiffness without the addition of PM2.5. This data further suggested that substrate stiffness alone is capable of increasing levels of ROS.

A recent pulmonary fibrosis drug trial that utilized treatment with the antioxidant N-acetyl-cysteine showed some benefit in delaying the progression of pulmonary fibrosis, but was not able to restore lung function or reverse any damage currently present (152). From the data presented, it is not surprising that NAC treatment alone was not a fully successful treatment, since it has clearly been shown that the mechanical environment is a crucial mediator of TGFβ activation, progression of EMT, and the subsequent onset of a fibrotic scar. Therefore, in a final experiment, it was explored if combinatorial treatment with the antioxidant NAC in conjunction with engagement of the epithelial maintaining matrix variant FnIII9*10, could mediate the significantly increased levels of TGFβ activation previously observed with epithelial cells cultured on increased substrate stiffness and exposed to PM2.5. When alveolar epithelial cells were cultured on FnIII9*10 and treated with NAC, levels of TGFβ were decreased to levels seen from cells cultured on laminin, the known epithelial maintaining substrate. This level of TGFβ activation was seen despite the stiffness of the substrate that cells were cultured on. This final piece of data strongly suggests that TGFβ activation is mediated by a combination of mechanical stimuli, i.e. tissue stiffness, and changes in the intracellular levels of ROS. Importantly, this result starts to explain why the clinical trial utilizing treatment with NAC alone was not highly effective.

This work shows that alveolar epithelial cells exhibit increased cell stiffness, TGFβ activation, and EMT events in response to PM2.5 exposure. These results highlight the importance of studying not only the micromechanical environment in lung disease but also the exposure to environmental injury adjuvants in already diseased lung models. Previous findings have indicated that increased tissue stiffness is able to lead to increased cell contraction, TGFβ activation, and subsequent EMT and represents one of the initial stages of pulmonary fibrosis (58, 61). Here these findings are expanded and show that in addition to the delicate balance between ECM stiffness, TGFβ, and EMT, exposure to environmental stimuli, such as PM2.5, additionally mediates this interaction through increased levels of intracellular ROS. Furthermore, it appears that there is an additive effect on TGFβ activation from mechanical stimuli and ROS from environmental stimuli, resulting in significantly increased EMT events.

Finally, it is shown that by controlling *both* the micromechanical environment through a3 integrin engaging substrates and reducing intracellular levels of ROS, that TGFβ activation can be reduced to levels typically seen in healthy epithelial cells. This work suggests that PM2.5 has a role in additionally driving a pre-existing fibrotic phenotype in pulmonary cells and that approaches to treat pulmonary fibrosis must focus on controlling both the micromechanical stimuli presented to alveolar epithelial cells while also controlling the oxidative effect of increased ROS. Future work should focus on further elucidation of the pathways that both tissue stiffness and PM2.5 engage to initiate the EMT program and additionally how these pathways intersect in order to develop novel treatment therapies for pulmonary fibrosis.

CHAPTER 6

FUTURE CONSIDERATIONS

Idiopathic pulmonary fibrosis is a chronic, progressive, untreatable disease, characterized by the emergence of mesenchymal cells and alterations in the ECM that result in increased tissue stiffness. Classically, changes in the ECM have been considered the final result of fibrosis. However, recently a much more active role for the ECM is starting to emerge. Both the biophysical and biochemical properties of the matrix can influence cellular processes relevant in the development of fibrosis, such as the emergence of a myofibroblastic population through EMT.

Specifically, the mechanical properties of the fibrotic ECM have the ability to affect cell behavior. In fibrosis, there is a notable increase in tissue stiffness, largely due to the deposition of increased amounts of unstructured extracellular matrix proteins as well as increased crosslinking of collagen and elastin due to an up regulation of lysyl oxidase. Numerous studies have shown that this increased matrix rigidity results in cells matching their cytoskeletal tension to their external environment and activating increased levels of latent TGFβ, the potent inducer of EMT (29, 30). Interestingly, cellular fibronectin binds to lysyl oxidase with high affinity (99) and crosslinking of the matrix by lysyl oxidase producing ROS, which can in turn activate TGFβ (95, 98). In addition, biochemical changes, such as the emergence of a provisional matrix composed predominantly of fibrin-fibronectin during wound healing and pathogenesis can lead to marked changes in cell behavior and phenotype. Studies from Kim et al showed that *in vitro,* ATII cells undergo spontaneous EMT in response to fibrin-fibronectin matrices but

not in response to laminin-collagen matrices through a mechanism involving αvβ6 integrin mediated activation of TGFβ (142). Furthermore, here it is shown that variations in the 9th and 10th type III repeats of fibronectin that closely model folded or unfolded states of Fn, determine integrin specific cell attachment, and result in marked cellular phenotype differences. Notably, cells that predominantly attach and engage the underlying matrix through α3 integrins (FnIII9*10) maintain a rounded, epithelial morphology, while predominantly αv integrin engagement (FnIII^{4G}10) results in elongated cells and intense actin staining typical of more mesenchymal-like cells. Taken together, it is clear that during the development of fibrosis, the cells and the matrix form an interactive system. This reciprocal interaction between the matrix properties and the cell may result in a positive feedback loop; amplifying fibrotic disease progression. By understanding the fine control of the biophysical and biochemical properties of the matrix and how they interact together to control cell phenotype, new, targeted therapeutics for pulmonary fibrosis may be developed that are more effective.

In Aim 1 of this work it is shown that both the biochemical and biophysical properties of the ECM play a role in activation of the EMT program. Interestingly, the data suggest that neither the conformation of Fn nor the substrate rigidity is fully a dominant effector of EMT and that there appears to be an integrated response to combinations of integrin engagement and compliance matching. The first major contribution of this work is the finding that while increased tissue rigidity can induce TGFβ activation and subsequent EMT, integrin specificity can highly modulate this response. Most notably, it is shown that on stiff matrices with elastic moduli in the range of fibrotic lung tissue (16 kPa), that sustained α3β1 integrin engagement by ATII cells,

results in low levels of TGFβ activation and maintenance of an epithelial phenotype, despite the increased tissue stiffness. Alternatively, cells cultured on soft matrices that engage αv integrins, activate increased levels of TGFβ and undergo EMT. From a therapeutic standpoint, these results suggest that a simple option for fibrosis treatment would be administration of a αv-blocking antibody. However, a major difficulty with this approach is the large chance of side effects, due to the ubiquitous expression and function of αv integrins within human tissues. Although more complicated, a possible effective solution may be to target the conformation of Fn in the underlying matrix in order to stabilize the integrin binding domains in the 9^{th} and 10^{th} type III repeats. As shown in this work, this would result in sustained α3β1 integrin engagement and maintenance of an epithelial phenotype halting ECM production and concomitant tissue stiffening.

In addition to therapeutic options, the results presented here have large implications on biomaterial design. Biomaterials often elicit fibrotic responses, which are characterized by excessive deposition of ECM and stiffening of the surrounding tissue, exhibiting many similarities to other fibrotic pathologies, including pulmonary fibrosis. The literature has clearly shown that EMT occurs in response to increasingly rigid materials, likely perpetuating the fibrotic response and further stiffening the tissue. Therefore, to design effective materials, minimizing this response is desirable. This work suggests that addition of engineered ECM variants, such as the FnIII9*10 fragment, on the surface of the biomaterial may be able to modulate the formation of a fibrotic capsule commonly seen after implantation.

Additionally, these results lend themselves to applications for directing cell fate in tissue regeneration applications. Although this work has highlighted the role of EMT in

pathological progression, it is also known to be an important transition in development and regeneration of several tissues. The finding that epithelial cells can undergo EMT on soft substrates with the proper integrin engagement may lead to interesting approaches for biomaterial design. Specifically, these integrin specific fragments could be exploited in tissue engineering applications that aim to create complex tissues where epithelial and mesenchymal cells need to be in close proximity. For example, a soft biomaterial could be patterned with both the epithelial promoting variant (FnIII9*10) and the mesenchymal promoting fragment (FnIII9^{4G}10) in distinct spatial orientations. This further understanding of the interaction between the biophysical and biochemical properties of the matrix is a first step to developing new therapeutic options and novel tissue engineering strategies.

It is evident that major alterations in the ECM of the lung during the onset and progression of fibrosis are pivotal in directing cell fate through cellular processes such as EMT. However, alterations in the matrix are not the only factors involved in the progression of fibrotic diseases. Notably, the tissue of the lung is distinctive from many other epithelial tissues due to its high exposure to damaging stimuli from environmental components and these components have been linked to the progression of pulmonary disease. The work in this dissertation shows that in addition to increased matrix rigidity, repeated injury to ATII cells by exposure to PM2.5 further increases TGFβ and EMT and that this response is in part due to increased levels of ROS. Interestingly, it is shown that ATII cells cultured in the presence of PM2.5 on soft matrices exhibited increased contractility, TGFβ activation, and underwent EMT. It was hypothesized that the α3 engaging matrix variant FnIII9*10 would be able to modulate this response. However, it

was observed that culture on FnIII9*10 resulted in a decrease in the increased TGFβ activation levels, but not to the level seen without PM2.5 exposure, suggesting that there is likely an additional mechanism of TGFβ activation that acts synergistically to further drive EMT. The results further indicate ROS are increased not only in response to PM2.5 exposure, but also increased matrix rigidity. These findings are critical because ROS have been reported to activate TGFβ on their own. This suggests a paradigm connecting exposure of PM2.5 and the progression of lung fibrosis where initial insults of injury from PM2.5 would set off an inflammatory response, recruiting matrix-producing fibroblasts while also raising ROS levels allowing for latent TGFβ activation and subsequent ATII cell EMT. This initial cascade would result in a significantly increased population of cells laying down an abundance of ECM, ultimately increasing the matrix rigidity. This increase in rigidity would then be sensed by surrounding epithelial cells, resulting in additional EMT, leading to more ECM producing fibroblasts which would further drive the fibrotic diseased state **(Figure 6.1).** This information stresses the need to focus on the presence of positive feedback loops that amplify cell and matrix changes in both basic biologic studies as well as in the design of therapeutics for fibrotic diseases. Specifically, targeting at the level of this reciprocal cell-matrix interaction may lead to more effective treatments that focusing on the properties of the cell or microenvironment alone. Future studies that measure specific changes in matrix production due to exposure to PM2.5 may help to elucidate these interactions further.

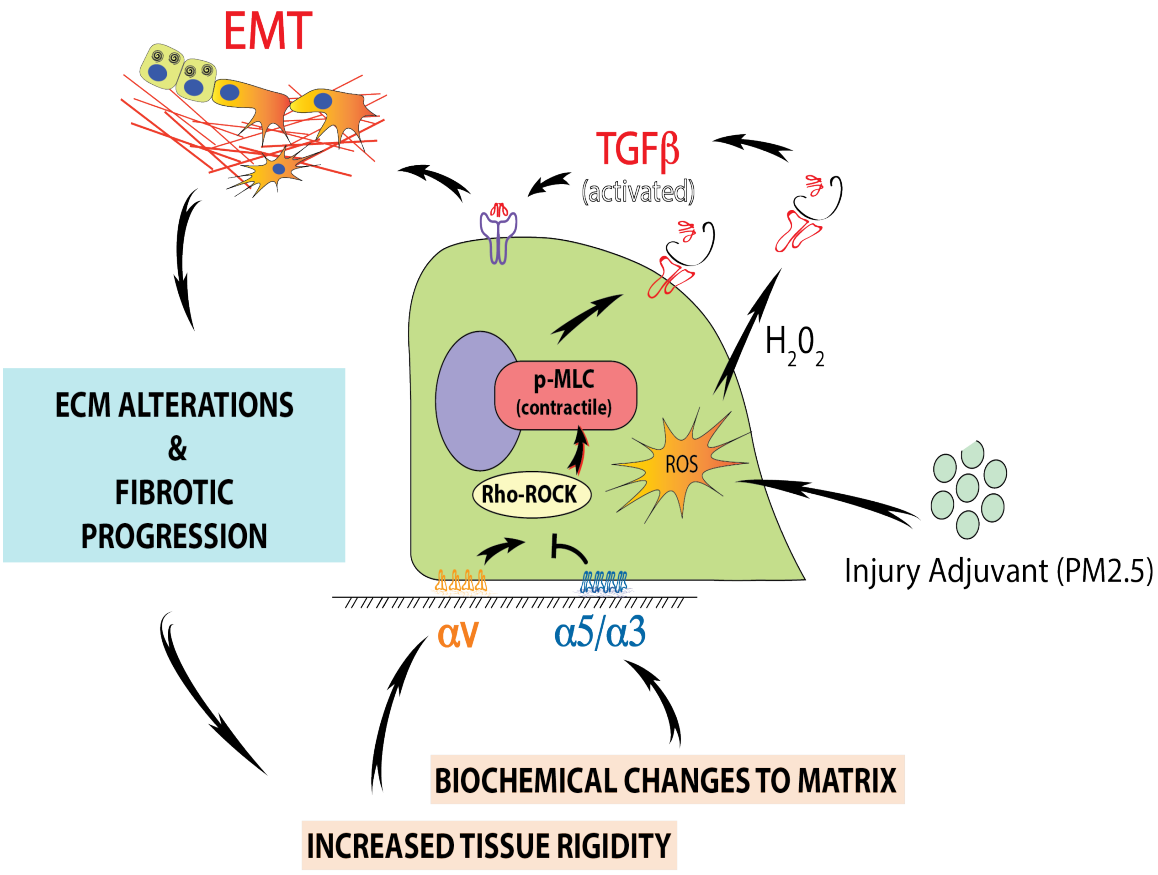

Figure 6.1. Schematic of positive feedback interactions that contribute to the progression of lung fibrosis. Initial insults of injury and αv integrin engaging matrices can activate latent TGFβ driving EMT. This process leads to further changes of the biochemical and biophysical properties of the matrix, which can drive cell contractility and additional TGFβ activation.

In patients, IPF is diagnosed at a late stage of disease progression due to the lack of symptoms until the lungs lose vital capacity. Due to this late diagnosis, the etiology of IPF is largely unknown, specifically about earlier stages of the disease. These studies focus largely on how already altered matrix properties drive ATII cell phenotype and the progression of fibrosis. While these studies have implications in halting the progression of fibrosis, future studies focused towards understanding earlier stages of the disease may have more promise towards completely healing those with IPF. In this work it is shown that there is a delicate balance between the properties of the matrix, ATII cell injury, and EMT. It appears that there is a threshold of these signals that must be met to drive EMT. We can speculate that a similar threshold may need to be met to initiate fibrosis, such that there may be light, transient states of fibrosis that are able to be resolved as well as progressive states of fibrosis that actually present in the clinic. It can be hypothesized that the progressive fibrosis may be a result of more severe and/or repeated injury events where a certain threshold of signals stimulates a strong positive feedback loop resulting in a "point of no return" which is suggested in this work. Alternatively, progressive fibrosis may be due to a lack of ability to resolve fibrosis possibly due to genetic predisposition or other secondary effects. Taking these possibilities into consideration future work should aim to explore 1) what is the key factor / factors in determining the "point of no return"? 2) How can recovery take place in a transient model? Specifically, what is able to interrupt the positive feedback loop characteristic of fibrosis demonstrated in this work? and 3) does the composition and state of the matrix change differently in transient vs. progressive models of fibrosis. Answers to these questions would provide

significant additional information to the results provided in this dissertation, and taken together, provide promising new leads for treatment options for lung fibrosis.

In conclusion, this dissertation shows for the first time that a fine balance between integrin specific engagements to Fn and substrate rigidity influences alveolar epithelial cell EMT, and that this balance can be shifted by additional injury events. The EMT observed due to the properties of the matrix are likely due to an increase in cell contractility, resulting in TGFβ activation, while exposure to PM2.5 results in additional TGFβ activation through increased levels of ROS. This work highlights that EMT is a complicated process resulting from changes in the biochemical and biophysical properties of the surrounding ECM as well as external stimuli. Additionally, it is shown that there is likely a certain threshold of pro-EMT signals that must be reached for ATII cells to undergo a transition, and that this threshold is not predominantly controlled by any single factor. However, this work suggests that these main drivers of EMT are interrelated and likely result in a strong positive feedback loop of pro-fibrotic signals leading to the severe progression of pulmonary fibrosis. Therefore, new potential treatments should focus on the interaction between the multiple drivers of EMT in order to interrupt this feedback loop. Finally, the findings that show that integrin specific engagement is able to drive differential ATII cell phenotypes on a single matrix rigidity offer the potential for new designs of cell instructive matrices and provide insight into designing more effective biomaterials.

APPENDIX A

SOUTH DEKALB PARTICULATE MATTER ELEMENT ANALYSIS

DATE	SD_NH4(ug/m3)	SD_Ca(ug/m3)	SD_K(ug/m3)	SD_Na(ug/m3)	SD_Ace(ug/m3)	SD_Cl(ug/m3)	SD_Form(ug/m3)
03/01/04	0.5822	0.0000	0.0381	0.1720	0.0235	0.1441	0.0000
03/04/04	1.2026	0.0000	0.0949	0.2121	0.0547	0.0744	0.0000
03/07/04	0.3956	0.0000	0.0220	0.0293	0.0000	0.1404	0.0000
03/10/04	1.8549	0.0000	0.0222	0.0094	0.0209	0.0000	0.0000
03/13/04	0.8667	0.0000	0.0322	0.0142	0.0711	0.0000	0.0000
03/16/04	1.0595	0.0000	0.0515	0.0419	0.0208	0.0588	0.0000
03/19/04	0.9079	0.0000	0.0262	0.0085	0.0509	0.0000	0.0000
03/22/04	1.4044	0.0000	0.0343	0.0486	0.0435	0.0000	0.0097
03/25/04	1.1221	0.0000	0.0588	0.0655	0.1044	0.0000	0.1389
03/28/04	0.8728	0.0000	0.0223	0.0700	0.0562	0.0000	0.0552
03/31/04	1.0926	0.0000	0.0402	0.0638	0.0071	0.0087	0.0000
04/03/04	1.3214	0.0000	0.0235	0.0578	0.0337	0.0000	0.0439
04/06/04	0.3844	0.0000	0.0145	0.0000	0.0000	0.0074	0.0000
04/09/04	1.5284	0.0000	0.0419	0.0159	0.0463	0.0000	0.0481
04/12/04	3.4317	0.0000	0.0539	0.0092	0.0640	0.0000	0.0691
04/15/04	0.7053	0.0000	0.0238	0.0088	0.0303	0.0000	0.0283
04/18/04	1.4805	0.0000	0.0822	0.0391	0.0697	0.0000	0.0611
04/21/04	0.7844	0.0000	0.0427	0.1219	0.0247	0.0000	0.0528
04/24/04	1.5439	0.0000	0.0786	0.1277	0.1495	0.0000	0.1742
04/27/04	1.0638	0.0000	0.0242	0.0237	0.0391	0.0000	0.0538
04/30/04	2.5667	0.0000	0.0553	0.2240	0.2215	0.0000	0.1345
05/03/04	1.3231	0.0000	0.0000	0.0000	0.0716	0.0000	0.0436
05/09/04	2.2487	0.0000	0.0527	0.0451	0.1322	0.0000	0.1241
05/12/04	2.3511	0.0000	0.0248	0.0619	0.1136	0.0000	0.1537
05/15/04	0.9264	0.0000	0.0187	0.1440	0.0251	0.0000	0.0061
05/18/04	0.8941	0.0000	0.0441	0.0793	0.0895	0.0000	0.0744
05/21/04	2.3969	0.0000	0.0185	0.0543	0.1445	0.0000	0.1302
05/24/04	1.8217	0.0000	0.0337	0.2081	0.1628	0.0000	0.1548
05/27/04	1.8289	0.0000	0.0348	0.1450	0.1124	0.0000	0.1250
05/30/04	1.3446	0.0000	0.0899	0.1688	0.1188	0.0000	0.1151
Average	1.3769	0.0000	0.0400	0.0757	0.0701	0.0145	0.0599
Standard Deviaton	0.695163471	0	0.023019435	0.068795152	0.054358474	0.03865411	0.058364848

SD_NO3(ug/m3)	SD_NO2(ug/m3)	SD_Oxalate(ug/m3)	SD_SO4 (ug/m3)	OC(ug/m3)	EC(ug/m3)
0.5218	0.0000	0.0510	1.9194	3.7767	0.3264
0.5796	0.0000	0.1938	3.7654	10.0305	1.5901
0.1549	0.0000	0.0000	1.3725	4.0551	1.1624
1.4188	0.0000	0.0000	4.6216	3.9131	0.6443
1.0879	0.0000	0.0220	1.9098	5.4367	0.3329
0.4262	0.0000	0.1071	3.1579	5.2483	0.6416
0.5570	0.0000	0.0885	2.9364	8.3052	2.2129
0.9724	0.0101	0.0477	3.5045	1.5912	0.2440
0.6131	0.0733	0.1705	3.6767	8.9087	0.7542
0.5921	0.0228	0.1945	2.6550	7.2370	1.0973
0.7470	0.0000	0.0522	2.7627	1.9392	0.5436
0.6678	0.0159	0.0948	3.7424	2.7707	0.3162
0.2960	0.0121	0.0591	1.5176	4.5491	1.5603
0.5665	0.0324	0.1097	4.8397	5.3699	1.1097
2.0284	0.0317	0.2089	7.9279	4.7972	0.2665
0.5262	0.0112	0.0648	2.3165	3.7095	0.9992
0.5723	0.0142	0.1869	4.9996	8.8146	1.0789
0.4980	0.0000	0.1423	2.6911	4.2996	0.5176
0.7845	0.3712	0.2602	4.3773	8.1461	1.5976
0.4831	0.0000	0.0887	3.1429	3.2957	0.8845
0.5078	0.0000	0.1944	7.0653	2.8399	0.0646
0.3165	0.0000	0.0577	3.8384	1.7928	0.4822
0.8004	0.0020	0.3159	6.3695	9.7642	0.5648
0.5203	0.0000	0.1454	6.5548	3.3388	0.1054
0.5831	0.0000	0.0906	3.0929	3.3611	0.1762
0.4855	0.0000	0.1025	3.1017	3.7464	0.8950
0.7246	0.1963	0.2012	7.7311	8.5583	2.0416
0.5863	0.0000	0.1779	6.0983	4.9453	1.3560
0.4686	0.0000	0.1627	5.6452	4.4140	0.7130
0.6115	0.0000	0.1588	4.8632	3.5952	0.3991
0.6566	0.0264	0.1250	4.0732	5.0850	0.8226
0.352049804	0.075236106	0.076751541	1.811524864	2.46084107	0.567014298

REFERENCES

1. Buttery RC, Rintoul RC, Sethi T. Small cell lung cancer: The importance of the extracellular matrix. *Int J Biochem Cell Biol* 2004;36(7):1154-1160.

2. Cox TR, Erler JT. Remodeling and homeostasis of the extracellular matrix: Implications for fibrotic diseases and cancer. *Dis Model Mech*;4(2):165-178.

3. Hallgren O, Nihlberg K, Dahlback M, Bjermer L, Eriksson LT, Erjefalt JS, Lofdahl CG, Westergren-Thorsson G. Altered fibroblast proteoglycan production in copd. *Respir Res*;11:55.

4. Horowitz JC, Martinez FJ, Thannickal VJ. Mesenchymal cell fate and phenotypes in the pathogenesis of emphysema. *COPD* 2009;6(3):201-210.

5. Spruit MA, Janssen DJ, Franssen FM, Wouters EF. Rehabilitation and palliative care in lung fibrosis. *Respirology* 2009;14(6):781-787.

6. Engler AJ, Griffin MA, Sen S, Bonnemann CG, Sweeney HL, Discher DE. Myotubes differentiate optimally on substrates with tissue-like stiffness: Pathological implications for soft or stiff microenvironments. *J Cell Biol* 2004;166(6):877-887.

7. Engler AJ, Sen S, Sweeney HL, Discher DE. Matrix elasticity directs stem cell lineage specification. *Cell* 2006;126(4):677-689.

8. Liu Q, Mao H, Nie J, Chen W, Yang Q, Dong X, Yu X. Transforming growth factor {beta}1 induces epithelial-mesenchymal transition by activating the jnk-smad3 pathway in rat peritoneal mesothelial cells. *Perit Dial Int* 2008;28 Suppl 3:S88-95.

9. Paszek MJ, Zahir N, Johnson KR, Lakins JN, Rozenberg GI, Gefen A, Reinhart-King CA, Margulies SS, Dembo M, Boettiger D, et al. Tensional homeostasis and the malignant phenotype. *Cancer Cell* 2005;8(3):241-254.

10. Pelham RJ, Jr., Wang Y. Cell locomotion and focal adhesions are regulated by substrate flexibility. *Proc Natl Acad Sci U S A* 1997;94(25):13661-13665.

11. Pelham RJ, Jr., Wang YL. Cell locomotion and focal adhesions are regulated by the mechanical properties of the substrate. *Biol Bull* 1998;194(3):348-349; discussion 349-350.

12. Wozniak MA, Desai R, Solski PA, Der CJ, Keely PJ. Rock-generated contractility regulates breast epithelial cell differentiation in response to the physical properties of a three-dimensional collagen matrix. *J Cell Biol* 2003;163(3):583-595.

13. Smith ML, Gourdon D, Little WC, Kubow KE, Eguiluz RA, Luna-Morris S, Vogel V. Force-induced unfolding of fibronectin in the extracellular matrix of living cells. *PLoS Biol* 2007;5(10):e268.

14. Levental KR, Yu H, Kass L, Lakins JN, Egeblad M, Erler JT, Fong SF, Csiszar K, Giaccia A, Weninger W, et al. Matrix crosslinking forces tumor progression by enhancing integrin signaling. *Cell* 2009;139(5):891-906.

15. Santhanam L, Tuday EC, Webb AK, Dowzicky P, Kim JH, Oh YJ, Sikka G, Kuo M, Halushka MK, Macgregor AM, et al. Decreased s-nitrosylation of tissue transglutaminase contributes to age-related increases in vascular stiffness. *Circ Res*;107(1):117-125.

16. Baneyx G, Baugh L, Vogel V. Fibronectin extension and unfolding within cell matrix fibrils controlled by cytoskeletal tension. *Proc Natl Acad Sci U S A* 2002;99(8):5139-5143.

17. Krammer A, Craig D, Thomas WE, Schulten K, Vogel V. A structural model for force regulated integrin binding to fibronectin's rgd-synergy site. *Matrix Biol* 2002;21(2):139-147.

18. Friedland JC, Lee MH, Boettiger D. Mechanically activated integrin switch controls alpha5beta1 function. *Science* 2009;323(5914):642-644.

19. Herard AL, Pierrot D, Hinnrasky J, Kaplan H, Sheppard D, Puchelle E, Zahm JM. Fibronectin and its alpha 5 beta 1-integrin receptor are involved in the wound-repair process of airway epithelium. *The American journal of physiology* 1996;271(5 Pt 1):L726-733.

20. Margadant C, Sonnenberg A. Integrin-tgf-beta crosstalk in fibrosis, cancer and wound healing. *EMBO Rep*;11(2):97-105.

21. Birchmeier C, Birchmeier W, Brand-Saberi B. Epithelial-mesenchymal transitions in cancer progression. *Acta Anat (Basel)* 1996;156(3):217-226.

22. Chaffer CL, Thompson EW, Williams ED. Mesenchymal to epithelial transition in development and disease. *Cells Tissues Organs* 2007;185(1-3):7-19.

23. Geiser T. Idiopathic pulmonary fibrosis--a disorder of alveolar wound repair? *Swiss Med Wkly* 2003;133(29-30):405-411.

24. Lopez-Novoa JM, Nieto MA. Inflammation and emt: An alliance towards organ fibrosis and cancer progression. *EMBO Mol Med* 2009;1(6-7):303-314.

25. Thiery JP, Acloque H, Huang RY, Nieto MA. Epithelial-mesenchymal transitions in development and disease. *Cell* 2009;139(5):871-890.

26. Thiery JP, Sleeman JP. Complex networks orchestrate epithelial-mesenchymal transitions. *Nat Rev Mol Cell Biol* 2006;7(2):131-142.

27. Zeisberg M, Neilson EG. Biomarkers for epithelial-mesenchymal transitions. *J Clin Invest* 2009;119(6):1429-1437.

28. Wu Z, Yang L, Cai L, Zhang M, Cheng X, Yang X, Xu J. Detection of epithelial to mesenchymal transition in airways of a bleomycin induced pulmonary fibrosis model derived from an alpha-smooth muscle actin-cre transgenic mouse. *Respir Res* 2007;8:1.

29. Brown AC, Fiore VF, Sulchek TA, Barker TH. Physical and chemical microenvironmental cues orthogonally control the degree and duration of fibrosis-associated epithelial-to-mesenchymal transitions. *J Pathol* 2013;229(1):25-35.

30. Kim KK, Kugler MC, Wolters PJ, Robillard L, Galvez MG, Brumwell AN, Sheppard D, Chapman HA. Alveolar epithelial cell mesenchymal transition develops in vivo during pulmonary fibrosis and is regulated by the extracellular matrix. *Proc Natl Acad Sci U S A* 2006;103(35):13180-13185.

31. Jain R, Shaul PW, Borok Z, Willis BC. Endothelin-1 induces alveolar epithelial-mesenchymal transition through endothelin type a receptor-mediated production of tgf-beta1. *Am J Respir Cell Mol Biol* 2007;37(1):38-47.

32. Kasai H, Allen JT, Mason RM, Kamimura T, Zhang Z. Tgf-beta1 induces human alveolar epithelial to mesenchymal cell transition (emt). *Respir Res* 2005;6:56.

33. Park SH, Choi MJ, Song IK, Choi SY, Nam JO, Kim CD, Lee BH, Park RW, Park KM, Kim YJ, et al. Erythropoietin decreases renal fibrosis in mice with ureteral obstruction: Role of inhibiting tgf-beta-induced epithelial-to-mesenchymal transition. *J Am Soc Nephrol* 2007;18(5):1497-1507.

34. Taipale J, Saharinen J, Keski-Oja J. Extracellular matrix-associated transforming growth factor-beta: Role in cancer cell growth and invasion. *Adv Cancer Res* 1998;75:87-134.

35. Willis BC, Borok Z. Tgf-beta-induced emt: Mechanisms and implications for fibrotic lung disease. *Am J Physiol Lung Cell Mol Physiol* 2007;293(3):L525-534.

36. Xu J, Lamouille S, Derynck R. Tgf-beta-induced epithelial to mesenchymal transition. *Cell Res* 2009;19(2):156-172.

37. Yao HW, Xie QM, Chen JQ, Deng YM, Tang HF. Tgf-beta1 induces alveolar epithelial to mesenchymal transition in vitro. *Life Sci* 2004;76(1):29-37.

38. Annes JP, Munger JS, Rifkin DB. Making sense of latent tgfbeta activation. *J Cell Sci* 2003;116(Pt 2):217-224.

39. Barcellos-Hoff MH, Dix TA. Redox-mediated activation of latent transforming growth factor-beta 1. *Mol Endocrinol* 1996;10(9):1077-1083.

40. Munger JS, Huang X, Kawakatsu H, Griffiths MJ, Dalton SL, Wu J, Pittet JF, Kaminski N, Garat C, Matthay MA, et al. The integrin alpha v beta 6 binds and activates latent tgf beta 1: A mechanism for regulating pulmonary inflammation and fibrosis. *Cell* 1999;96(3):319-328.

41. Stetler-Stevenson WG, Aznavoorian S, Liotta LA. Tumor cell interactions with the extracellular matrix during invasion and metastasis. *Annu Rev Cell Biol* 1993;9:541-573.

42. Yu Q, Stamenkovic I. Cell surface-localized matrix metalloproteinase-9 proteolytically activates tgf-beta and promotes tumor invasion and angiogenesis. *Genes Dev* 2000;14(2):163-176.

43. Yue J, Mulder KM. Transforming growth factor-beta signal transduction in epithelial cells. *Pharmacol Ther* 2001;91(1):1-34.

44. Brown AC, Rowe JA, Barker TH. Guiding epithelial cell phenotypes with engineered integrin-specific recombinant fibronectin fragments. *Tissue Eng Part A*;17(1-2):139-150.

45. Wipff PJ, Hinz B. Integrins and the activation of latent transforming growth factor beta1 - an intimate relationship. *Eur J Cell Biol* 2008;87(8-9):601-615.

46. Wipff PJ, Rifkin DB, Meister JJ, Hinz B. Myofibroblast contraction activates latent tgf-beta1 from the extracellular matrix. *J Cell Biol* 2007;179(6):1311-1323.

47. Amara N, Goven D, Prost F, Muloway R, Crestani B, Boczkowski J. Nox4/nadph oxidase expression is increased in pulmonary fibroblasts from patients with idiopathic

pulmonary fibrosis and mediates tgfbeta1-induced fibroblast differentiation into myofibroblasts. *Thorax* 2010;65(8):733-738.

48. Bocchino M, Agnese S, Fagone E, Svegliati S, Grieco D, Vancheri C, Gabrielli A, Sanduzzi A, Avvedimento EV. Reactive oxygen species are required for maintenance and differentiation of primary lung fibroblasts in idiopathic pulmonary fibrosis. *PloS one* 2010;5(11):e14003.

49. Cui Y, Robertson J, Maharaj S, Waldhauser L, Niu J, Wang J, Farkas L, Kolb M, Gauldie J. Oxidative stress contributes to the induction and persistence of tgf-beta1 induced pulmonary fibrosis. *Int J Biochem Cell Biol* 2011;43(8):1122-1133.

50. Jobling MF, Mott JD, Finnegan MT, Jurukovski V, Erickson AC, Walian PJ, Taylor SE, Ledbetter S, Lawrence CM, Rifkin DB, et al. Isoform-specific activation of latent transforming growth factor beta (ltgf-beta) by reactive oxygen species. *Radiation research* 2006;166(6):839-848.

51. Teramoto S, Fukuchi Y, Uejima Y, Shu CY, Orimo H. Superoxide anion formation and glutathione metabolism of blood in patients with idiopathic pulmonary fibrosis. *Biochemical and molecular medicine* 1995;55(1):66-70.

52. Bakand S, Hayes A, Dechsakulthorn F. Nanoparticles: A review of particle toxicology following inhalation exposure. *Inhalation toxicology* 2012;24(2):125-135.

53. Becquemin MH, Roy M, Robeau D, Bonnefous S, Piechowski J, Teillac A. Inhaled particle deposition and clearance from the normal respiratory tract. *Respiration physiology* 1987;67(2):147-158.

54. Borm PJ. Particle toxicology: From coal mining to nanotechnology. *Inhalation toxicology* 2002;14(3):311-324.

55. Hofmann W, Sturm R, Winkler-Heil R, Pawlak E. Stochastic model of ultrafine particle deposition and clearance in the human respiratory tract. *Radiation protection dosimetry* 2003;105(1-4):77-80.

56. Kappos AD, Bruckmann P, Eikmann T, Englert N, Heinrich U, Hoppe P, Koch E, Krause GH, Kreyling WG, Rauchfuss K, et al. Health effects of particles in ambient air. *International journal of hygiene and environmental health* 2004;207(4):399-407.

57. Katsouyanni K, Touloumi G, Samoli E, Gryparis A, Le Tertre A, Monopolis Y, Rossi G, Zmirou D, Ballester F, Boumghar A, et al. Confounding and effect modification in the short-term effects of ambient particles on total mortality: Results from 29 european cities within the aphea2 project. *Epidemiology* 2001;12(5):521-531.

58. Ostro B, Broadwin R, Green S, Feng WY, Lipsett M. Fine particulate air pollution and mortality in nine california counties: Results from calfine. *Environmental health perspectives* 2006;114(1):29-33.

59. Pope CA, 3rd, Burnett RT, Thun MJ, Calle EE, Krewski D, Ito K, Thurston GD. Lung cancer, cardiopulmonary mortality, and long-term exposure to fine particulate air pollution. *JAMA : the journal of the American Medical Association* 2002;287(9):1132-1141.

60. Tao F, Gonzalez-Flecha B, Kobzik L. Reactive oxygen species in pulmonary inflammation by ambient particulates. *Free radical biology & medicine* 2003;35(4):327-340.

61. Zanobetti A, Schwartz J, Dockery DW. Airborne particles are a risk factor for hospital admissions for heart and lung disease. *Environmental health perspectives* 2000;108(11):1071-1077.

62. Maher TM, Wells AU, Laurent GJ. Idiopathic pulmonary fibrosis: Multiple causes and multiple mechanisms? *Eur Respir J* 2007;30(5):835-839.

63. Meltzer EB, Noble PW. Idiopathic pulmonary fibrosis. *Orphanet J Rare Dis* 2008;3:8.

64. Degryse AL, Tanjore H, Xu XC, Polosukhin VV, Jones BR, Boomershine CS, Ortiz C, Sherrill TP, McMahon FB, Gleaves LA, et al. Tgf{beta} signaling in lung epithelium regulates bleomycin induced alveolar injury and fibroblast recruitment. *Am J Physiol Lung Cell Mol Physiol*.

65. Willis BC, Liebler JM, Luby-Phelps K, Nicholson AG, Crandall ED, du Bois RM, Borok Z. Induction of epithelial-mesenchymal transition in alveolar epithelial cells by transforming growth factor-beta1: Potential role in idiopathic pulmonary fibrosis. *Am J Pathol* 2005;166(5):1321-1332.

66. Wynn TA. Cellular and molecular mechanisms of fibrosis. *J Pathol* 2008;214(2):199-210.

67. Iwano M, Plieth D, Danoff TM, Xue C, Okada H, Neilson EG. Evidence that fibroblasts derive from epithelium during tissue fibrosis. *J Clin Invest* 2002;110(3):341-350.

68. Duband JL, Thiery JP. Appearance and distribution of fibronectin during chick embryo gastrulation and neurulation. *Dev Biol* 1982;94(2):337-350.

69. Hay ED. An overview of epithelio-mesenchymal transformation. *Acta Anat (Basel)* 1995;154(1):8-20.

70. Vicovac L, Aplin JD. Epithelial-mesenchymal transition during trophoblast differentiation. *Acta Anat (Basel)* 1996;156(3):202-216.

71. Arnoux V, Nassour M, L'Helgoualc'h A, Hipskind RA, Savagner P. Erk5 controls slug expression and keratinocyte activation during wound healing. *Mol Biol Cell* 2008;19(11):4738-4749.

72. Camara J, Jarai G. Epithelial-mesenchymal transition in primary human bronchial epithelial cells is smad-dependent and enhanced by fibronectin and tnf-alpha. *Fibrogenesis Tissue Repair*;3(1):2.

73. Felton VM, Borok Z, Willis BC. N-acetylcysteine inhibits alveolar epithelial-mesenchymal transition. *Am J Physiol Lung Cell Mol Physiol* 2009;297(5):L805-812.

74. Gharaee-Kermani M, Hu B, Phan SH, Gyetko MR. Recent advances in molecular targets and treatment of idiopathic pulmonary fibrosis: Focus on tgfbeta signaling and the myofibroblast. *Curr Med Chem* 2009;16(11):1400-1417.

75. Derynck R, Zhang YE. Smad-dependent and smad-independent pathways in tgf-beta family signalling. *Nature* 2003;425(6958):577-584.

76. Rahimi RA, Leof EB. Tgf-beta signaling: A tale of two responses. *J Cell Biochem* 2007;102(3):593-608.

77. Shi Y, Massague J. Mechanisms of tgf-beta signaling from cell membrane to the nucleus. *Cell* 2003;113(6):685-700.

78. Batlle E, Sancho E, Franci C, Dominguez D, Monfar M, Baulida J, Garcia De Herreros A. The transcription factor snail is a repressor of e-cadherin gene expression in epithelial tumour cells. *Nat Cell Biol* 2000;2(2):84-89.

79. Boutet A, De Frutos CA, Maxwell PH, Mayol MJ, Romero J, Nieto MA. Snail activation disrupts tissue homeostasis and induces fibrosis in the adult kidney. *EMBO J* 2006;25(23):5603-5613.

80. Guaita S, Puig I, Franci C, Garrido M, Dominguez D, Batlle E, Sancho E, Dedhar S, De Herreros AG, Baulida J. Snail induction of epithelial to mesenchymal transition in tumor cells is accompanied by muc1 repression and zeb1 expression. *J Biol Chem* 2002;277(42):39209-39216.

81. Magnusson MK, Mosher DF. Fibronectin: Structure, assembly, and cardiovascular implications. *Arteriosclerosis, thrombosis, and vascular biology* 1998;18(9):1363-1370.

82. Beers MF, Morrisey EE. The three r's of lung health and disease: Repair, remodeling, and regeneration. *J Clin Invest* 2011;121(6):2065-2073.

83. Worthington JJ, Klementowicz JE, Travis MA. Tgfbeta: A sleeping giant awoken by integrins. *Trends Biochem Sci*;36(1):47-54.

84. Kantola AK, Keski-Oja J, Koli K. Fibronectin and heparin binding domains of latent tgf-beta binding protein (ltbp)-4 mediate matrix targeting and cell adhesion. *Exp Cell Res* 2008;314(13):2488-2500.

85. Chen Q, Sivakumar P, Barley C, Peters DM, Gomes RR, Farach-Carson MC, Dallas SL. Potential role for heparan sulfate proteoglycans in regulation of transforming growth factor-beta (tgf-beta) by modulating assembly of latent tgf-beta-binding protein-1. *J Biol Chem* 2007;282(36):26418-26430.

86. Mu D, Cambier S, Fjellbirkeland L, Baron JL, Munger JS, Kawakatsu H, Sheppard D, Broaddus VC, Nishimura SL. The integrin alpha(v)beta8 mediates epithelial homeostasis through mt1-mmp-dependent activation of tgf-beta1. *J Cell Biol* 2002;157(3):493-507.

87. Jenkins RG, Su X, Su G, Scotton CJ, Camerer E, Laurent GJ, Davis GE, Chambers RC, Matthay MA, Sheppard D. Ligation of protease-activated receptor 1 enhances alpha(v)beta6 integrin-dependent tgf-beta activation and promotes acute lung injury. *J Clin Invest* 2006;116(6):1606-1614.

88. Wells RG, Discher DE. Matrix elasticity, cytoskeletal tension, and tgf-beta: The insoluble and soluble meet. *Science signaling* 2008;1(10):pe13.

89. Bonner JC. Lung fibrotic responses to particle exposure. *Toxicologic pathology* 2007;35(1):148-153.

90. Holgate ST, Davies DE, Lackie PM, Wilson SJ, Puddicombe SM, Lordan JL. Epithelial-mesenchymal interactions in the pathogenesis of asthma. *The Journal of allergy and clinical immunology* 2000;105(2 Pt 1):193-204.

91. Anderson JM, Rodriguez A, Chang DT. Foreign body reaction to biomaterials. *Semin Immunol* 2008;20(2):86-100.

92. Becker S, Soukup JM, Gilmour MI, Devlin RB. Stimulation of human and rat alveolar macrophages by urban air particulates: Effects on oxidant radical generation and cytokine production. *Toxicology and applied pharmacology* 1996;141(2):637-648.

93. Behr J, Demedts M, Buhl R, Costabel U, Dekhuijzen RP, Jansen HM, MacNee W, Thomeer M, Wallaert B, Laurent F, et al. Lung function in idiopathic pulmonary fibrosis--extended analyses of the ifigenia trial. *Respir Res* 2009;10:101.

94. Oberdorster G, Oberdorster E, Oberdorster J. Nanotoxicology: An emerging discipline evolving from studies of ultrafine particles. *Environmental health perspectives* 2005;113(7):823-839.

95. El-Haibi CP, Bell GW, Zhang J, Collmann AY, Wood D, Scherber CM, Csizmadia E, Mariani O, Zhu C, Campagne A, et al. Critical role for lysyl oxidase in mesenchymal stem cell-driven breast cancer malignancy. *Proc Natl Acad Sci U S A* 2012;109(43):17460-17465.

96. Diaz-Sanchez D, Jyrala M, Ng D, Nel A, Saxon A. In vivo nasal challenge with diesel exhaust particles enhances expression of the cc chemokines rantes, mip-1alpha, and mcp-3 in humans. *Clin Immunol* 2000;97(2):140-145.

97. Dreher KL, Jaskot RH, Lehmann JR, Richards JH, McGee JK, Ghio AJ, Costa DL. Soluble transition metals mediate residual oil fly ash induced acute lung injury. *Journal of toxicology and environmental health* 1997;50(3):285-305.

98. Li W, Zhou J, Chen L, Luo Z, Zhao Y. Lysyl oxidase, a critical intra- and extra-cellular target in the lung for cigarette smoke pathogenesis. *International journal of environmental research and public health* 2011;8(1):161-184.

99. Fogelgren B, Polgar N, Szauter KM, Ujfaludi Z, Laczko R, Fong KS, Csiszar K. Cellular fibronectin binds to lysyl oxidase with high affinity and is critical for its proteolytic activation. *J Biol Chem* 2005;280(26):24690-24697.

100. Zhou G, Dada LA, Wu M, Kelly A, Trejo H, Zhou Q, Varga J, Sznajder JI. Hypoxia-induced alveolar epithelial-mesenchymal transition requires mitochondrial ros and hypoxia-inducible factor 1. *Am J Physiol Lung Cell Mol Physiol* 2009;297(6):L1120-1130.

101. Lee IT, Yang CM. Inflammatory signalings involved in airway and pulmonary diseases. *Mediators of inflammation* 2013;2013:791231.

102. Lee IT, Yang CM. Role of nadph oxidase/ros in pro-inflammatory mediators-induced airway and pulmonary diseases. *Biochemical pharmacology* 2012;84(5):581-590.

103. Kettle AJ, Anderson RF, Hampton MB, Winterbourn CC. Reactions of superoxide with myeloperoxidase. *Biochemistry* 2007;46(16):4888-4897.

104. Gamaley IA, Kirpichnikova KM, Klyubin IV. Activation of murine macrophages by hydrogen peroxide. *Cellular signalling* 1994;6(8):949-957.

105. Qi S, den Hartog GJ, Bast A. Superoxide radicals increase transforming growth factor-beta1 and collagen release from human lung fibroblasts via cellular influx through chloride channels. *Toxicology and applied pharmacology* 2009;237(1):111-118.

106. Fehrenbach H. Alveolar epithelial type ii cell: Defender of the alveolus revisited. *Respir Res* 2001;2(1):33-46.

107. Mason RJ. Biology of alveolar type ii cells. *Respirology* 2006;11 Suppl:S12-15.

108. Jain L, Chen XJ, Ramosevac S, Brown LA, Eaton DC. Expression of highly selective sodium channels in alveolar type ii cells is determined by culture conditions. *Am J Physiol Lung Cell Mol Physiol* 2001;280(4):L646-658.

109. Selman M, Pardo A. Role of epithelial cells in idiopathic pulmonary fibrosis: From innocent targets to serial killers. *Proceedings of the American Thoracic Society* 2006;3(4):364-372.

110. Thannickal VJ, Horowitz JC. Evolving concepts of apoptosis in idiopathic pulmonary fibrosis. *Proceedings of the American Thoracic Society* 2006;3(4):350-356.

111. Uhal BD, Joshi I, Hughes WF, Ramos C, Pardo A, Selman M. Alveolar epithelial cell death adjacent to underlying myofibroblasts in advanced fibrotic human lung. *The American journal of physiology* 1998;275(6 Pt 1):L1192-1199.

112. Sheppard D. Functions of pulmonary epithelial integrins: From development to disease. *Physiological reviews* 2003;83(3):673-686.

113. Lubman RL, Zhang XL, Zheng J, Ocampo L, Lopez MZ, Veeraraghavan S, Zabski SM, Danto SI, Borok Z. Integrin alpha(3)-subunit expression modulates alveolar epithelial cell monolayer formation. *Am J Physiol Lung Cell Mol Physiol* 2000;279(1):L183-193.

114. Kumar NM, Sigurdson SL, Sheppard D, Lwebuga-Mukasa JS. Differential modulation of integrin receptors and extracellular matrix laminin by transforming growth factor-beta 1 in rat alveolar epithelial cells. *Exp Cell Res* 1995;221(2):385-394.

115. Eble JA, Wucherpfennig KW, Gauthier L, Dersch P, Krukonis E, Isberg RR, Hemler ME. Recombinant soluble human alpha 3 beta 1 integrin: Purification, processing, regulation, and specific binding to laminin-5 and invasin in a mutually exclusive manner. *Biochemistry* 1998;37(31):10945-10955.

116. Pankov R YK. Fibronectin at a glance. *J Cell Sci* 2002;115(20):3861-3863.

117. Kaufmann R, Frosch D, Westphal C, Weber L, Klein CE. Integrin vla-3: Ultrastructural localization at cell-cell contact sites of human cell cultures. *J Cell Biol* 1989;109(4 Pt 1):1807-1815.

118. Elices MJ, Urry LA, Hemler ME. Receptor functions for the integrin vla-3: Fibronectin, collagen, and laminin binding are differentially influenced by arg-gly-asp peptide and by divalent cations. *J Cell Biol* 1991;112(1):169-181.

119. Humphries J, Byron, A, Humphries, M. Integrin ligands at a glance. *J Cell Sci* 2006;119:3901-3903.

120. Mould AP, Askari JA, Aota S, Yamada KM, Irie A, Takada Y, Mardon HJ, Humphries MJ. Defining the topology of integrin alpha5beta1-fibronectin interactions using inhibitory anti-alpha5 and anti-beta1 monoclonal antibodies. Evidence that the synergy sequence of fibronectin is recognized by the amino-terminal repeats of the alpha5 subunit. *J Biol Chem* 1997;272(28):17283-17292.

121. Mould AP, Akiyama SK, Humphries MJ. Regulation of integrin alpha 5 beta 1-fibronectin interactions by divalent cations. Evidence for distinct classes of binding sites for mn2+, mg2+, and ca2+. *J Biol Chem* 1995;270(44):26270-26277.

122. Mardon HJ, Grant KE. The role of the ninth and tenth type iii domains of human fibronectin in cell adhesion. *FEBS letters* 1994;340(3):197-201.

123. Grant RP, Spitzfaden C, Altroff H, Campbell ID, Mardon HJ. Structural requirements for biological activity of the ninth and tenth fiii domains of human fibronectin. *J Biol Chem* 1997;272(10):6159-6166.

124. Ng SP, Billings KS, Ohashi T, Allen MD, Best RB, Randles LG, Erickson HP, Clarke J. Designing an extracellular matrix protein with enhanced mechanical stability. *Proc Natl Acad Sci U S A* 2007;104(23):9633-9637.

125. Altroff H, Schlinkert R, van der Walle CF, Bernini A, Campbell ID, Werner JM, Mardon HJ. Interdomain tilt angle determines integrin-dependent function of the ninth and tenth fiii domains of human fibronectin. *J Biol Chem* 2004;279(53):55995-56003.

126. Stephansson SN, Byers BA, Garcia AJ. Enhanced expression of the osteoblastic phenotype on substrates that modulate fibronectin conformation and integrin receptor binding. *Biomaterials* 2002;23(12):2527-2534.

127. Gronthos S, Simmons PJ, Graves SE, Robey PG. Integrin-mediated interactions between human bone marrow stromal precursor cells and the extracellular matrix. *Bone* 2001;28(2):174-181.

128. Koistinen P, Pulli T, Uitto VJ, Nissinen L, Hyypia T, Heino J. Depletion of alphav integrins from osteosarcoma cells by intracellular antibody expression induces bone differentiation marker genes and suppresses gelatinase (mmp-2) synthesis. *Matrix Biol* 1999;18(3):239-251.

129. Chang CJ, Chao CH, Xia W, Yang JY, Xiong Y, Li CW, Yu WH, Rehman SK, Hsu JL, Lee HH, et al. P53 regulates epithelial-mesenchymal transition and stem cell properties through modulating mirnas. *Nat Cell Biol*;13(3):317-323.

130. Choquet D, Felsenfeld DP, Sheetz MP. Extracellular matrix rigidity causes strengthening of integrin-cytoskeleton linkages. *Cell* 1997;88(1):39-48.

131. Georges PC, Janmey PA. Cell type-specific response to growth on soft materials. *J Appl Physiol* 2005;98(4):1547-1553.

132. Vogel V, Sheetz M. Local force and geometry sensing regulate cell functions. *Nat Rev Mol Cell Biol* 2006;7(4):265-275.

133. Liu F, Mih JD, Shea BS, Kho AT, Sharif AS, Tager AM, Tschumperlin DJ. Feedback amplification of fibrosis through matrix stiffening and cox-2 suppression. *J Cell Biol* 2010;190(4):693-706.

134. Markowski MC, Brown AC, Barker TH. Directing epithelial to mesenchymal transition through engineered microenvironments displaying orthogonal adhesive and mechanical cues. *Journal of biomedical materials research Part A* 2012;100(8):2119-2127.

135. Clause KC, Barker TH. Extracellular matrix signaling in morphogenesis and repair. *Current opinion in biotechnology* 2013;24(5):830-833.

136. Ruoslahti E. Rgd and other recognition sequences for integrins. *Annu Rev Cell Dev Biol* 1996;12:697-715.

137. Humphries MJ. The molecular basis and specificity of integrin-ligand interactions. *J Cell Sci* 1990;97 (Pt 4):585-592.

138. Plow EF, Haas TA, Zhang L, Loftus J, Smith JW. Ligand binding to integrins. *J Biol Chem* 2000;275(29):21785-21788.

139. Mao Y, Schwarzbauer JE. Fibronectin fibrillogenesis, a cell-mediated matrix assembly process. *Matrix Biol* 2005;24(6):389-399.

140. Barker TH, Baneyx G, Cardo-Vila M, Workman GA, Weaver M, Menon PM, Dedhar S, Rempel SA, Arap W, Pasqualini R, et al. Sparc regulates extracellular matrix organization through its modulation of integrin-linked kinase activity. *J Biol Chem* 2005;280(43):36483-36493.

141. Sriramarao P, Steffner P, Gehlsen KR. Biochemical evidence for a homophilic interaction of the alpha 3 beta 1 integrin. *J Biol Chem* 1993;268(29):22036-22041.

142. Kim KK, Wei Y, Szekeres C, Kugler MC, Wolters PJ, Hill ML, Frank JA, Brumwell AN, Wheeler SE, Kreidberg JA, et al. Epithelial cell alpha3beta1 integrin links beta-catenin and smad signaling to promote myofibroblast formation and pulmonary fibrosis. *J Clin Invest* 2009;119(1):213-224.

143. Kim Y, Kugler MC, Wei Y, Kim KK, Li X, Brumwell AN, Chapman HA. Integrin alpha3beta1-dependent beta-catenin phosphorylation links epithelial smad signaling to cell contacts. *J Cell Biol* 2009;184(2):309-322.

144. Martino MM, Mochizuki M, Rothenfluh DA, Rempel SA, Hubbell JA, Barker TH. Controlling integrin specificity and stem cell differentiation in 2d and 3d environments through regulation of fibronectin domain stability. *Biomaterials* 2009;30(6):1089-1097.

145. Stabenfeldt SE, Gossett JJ, Barker TH. Building better fibrin knob mimics: An investigation of synthetic fibrin knob peptide structures in solution and their dynamic binding with fibrinogen/fibrin holes. *Blood*;116(8):1352-1359.

146. Petrie TA, Capadona JR, Reyes CD, Garcia AJ. Integrin specificity and enhanced cellular activities associated with surfaces presenting a recombinant fibronectin fragment compared to rgd supports. *Biomaterials* 2006;27(31):5459-5470.

147. Morton TA, Myszka DG. Kinetic analysis of macromolecular interactions using surface plasmon resonance biosensors. *Methods Enzymol* 1998;295:268-294.

148. Joss L, Morton TA, Doyle ML, Myszka DG. Interpreting kinetic rate constants from optical biosensor data recorded on a decaying surface. *Anal Biochem* 1998;261(2):203-210.

149. Myszka DG, Morton TA. Clamp: A biosensor kinetic data analysis program. *Trends Biochem Sci* 1998;23(4):149-150.

150. Myszka DG. Improving biosensor analysis. *J Mol Recognit* 1999;12(5):279-284.

151. Rao SP, Gehlsen KR, Catanzaro A. Identification of a beta 1 integrin on mycobacterium avium-mycobacterium intracellulare. *Infect Immun* 1992;60(9):3652-3657.

152. Harburger DS, Calderwood DA. Integrin signalling at a glance. *J Cell Sci* 2009;122(Pt 2):159-163.

153. Roca-Cusachs P, Gauthier NC, Del Rio A, Sheetz MP. Clustering of alpha(5)beta(1) integrins determines adhesion strength whereas alpha(v)beta(3) and talin enable mechanotransduction. *Proc Natl Acad Sci U S A* 2009;106(38):16245-16250.

154. Wang Z, Symons JM, Goldstein SL, McDonald A, Miner JH, Kreidberg JA. (alpha)3(beta)1 integrin regulates epithelial cytoskeletal organization. *J Cell Sci* 1999;112 (Pt 17):2925-2935.

155. Truong H, Danen EH. Integrin switching modulates adhesion dynamics and cell migration. *Cell Adh Migr* 2009;3(2):179-181.

156. Carson AE, Barker TH. Emerging concepts in engineering extracellular matrix variants for directing cell phenotype. *Regen Med* 2009;4(4):593-600.

157. Schwartz MA. Integrins and extracellular matrix in mechanotransduction. *Cold Spring Harb Perspect Biol*;2(12):a005066.

158. Li J, Zhao Z, Wang J, Chen G, Yang J, Luo S. The role of extracellular matrix, integrins, and cytoskeleton in mechanotransduction of centrifugal loading. *Mol Cell Biochem* 2008;309(1-2):41-48.

159. Masszi A, Fan L, Rosivall L, McCulloch CA, Rotstein OD, Mucsi I, Kapus A. Integrity of cell-cell contacts is a critical regulator of tgf-beta 1-induced epithelial-to-myofibroblast transition: Role for beta-catenin. *Am J Pathol* 2004;165(6):1955-1967.

160. Hinz B. Tissue stiffness, latent tgf-beta1 activation, and mechanical signal transduction: Implications for the pathogenesis and treatment of fibrosis. *Curr Rheumatol Rep* 2009;11(2):120-126.

161. Tse JR, Engler AJ. Preparation of hydrogel substrates with tunable mechanical properties. *Current protocols in cell biology / editorial board, Juan S Bonifacino [et al*;Chapter 10:Unit 10 16.

162. Abe M, Harpel JG, Metz CN, Nunes I, Loskutoff DJ, Rifkin DB. An assay for transforming growth factor-beta using cells transfected with a plasminogen activator inhibitor-1 promoter-luciferase construct. *Anal Biochem* 1994;216(2):276-284.

163. Chan TL, Lee PS, Hering WE. Deposition and clearance of inhaled diesel exhaust particles in the respiratory tract of fischer rats. *Journal of applied toxicology : JAT* 1981;1(2):77-82.

164. Butler AJ, Andrew MS, Russell AG. Daily sampling of pm2.5 in atlanta: Results of the first year of the assessment of spatial aerosol composition in atlanta study. *J Geophys Res-Atmos* 2003;108(D1).

165. Lee S, Russell AG, Baumann K. Source apportionment of fine particulate matter in the southeastern united states. *J Air Waste Manag Assoc* 2007;57(9):1123-1135.

166. Nawijn MC, Hackett TL, Postma DS, van Oosterhout AJ, Heijink IH. E-cadherin: Gatekeeper of airway mucosa and allergic sensitization. *Trends in immunology* 2011;32(6):248-255.

167. Zou W, Zou Y, Zhao Z, Li B, Ran P. Nicotine induced epithelial-mesenchymal transition via wnt/beta-catenin signaling in human airway epithelial cells. *Am J Physiol Lung Cell Mol Physiol* 2012.

VITA

MARILYN M. DYSART

Marilyn M. Dysart was born in Norfolk, Virginia. She attended public schools in Virginia Beach, Virginia and received a B.S. in Biomedical Engineering from the University of Virginia, Charlottesville, Virginia in 2008 before coming to Georgia Tech to pursue a doctorate in Biomedical Engineering. When she is not working on her research, Mrs. Dysart enjoys baking, hiking and snowboarding with her husband Fred, and spending time with their dog Riley.